VOLUME XLVI

GEMS & GEMOLOGY

WINTER 2010

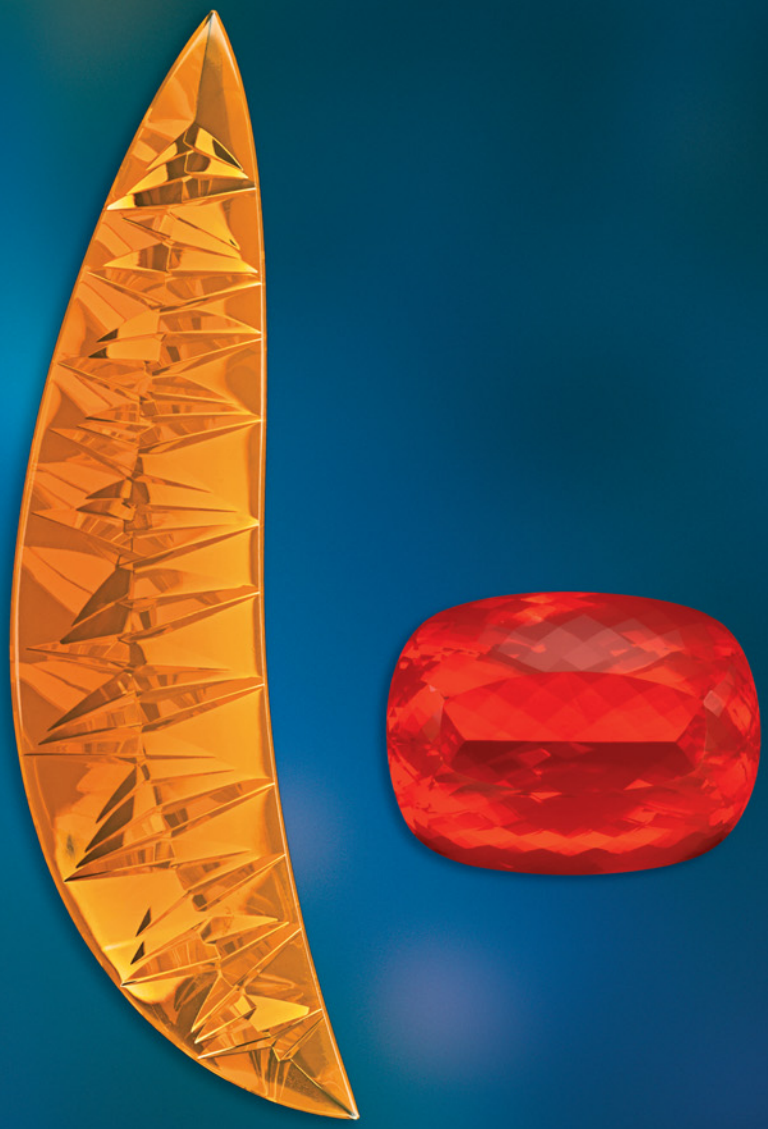

Synthetics Retrospective . . . Scapolite from Madagascar . . . Pietersite from China and Namibia . . . New Mexifire Synthetic Opal . . . Identifying Historic Gems

THE QUARTERLY JOURNAL OF THE GEMOLOGICAL INSTITUTE OF AMERICA

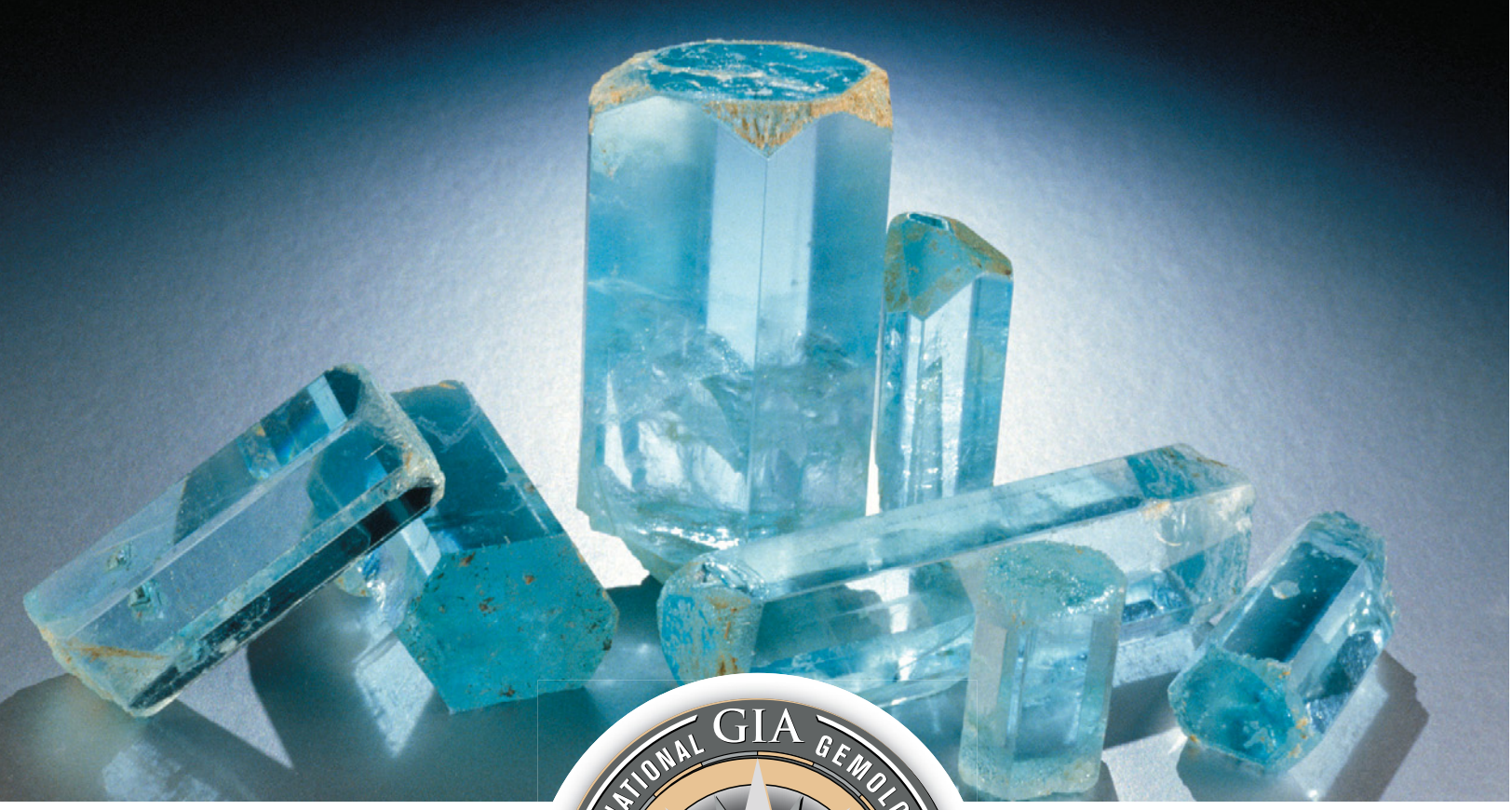

INTERNATIONAL GIA GEMOLOGICAL SYMPOSIUM

SYMPOSIUM 2011

ADVANCING THE SCIENCE AND BUSINESS OF GEMS

MAY 29 – 30, 2011

GIA World Headquarters

Robert Mouawad Campus | Carlsbad, California

www.symposium2011.gia.edu

GIA®

Winter 2010 GEMS & GEMOLOGY® Volume 46, No. 4

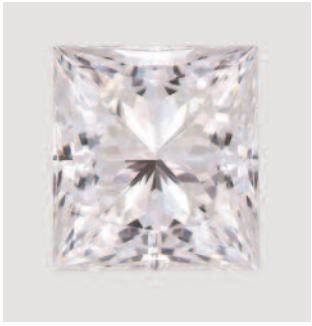

pg. 262

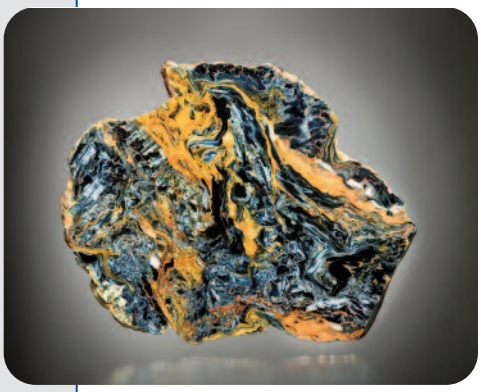

pg. 286

EDITORIAL

FEATURE ARTICLE

NOTES & NEW TECHNIQUES

RAPID COMMUNICATIONS

REGULAR FEATURES

pg. 319

GEMS & GEMOLOGY®

www.gia.edu/gandg

SUBSCRIPTIONS

Copies of the current issue may be purchased for **$29.95** plus shipping. Online subscriptions are $74.95 for one year (4 issues), $129.95 for two years (8 issues). Combination print + online subscriptions are $139.95 in the U.S. and $160 elsewhere for one year, and $269.95 in the U.S. and $305 elsewhere for two years. Canadian subscribers should add GST. Discounts are available for group subscriptions, renewals, GIA alumni, and current GIA students. For institutional rates, go to gia.edu/gandg. Subscriptions include *G&G's* monthly gemological e-newsletter, the *G&G eBrief*.

To purchase subscriptions and single issues (print or PDF), visit **store.gia.edu** or contact the Circulation Coordinator.

PDF versions of individual articles and sections from Spring 1981 forward can be purchased at **gia.metapress.com** for $12 each. Visit gia.edu/gandg for free online access to the 1934–2009 subject and author index and all 1934–1980 issues.

To obtain a Japanese translation of *Gems & Gemology,* contact GIA Japan at info@giajpn.gr.jp. Our Canadian goods and service registration number is 126142892RT.

DATABASE COVERAGE

Gems & Gemology's five-year impact factor (for 2004–2008) is 1.197, according to the 2009 Thomson Reuters Journal Citation Reports (issued July 2010). The journal ranked 17th out of 27 titles in the mineralogy category. *Gems & Gemology* is abstracted in Thomson Reuters products (*Current Contents: Physical, Chemical & Earth Sciences* and Science Citation Index—Expanded, including the Web of Knowledge) and other databases. For a complete list of sources abstracting *G&G*, go to gia.edu/gandg.

MANUSCRIPT SUBMISSIONS

Gems & Gemology welcomes the submission of articles on all aspects of the field. Please see the Guidelines for Authors at gia.edu/gandg or contact the Managing Editor. Letters on articles published in *Gems & Gemology* are also welcome.

COPYRIGHT AND REPRINT PERMISSIONS

Gems & Gemology is published quarterly by the Gemological Institute of America, a nonprofit educational organization for the gem and jewelry industry.

Postmaster: Return undeliverable copies of *Gems & Gemology* to GIA, The Robert Mouawad Campus, 5345 Armada Drive, Carlsbad, CA 92008.

ABOUT THE COVER

The desirability of natural fire opal has stimulated the production of synthetic counterparts. In this issue, Rajneesh Bhandari and Gagan Choudhary characterize the new version of Mexifire synthetic opal, which has RI and SG values much closer to those of natural fire opal, such as these two superb examples. Bernd Munsteiner's "Changing Perspectives" 181.36 ct fire opal carving (left) measures 100 × 23 mm. The 132 ct faceted fire opal on the right is courtesy of W. Constantin Wild & Co., Idar-Oberstein, Germany. Photos by Robert Weldon.

Color separations for *Gems & Gemology* are by Pacific Plus, Carlsbad, California.
Printing is by Allen Press, Lawrence, Kansas.

 ISSN 0016-626X

A Fond Farewell

This is indeed a fond farewell. In January 2011, I am stepping down from *G&G*, and retiring from GIA, after 30 years first as managing editor, then editor, and most recently editor-in-chief of the journal. As is so often stated, I am doing so "for personal reasons." But there are no secrets here. My daughter, Elizabeth, is expecting twins in February, my first grandchildren. She has asked for my help. How can I say no?

Elizabeth was less than a year old when Richard Liddicoat hired me in 1980 to remake *G&G* as a true professional journal. I arrived at GIA with several years' experience working for peer-reviewed marketing and medical journals and with some knowledge of the geology and gemology communities. I thought I would rework the journal and move on. But as so many of you know, gemology is addictive. Soon I was enthralled with the possibilities *G&G* offered to promote this relatively new science.

In the early years of the "new" *G&G*, most of our articles revolved around colored stones: separation from simulants and synthetics, identification of treatments, and especially characterization of new and historic localities, such as emeralds from Colombia and lapis lazuli from Afghanistan. In the 1990s, we published some of the earliest reports on copper-bearing tourmalines from Paraíba, Brazil; rubies and sapphires from Vietnam; and rubies from Mong Hsu, Myanmar. Since then, groundbreaking articles on emerging gem deposits in Madagascar and countries on the African continent have appeared.

Over the years, though, diamonds became more prominent in the pages of the journal. Perhaps *G&G*'s strongest contribution to the diamond community over the last three decades has been the articles on the characterization and identification of synthetic diamonds. Yet I am equally proud of our reporting on diamond treatments and especially the identification of glass-filled diamonds in the late '80s and early '90s. A decade later, the more sophisticated—and potentially more devastating—HPHT treatment of diamonds was successfully tackled in *G&G* by researchers from the GIA, Gübelin, De Beers, and SSEF laboratories, among others. We know that it is only by cooperation and collaboration—and the sharing of information in a respected forum—that gemology can progress as a science in support of public confidence in the gem and jewelry industry.

I can take little credit, though, for what is one of *G&G*'s most important contributions to the science of gemology: becoming the first gemological journal admitted to the Thomson Reuters (formerly ISI) database, the world's foremost resource for accessing scientific content. Editor Brendan Laurs rallied the support of leading researchers to secure this honor and thus enhance the stature of gemology in the scientific community.

With this, my last issue, I extend to you—the readers of *G&G*—my heartfelt thanks for your support all these years. I have loved interacting with you first by mail then by e-mail, visiting with you at trade shows, and sharing experiences at the GIA International Symposia. In fact, GIA has asked me to complete one last project—my role as co-chair of the business track of GIA Symposium 2011, which will be held May 29–30 at GIA headquarters in Carlsbad, California. It will give me great pleasure to see many of you there and thank you in person.

At this time, I turn the journal over to the capable hands of interim editor-in-chief Brendan Laurs, managing editor Tom Overton, and associate editor Stuart Overlin. Please give them your support as well. They are the future of gemology, as told through the pages of *G&G*.

With best personal regards,

Alice S. Keller
Editor-in-Chief
akeller@gia.edu

’10

SYNTHETIC GEM MATERIALS IN THE 2000S: A DECADE IN REVIEW

Nathan Renfro, John I. Koivula, Wuyi Wang, and Gary Roskin

The first decade of the 2000s brought a constant flow of previously known synthetics into the marketplace, but little in the way of new technology. The biggest development was the commercial introduction of faceted single-crystal gem-quality CVD synthetic diamonds. A few other interesting and noteworthy synthetics, such as Malossi hydrothermal synthetic emeralds and Mexifire synthetic opals, also entered the market. Identification of synthetic gem materials continued to be an important function of—and, in some cases, challenge for—gemologists worldwide.

The development of synthetics and the methodologies used to detect new and existing materials is of great importance to the international gem community. Indeed, whether a synthetic gem was grown in the 2000s or the 1880s, today’s gemologists must still be prepared to deal with it. Many synthetic gems were prominent in the marketplace in the first decade of the 2000s (see, e.g., figure 1).

The decade also saw some new synthetics. Among the synthetic colored stones introduced was the Malossi hydrothermal synthetic emerald (Adamo et al., 2005), which was gemologically similar to both Russian synthetic emeralds and those manufactured by Linde-Regency in the United States. Also new to this decade was a synthetic fire opal marketed as Mexifire (Choudhary and Bhandari, 2008). On initial examination, this nonphenomenal synthetic opal resembled manufactured glass.

Yet it is clear from the overall volume of published literature that the most significant developments—and the focus of most research—during this decade involved the production of gem-quality synthetic diamonds, primarily those grown by the comparatively new CVD (chemical vapor deposition) process. Who can forget the September 2003 cover of *Wired* magazine, with a diamond-pavéd “supermodel” next to the headlines “$5 a carat. Flawless. Made in a lab.”? This article proclaimed that “The diamond wars have begun,” and touted the potential for outright cheap but extremely high-quality colorless and fancy-colored synthetic diamonds grown by two very different processes (CVD and HPHT). Although neither of these technologies was new to the 2000s—and neither has even approached a price as low as $5 a carat—both made important commercial statements and had a major impact on the diamond trade and gemological research during this first decade.

It is important to state that reviews such as this can serve only as guides to the available gemological literature. Anyone seeking in-depth information regarding synthetic gems and their identification

See end of article for About the Authors and Acknowledgments.
GEMS & GEMOLOGY, Vol. 46, No. 4, pp. 260–273.

Figure 1. Consisting of synthetic alexandrite, amethyst, beryl, corundum, diamond, and fire opal, this collection represents some of the interesting and unusual synthetic gem materials encountered in the decade of the 2000s. The three smallest stones are synthetic diamonds weighing 0.06–0.14 ct. Photo by Robert Weldon.

should consult the references at the end of the article to gain the knowledge required to recognize and correctly identify the various materials under discussion. In addition, useful reviews of synthetic materials that have impacted the gem trade were previously published in *Gems & Gemology* (Nassau, 1990; Koivula et al., 2000) and in *Elements* magazine (Kane, 2009), while the largest collection of images detailing inclusions and other microfeatures in gemologically significant synthetics can be found in the three volumes of the *Photoatlas of Inclusions in Gemstones* (Gübelin and Koivula, 1986, 2005, 2008).

It should also be noted that only those synthetic products that are actually new to the prior decade are included in this review. For example, although hydrothermally grown cobalt-colored synthetic blue quartz was described in the Winter 2008 issue of *Gems & Gemology* (Choudhary, 2008), it is actually a material that was introduced in the 1990s (see Koivula et al., 1993), so it was not included in this retrospective.

SYNTHETIC DIAMOND

Synthetic diamonds were an important concern throughout the past decade, although supplies of gem-quality material were never extensive, and fashioned synthetic diamonds were only occasionally submitted for diamond grading reports. In the GIA Laboratory, for example, gem-quality synthetic diamonds have been seen only rarely (a fraction of a percent of the large volume of diamonds examined daily), and the vast majority have had a (fancy) bodycolor. Kitawaki et al. (2008) of the GAAJ-Zenhokyo Laboratory in Tokyo reported identifying more than 100 yellow synthetic melee diamonds (smaller than 0.20 ct) among material received for identification over the course of four months, a significant amount but still a small portion of the total number of melee stones examined.

The big shift between the 1990s and the 2000s came in the processes used to synthesize diamonds. In the 1990s, synthetic diamonds grown by the application of both high pressure and high temperature in molten iron/nickel fluxes (the HPHT process) were of primary concern. Such lab-grown diamonds produced today are still commonly yellow to brownish orange as grown (due to nitrogen; Shigley et al., 2002), but they can also be grown with a blue body-

color and treated to pink (Shigley et al., 2004). While the quality, quantity, and size of these synthetics have increased over the past decade—with the largest faceted HPHT synthetic diamond submitted to the GIA lab being 4.09 ct (Wang and Moses, 2010)—the detection methods used to separate them from natural diamonds have remained essentially the same.

Early in the decade, companies like Gemesis Corp. in Sarasota, Florida, began to produce and market HPHT-grown synthetic diamonds, primarily in shades of yellow to orange (again, see Shigley et al., 2002). Chatham Created Gems began to sell their own branded HPHT-grown stones in a variety of colors (again, see Shigley et al., 2004), such as blue, yellow, and pink. It was CVD synthesis by Apollo Diamond, however, that caused the largest stir in the trade.

The CVD method involves bringing together the needed gaseous reagents—typically a small amount of methane (CH_4) in hydrogen (H_2)—in a chamber with a substrate. A reaction among these components is initiated at high temperatures and low pressures. The reactants, products, and reactive species are transported throughout the chamber by diffusion and convection. Over the substrate surface, various reactions (adsorption, diffusion, and desorption) occur among the chemical species, leading to the deposition of synthetic diamond and, ultimately, the growth of a continuous layer of material (Butler and Woodin, 1993; Davis, 1993; Spear and Dismukes, 1994, Butler et al., 2009). When a diamond (natural or synthetic) is used as the substrate, single-crystal CVD gem-quality synthetic diamond can be produced.

The first successful and reproducible growth of synthetic diamond as a thin film using a CVD technique was achieved by W. G. Eversole in 1952 (Kiffer, 1956, as referenced in Angus, 1994). It is interesting to note that this event predated General Electric's 1955 announcement that its researchers had created single-crystal synthetic diamonds by the HPHT method (Bundy et al., 1955, as referenced in Angus, 1994). However, the early CVD products were exclusively polycrystalline (and, therefore, not gem quality), and the first single-crystal CVD-grown synthetic diamonds were extremely small (on the order of a few micrometers). Not until 1993 did Badzian and Badzian report the growth of single-crystal CVD synthetic diamond as thick as 1.2 mm; subsequently, several other groups (e.g., Doering and Linares, 1999; Linares and Doering, 1999) reported the CVD growth of undoped and boron-doped single-crystal synthetic diamond of approximately 1 mm thickness.

Figure 2. This near-colorless synthetic diamond (0.30 ct) illustrates the improvements in color and clarity seen in the later CVD-grown products offered by Apollo Diamond. Photo by Jian Xin Liao.

Early in the 2000s, however, Wang et al. (2003) reported on the gemological and spectroscopic properties of 15 CVD synthetic diamonds from Apollo Diamond; only a few were faceted. As a common feature, these samples had a limited thickness or depth (0.6–2.5 mm) and all displayed varying saturation of a brown hue. The faceted samples were small (<0.30 ct) and contained abundant cleavage cracks and pinpoint-sized black inclusions. Martineau et al. (2004) described the experimental CVD products from De Beers. More than a thousand samples (produced for research purposes only) were studied for that report, including high-purity type IIa colorless, brown, pink, and boron-doped type IIb blue synthetic diamonds. The faceted goods ranged from ~0.3 to 2.6 ct, with clarities varying from IF to I_3. Since then, significant improvements in the CVD growth technique and, consequently, crystal quality have been reported (Yan et al., 2004; Tallaire et al., 2005; Wang et al., 2005; Miyatake et al., 2007).

Wang et al. (2007) analyzed the gemological and spectroscopic properties of 43 samples of Apollo's later production (figure 2), which showed major improvements in size, color, and clarity. In addition to colorless and near-colorless material, fancy orange-to-pink hues were produced—comparable in color

Figure 3. This 0.61 ct round brilliant from Apollo Diamond is an example of the strongly colored pink synthetic diamonds now being produced by the CVD method. Photo by Jian Xin Liao.

and clarity to natural diamonds. These colors were attributed to a broad absorption band at ~520 nm, which has not yet been observed in natural diamonds and is distinctly different from the 550 nm band seen in natural pinks. More recently, Apollo Diamond introduced strongly colored pink CVD synthetic diamonds (Wang et al., 2010; figure 3), with relatively high concentrations of nitrogen-vacancy (NV) centers. These were color graded mainly as Intense to Vivid pink, and weighed ~0.3–0.7 ct.

Figure 4. Although they are also observed in some natural diamonds, high-order interference colors are considered an indicator of CVD-grown synthetic diamonds, as is the case with the sample illustrated here. Photomicrograph by Jian Xin Liao; magnified 46×.

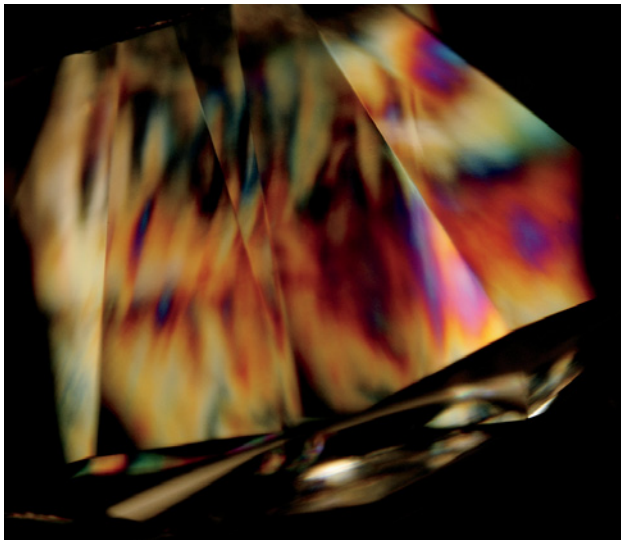

It is important to note that—though still quite rare—faceted CVD-grown diamonds are being traded in the jewelry market, with a few having been identified in gem laboratories during routine testing (e.g., Chadwick, 2008; Chadwick and Breeding, 2008; Wang, 2009; Kitawaki et al., 2010; Wang and Johnson, 2010). A near-colorless faceted CVD synthetic diamond weighing over 1 ct was identified recently by the GIA lab (Wang and Moe, 2010).

CVD synthetic diamonds can be identified through careful attention to their gemological and spectroscopic properties. While not conclusive, several gemological observations serve as good indications: strong internal graining with an indistinct "fuzzy" appearance, high-order interference colors (figure 4), and the presence of pinpoints. These gemological features do, however, appear in some natural diamonds as well.

Early products from Apollo with varying saturations of brown color displayed a weak orange fluorescence to UV radiation that was considered a useful indication of CVD synthesis (Roskin, 2003; Wang et al., 2003; Martineau et al., 2004). However, this feature is absent from most of the new products. Fluorescence and phosphorescence images obtained with the DTC DiamondView continue to be very useful for the identification of CVD synthetic diamonds. In particular, orange fluorescence with irregularly patterned areas of blue fluorescence, as well as narrow growth bands, appear to be characteristic when they are present. Spectroscopic features are very important for CVD synthetic diamond identification. The 3123.5 cm^{-1} absorption in the mid-infrared region, strong emissions from NV centers, the 596/597 nm doublet emission, and the doublet $[Si\text{-}V]^-$ emission at 736.6 and 736.9 nm are very useful (figure 5).

LifeGem Synthetic Diamonds. One synthetic diamond innovation the trade likely did not expect was announced by LifeGem (now LifeGem Created Diamonds), of Elk Grove Village, Illinois, in 2003 (Laurs and Overton, 2003). In 2004 during an Accredited Gemologists Association panel in Tucson, Arizona, Alex Grizenko of Lucent Diamonds stated that LifeGem diamonds were being processed from

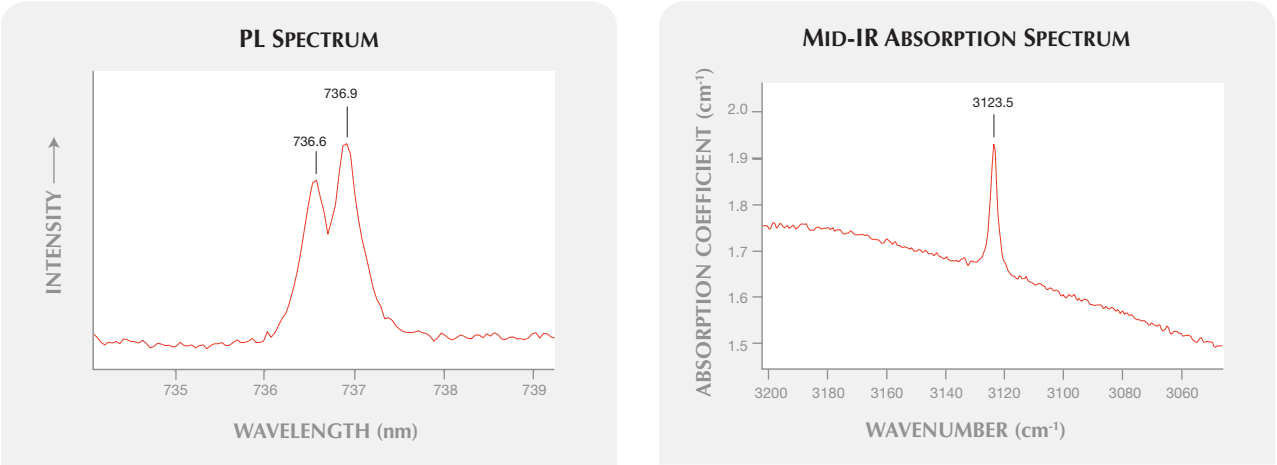

Figure 5. Absorption at 3123.5 cm^{-1} in the mid-IR region (right), strong emissions from NV centers, a 596/597 nm doublet, and another doublet at 736.6 and 736.9 nm (left) are currently very useful features in the identification of CVD-grown diamonds.

"100% cremated carbon" (Roskin, 2004). When a person decides in advance to undergo the LifeGem process, a special cremation procedure preserves enough carbon to grow the diamond. In other cases, LifeGem needs to add carbon to complete the gem, as ash from traditional cremation doesn't retain enough for the diamond growth process (Grahm, 2003). The company reported having partners in the mortuary business worldwide and produced ~1,000 diamonds annually. Dean VandenBiesen, one of the company's founders, said they used 8 oz. (227 g) of cremated remains to retrieve the carbon needed to grow one LifeGem synthetic diamond (pers. comm., 2004). From those who are not being cremated but prepared for burial, Mr. VandenBiesen indicated that ~40% of the carbon needed for a LifeGem was retrieved from a 5 g sample of the deceased's hair.

Figure 6. Possibly resulting from autoclave contamination, phantom planes consisting of dark blue crystallites of copper chloride were observed for the first time in Russian hydrothermal synthetic rubies. Photomicrograph by J. I. Koivula; magnified 20×.

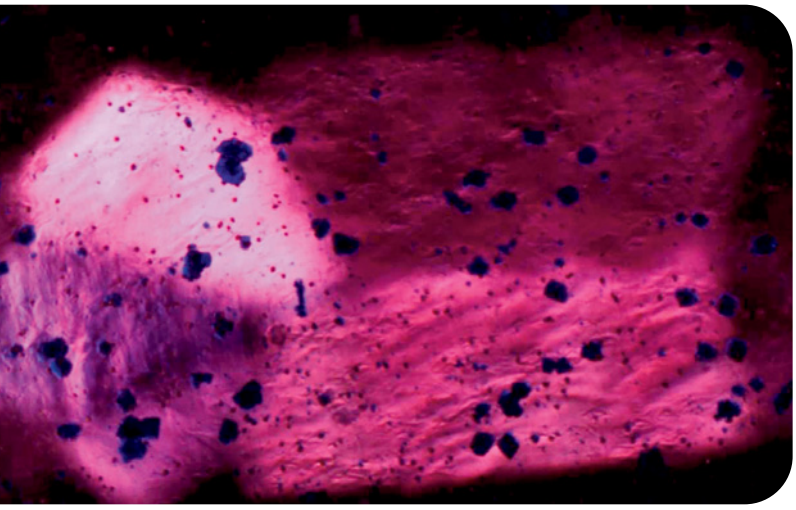

A Worried Trade. While the gem industry was well aware of the commercial advances in gem-quality synthetic diamonds, it was September 2003 when the consumer was thrust into the mix. But the news was not passed through the jewelry trade—it came from a story in the technology magazine *Wired* (Davis, 2003).

Davis's "The New Diamond Age" article was a well-researched and entertaining docudrama: "Armed with inexpensive, mass-produced gems, two startups are launching an assault on the De Beers cartel." *JCK*'s senior diamond editor Rob Bates (2003) later wrote, "*Wired* magazine sent shock waves through the industry . . . . The story on diamond synthetics covered mostly familiar territory for the industry—but its sensational tone caused some to worry."

The article described a concerned "Antwerp dealer," who was quoted as saying that "unless [CVD synthetics] can be detected, they will bankrupt the industry." Davis also noted "a De Beers executive" who had "gone pale and hands shaking" at the thought of mass-produced synthetic gem-quality diamonds. The *Wired* feature did give consumers their first glimpse of Gemesis' HPHT and Apollo's CVD gem-quality synthetic diamonds, even going so far as to mention their potential future use as a replacement for silicon in computer microprocessors. As noted above, how-

Figure 7. To produce a novelty, flame-fusion synthetic rubies and sapphires can be easily cut from areas within a boule where near-colorless portions join with the colored overgrowths. When this is done, a strongly color-zoned synthetic is the result, as shown by this 1.05 ct example. Composite photo by H. A. Hänni, © SSEF.

ever, well-equipped gemological laboratories can identify all synthetic diamonds, and the "$5 a carat" flawless lab-grown diamond remains a journalist's attention grabber—with no basis in the marketplace.

SYNTHETIC RUBY

No new types of synthetic rubies were introduced into the gem trade in the past decade. However, there were reports of interesting internal features in previously known and well-documented products. One of these inclusions consisted of phantom planes in Russian hydrothermal synthetic rubies that were randomly dusted with intense dark blue crystallites (figure 6) of transparent-to-translucent copper chloride (Gübelin and Koivula, 2005). In theory, it is possible that the precipitation of these crystals resulted from contamination, perhaps caused by a small "leak" through the inert metal lining in a copper containment vessel.

Another unusual sample was a strongly color-zoned flame-fusion synthetic ruby that had been faceted into an off-round oval mixed cut with a purplish red color zone located near the culet (figure 7). In face-up position, this synthetic appeared purplish red, even though the bulk of the material, including most of the pavilion and the entire crown, was actually very pale blue to almost colorless (Kiefert et al., 2004). It is not known if the original crystal was intentionally grown to be strongly color zoned or whether this was an accident of the growth process. In the past, flame-fusion synthetic rubies and sapphires have been grown using colorless synthetic corundum rods as "seeds." Synthetic gems could be cut from those areas where the near-colorless portions join with the colored overgrowth.

A continuing problem for gemologists is the many treated synthetics in the marketplace—and the risk they could be misidentified as treated natural stones. One such synthetic product is lead glass–filled flame-fusion synthetic ruby (see, e.g., figure 8). Jang-Green and Befi (2007) reported on a 12.84 ct sample that was apparently quench crackled to induce surface-reaching fractures, and those frac-

Figure 8. Containing numerous glass-filled surface-reaching cracks, this 3.50 ct flame-fusion synthetic ruby illustrates that synthetics can be treated, and that the presence of a treatment should not be construed as indicating natural origin. Photo by Robert Weldon.

Figure 9. With immersion microscopy, curved striae were spotted in this quench-crackled, lead glass–filled 12.84 ct flame-fusion ruby, which readily served to identify it as a synthetic. Photomicrograph by Riccardo Befi and HyeJin Jang-Green; magnified 40×.

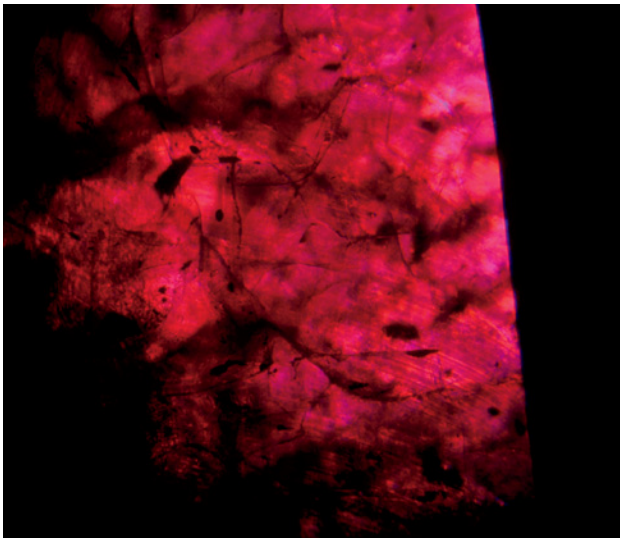

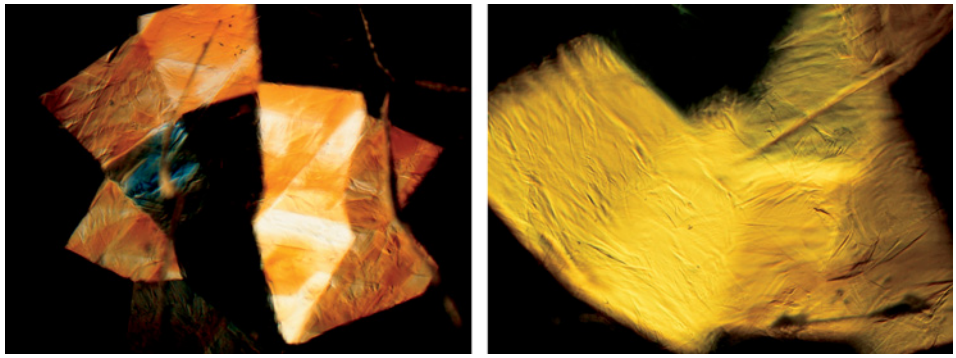

Figure 10. Distinctive roiled-to-angular growth structures, sometimes described as chevron shaped, make hydrothermally grown yellow synthetic sapphires relatively easy to identify. Photomicrographs by J. I. Koivula; magnified 15× and 40×.

tures were then filled with lead glass to reduce their visibility. When the sample was examined with immersion, curved striae readily identified it as a synthetic (figure 9). Relatively inexpensive, high-quality flame-fusion and Czochralski-pulled synthetics are available in large quantities, so it is not too surprising that they would be subjected to treatments of all types, including glass infilling. Therefore, it is important to identify not only the presence of a treatment, but also the natural or synthetic origin of the starting material to which that treatment has been applied.

SYNTHETIC SAPPHIRE

Hydrothermal synthetic sapphires grown in Russia continued to be available, in colors other than the normally expected blue. The Gem Testing Laboratory in Jaipur, India, examined ~20 faceted synthetic yellow sapphires that proved to be grown by the hydrothermal method (Choudhary, 2005). They ranged from 3.50 to 5.30 ct and had characteristic inclusions such as scattered flake-like "breadcrumbs" and distinctive roiled-to-angular growth structures (figure 10) sometimes described as chevron-shaped.

As with synthetic rubies, unusual internal features were also observed in synthetic sapphires during this decade. Koivula et al. (2008) reported on bluish green flame-fusion synthetic sapphires (e.g., figure 11) that contained numerous vibrant blue solid inclusions, as well as the more expected rounded and distorted gas bubbles (figure 12). Because of their color, the inclusions were suspected to contain cobalt. Indeed, a very weak visible-light absorption spectrum attributed to cobalt was detected with a standard gemological spectroscope. Raman analysis could not conclusively identify these isotropic inclusions, but it suggested that they were related to spinel.

SYNTHETIC EMERALD AND OTHER BERYLS

Available in the gem trade since 2004, the Malossi product (reportedly grown in the Czech Republic using Italian technology) was the only new develop-

Figure 11. This 0.91 ct bluish green flame-fusion synthetic sapphire displayed a bodycolor and inclusions the GIA Laboratory had never encountered before. Photo by Robert Weldon.

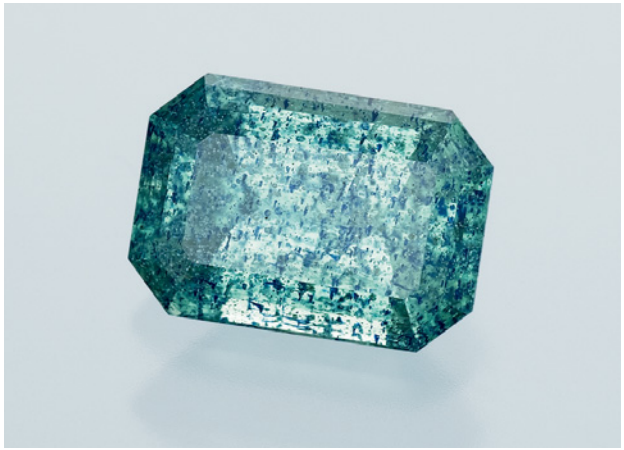

Figure 12. Associated with the gas bubbles more typical of flame-fusion material, these cobalt-colored blue inclusions in the synthetic sapphire in figure 11 could not be conclusively identified. Photomicrograph by J. I. Koivula; magnified 25×.

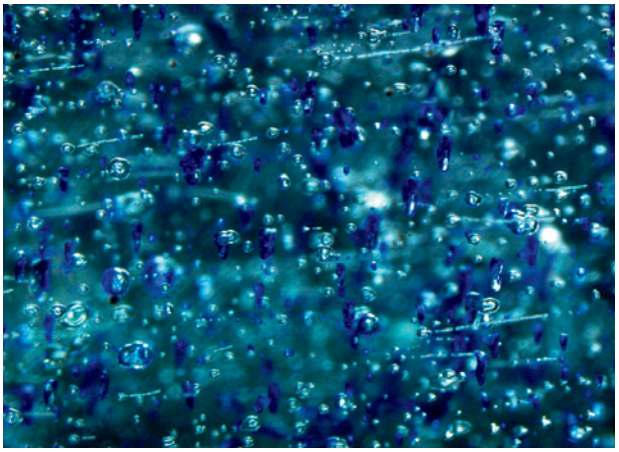

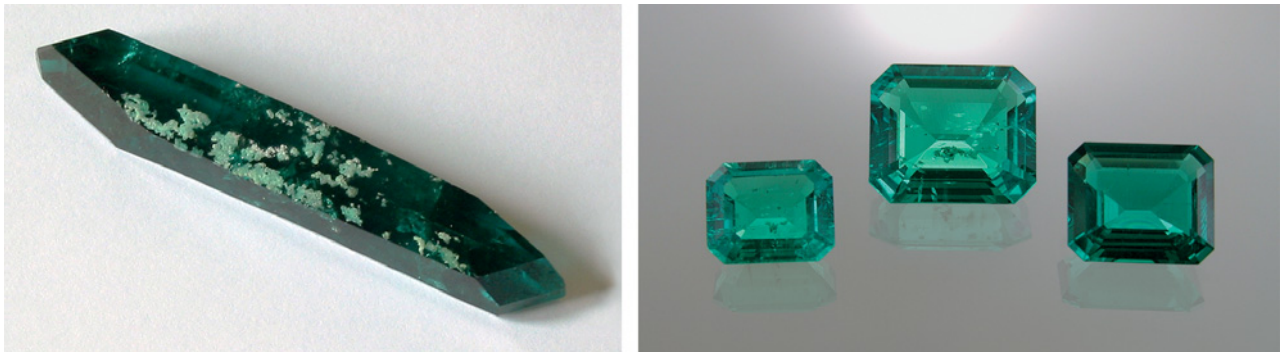

Figure 13. Malossi hydrothermal synthetic emeralds have been available in the trade since 2004. The rough specimen on the left (~6 cm long) is partially encrusted with white synthetic phenakite crystallites. Photos by Ilaria Adamo.

ment in the area of synthetic emeralds in the 2000s (see figure 13 and Adamo et al., 2005). This is believed to be a new type of synthetic emerald colored only by Cr^{3+}. The highly diagnostic growth structures normally encountered in hydrothermally grown material were all but absent from the samples examined. Nevertheless, the reported growth method is similar to that described for other hydrothermal synthetic emeralds: that is, use of a natural beryl seed plate in an autoclave. The producer indicated that hydrochloric acid is used to prevent Cr from precipitating out of the solution so it can instead be incorporated into the crystals (Adamo et al., 2005); features in the mid-IR spectrum are consistent with this statement.

Separation of the Malossi product from natural emerald is relatively straightforward. Irregular growth features, a seed plate, and synthetic phenakite-like crystals (figure 14) all readily indicate synthetic origin. Chemically, the presence of Cl concentrations greater than 0.2 wt.% and the absence of additional trace elements can provide supporting evidence for the Malossi product, but these criteria should not be relied on independently. Mid-IR spectroscopy can also be used to aid in the separation, as there are several bands related to Cl in the 3100–2500 cm^{-1} range.

Although Russian hydrothermal synthetic emeralds are not new to the 2000s, an excellent review article discussing their microscopic properties was published by Schmetzer et al. (2007).

Hydrothermally grown synthetic aquamarines, some violetish blue, were also reported in the 2000s as having been grown by Malossi in the Czech Republic (Adamo et al., 2008; see, e.g., figure 15). Just as with previously described synthetic aquamarine (Koivula and Kammerling, 1988) from Novosibirsk, Russia, that was marketed through the Tairus joint venture (Thailand-Russia), these new Malossi manufactured aquamarines also displayed characteristic

Figure 14. A cluster of small inclusions, probably synthetic phenakite, were observed in this Malossi hydrothermal synthetic emerald. Photomicrograph by Renata Marcon; magnified 50×.

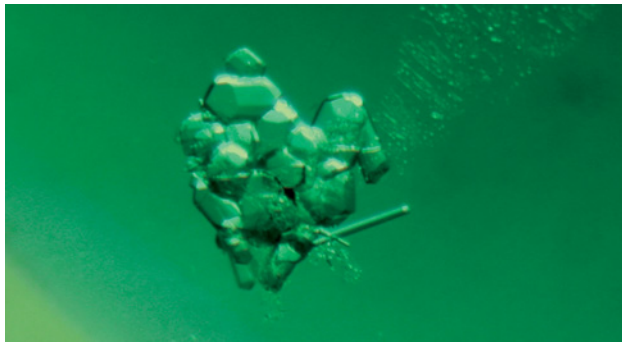

Figure 15. During the first decade of the 2000s, in addition to synthetic emeralds Malossi also produced hydrothermally grown synthetic aquamarines, such as the rough (14–16 g) and faceted (2.0–5.0 ct) material shown here. Photo by Alberto Malossi.

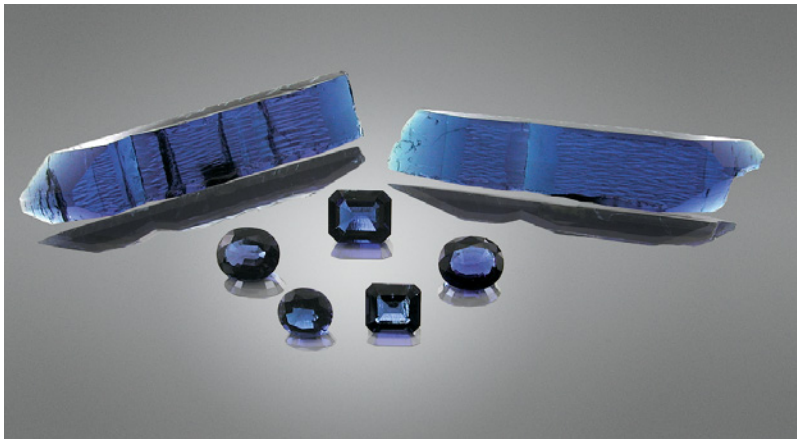

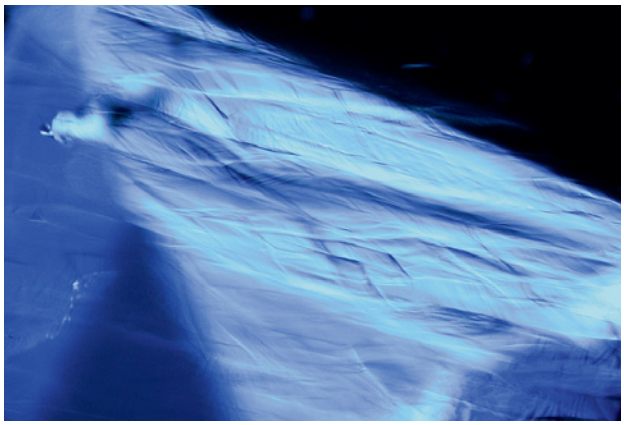

Figure 16. Like those previously produced in Russia, the Czech-Italian Malossi-manufactured blue beryls display characteristic roiled-to-angular structures or patterns of subgrain boundaries and intergrowths. Photomicrograph by Ilaria Adamo; magnified 25×.

roiled-to-angular growth structures or patterns of subgrain boundaries or intergrowths (figure 16).

Although hydrothermally grown synthetic red beryl was produced in earlier decades, the detailed descriptions by Shigley et al. (2001) and Fumagalli et al. (2003) are particularly useful in separating it from natural red beryl. Manufactured by the Institute of Crystallography and an affiliated company, Emcom Ltd., both located in Moscow, this material is produced under conditions similar to those used to grow other varieties of synthetic beryl. To give the red, pinkish red, and orange-red colors (figure 17), Co and Mn are introduced into the nutrient solution. RI and SG measurements were within published ranges for natural red beryl. Magnification revealed chevron-shaped growth zoning, typical of hydrothermal synthetic beryl products. Several absorption bands were seen between 530 and 590 nm; these are due to Co^{2+} and are not observed in natural red beryl. Chemical analysis showed that Co and Ni were the two most diagnostic trace elements, as these elements are not seen in natural red beryl. Another diagnostic feature is an absorption band in the infrared between 4200 and 3200 cm^{-1}. This band is related to water and is absent from natural red beryl, which formed in a pneumatolytic high-temperature igneous (rhyolitic) environment that contained very little water.

Figure 17. Manufactured in Moscow, these hydrothermally grown orange-red and pinkish red synthetic beryls derive their color from cobalt (left and center, 1.08 and 1.95 g) and manganese (right, 6.32 g) introduced into the nutrient solution. Photo by Robert Weldon.

SYNTHETIC JADEITE

The production of intense green, highly translucent synthetic "Imperial" jadeite was perhaps one of the most interesting and exciting developments in the first decade of the 2000s. While the synthesis of jadeite had been attempted by General Electric for more than 20 years (Nassau and Shigley, 1987), it was not until this decade that a truly successful product was achieved (Moses, 2002). As shown in figure 18, the quality of this synthetic rivals that of the finest natural green jadeite. Most of the material is very slightly mottled in white and intense green, with the overall effect being a rich green color. Only one cabochon examined contained an inclusion—an irregular black patch that could not be identified (figure 19). The small number of samples seen had gemological properties that overlapped those of natural jadeite of similar color and translucency. Fortunately, there are obvious differences in the IR region (Cao et al., 2008). Since FTIR analysis is a standard technique used to check jadeite for polymer impregnation, it is doubtful that any of these syn-

Figure 18. During the past decade, General Electric grew extremely high-quality synthetic jadeite, as illustrated by these two cabochons (5.20 and 6.73 ct). Photo by Robert Weldon.

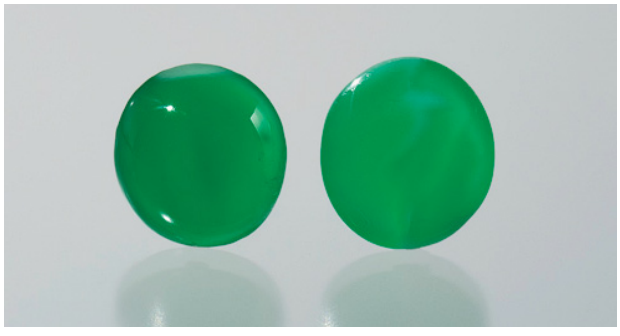

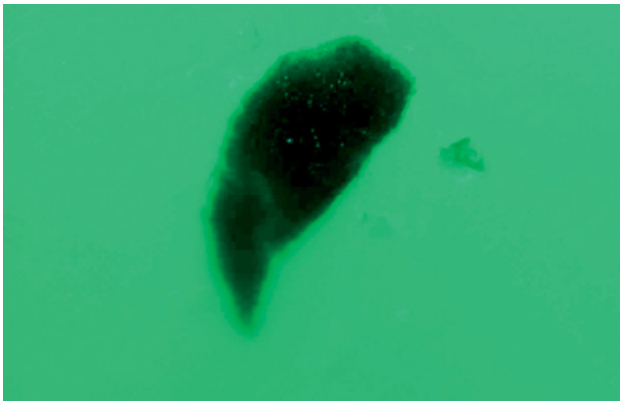

Figure 19. The only inclusion observed in the two cabochons of GE synthetic jadeite was this unidentifiable irregular dark spot. Photomicrograph by J. I. Koivula; magnified 20×.

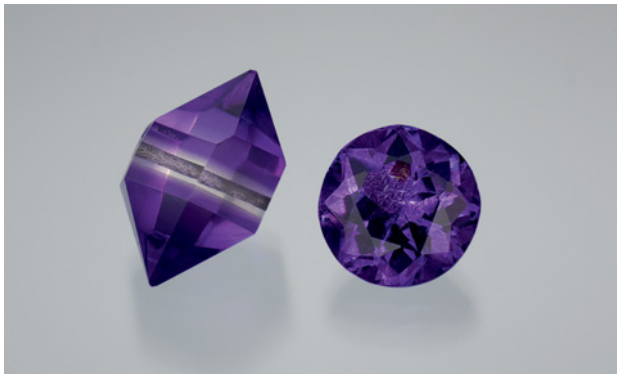

Figure 20. While synthetic amethyst, such as this 3.90 g crystal and 10.10 ct round brilliant, was not new in the last decade, advances were made in the use of FTIR spectroscopy to identify it. Photo by Robert Weldon.

thetic jadeite cabochons will be undetected in the laboratory if or when this synthetic is commercially manufactured and distributed (which, to the best of our knowledge, is not yet the case).

SYNTHETIC QUARTZ

Hydrothermal growth of synthetic quartz on prepared seed crystals was a significant synthesis technique throughout the 1990s. While synthetic amethyst (figure 20) is not a new development, a detailed study by Balitsky et al. (2004) compared the infrared absorption spectra of numerous synthetic amethyst samples grown from K_2CO_3 and NH_4F solutions, along with a limited number of Chinese and Japanese hydrothermal synthetics.

Absorption bands at ~3595 and 3543 cm^{-1} have diagnostic value in separating natural and synthetic amethyst (see also Karampelas et al., 2005). While the 3595 cm^{-1} band has not been observed in synthetic amethyst, it is occasionally also absent from natural material, which limits its diagnostic effectiveness. When the 3543 cm^{-1} band is found in amethyst grown in a near-neutral NH_4F solution (indicated by additional bands at 3680, 3664, and 3630 cm^{-1}), synthetic origin is certain. The 3543 cm^{-1} band, however, is commonly seen in more commercially significant synthetic amethyst grown in alkaline K_2CO_3 solutions, and it has occasionally been observed in natural amethyst from a few localities. For the most part, then, these features are not independently conclusive of natural or synthetic origin in amethyst, but they provide supporting evidence for origin determination (Balitsky and Balitskaya, 2009). A combination of microscopic observations, such as growth features and inclusions, should be used in conjunction with these IR features.

SYNTHETIC ALEXANDRITE

Synthetic alexandrite of high clarity is commonly grown by the Czochralski process, which was not new to the 2000s. Such material generally does not cause any real concern among gemologists, since we are immediately suspicious of any nearly flawless colored stone. Melt-grown synthetic alexandrites can be readily separated from natural stones by FTIR analysis (Stockton and Kane, 1988).

As with any gem material, however, unusual examples may occasionally appear. Some synthetic alexandrites contain odd-shaped "gas bubbles" (figure 21) that, on first observation, can appear very similar to the negative crystals seen in natural alexandrite (Mayerson and Kondo, 2005). While faceted synthetic alexandrites are often virtually flawless, cabochons usually contain at least a few easily observed gas bubbles that are useful in identification. However, if a few high-relief "negative crystals" are the only inclusions present, care should be exercised to make sure they are not the distorted gas bubbles found in a Czochralski-pulled synthetic.

SYNTHETIC OPAL

A nonphenomenal synthetic fire opal called Mexifire (figure 22) was one of the few new synthetic colored stones produced and marketed in the 2000s (Choudhary and Bhandari, 2008; Bhandari and Choudhary, 2010; Henn et al., 2010). While synthetic opal has been commercially produced since 1975, most of this material shows play-of-color. Mexifire does not, and its structure is reportedly similar to that of natural opal (i.e., composed of silica spheres); it also owes its orange color to traces of iron. One notable advantage to the synthetic material is that it does not appear to craze, as its natural counterpart often does.

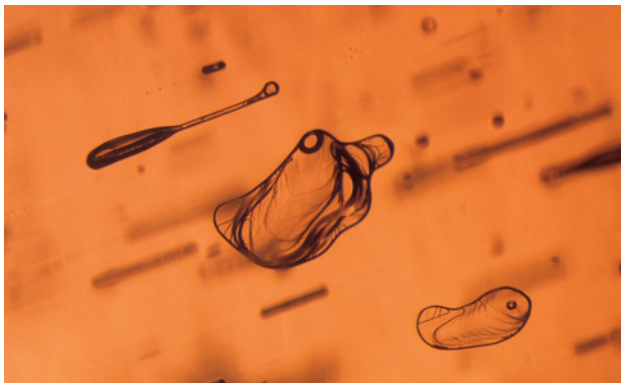

Figure 21. The distorted gas bubbles that sometimes occur in Czochralski melt-grown synthetic alexandrites can have the appearance of high-relief negative crystals. Such inclusions may be quite deceptive. Photomicrograph by J. I. Koivula; magnified 25×.

Gemological properties of the initial Mexifire product showed RI readings that were slightly lower (1.380–1.405) than those reported for natural fire opal (1.420–1.430). The SG (1.63–1.77) was also lower than what would be expected for natural fire opal (~2.00). The Mexifire product has a zonal turbid structure, and minute pinpoints are scattered throughout the material (figure 22, right). Unlike synthetic opals from other manufacturers, the Mexifire synthetic opals do not show a characteristic "chicken wire" or columnar structure. Energy-dispersive X-ray fluorescence (EDXRF) spectroscopy showed traces of Fe and Ca in the Mexifire product, which is consistent with natural fire opal. While Zr has been used to impregnate and stabilize opal in the past, it was not detected in this material. IR spectroscopy showed an absorption hump at 4600–4300 cm^{-1} that is sometimes absent from natural opal. While this feature cannot provide proof of natural or synthetic origin, the absence of this feature may suggest natural material.

Since late 2009, the process has been modified such that the new Mexifire product has gemological properties much more like those of natural fire opal. While the microscopic properties of the two generations of material are similar, the new Mexifire synthetic opal has a consistent RI reading of 1.47 and an SG of 2.19. Although these measurements are not exactly the same as natural material, they are close enough to cause concern, and careful testing is required if an opal is suspect. Fortunately, the new Mexifire material shows a characteristic infrared spectrum that allows conclusive separation from natural opal. Features observed in the new generation of Mexifire opal are a weak hump at ~5440 cm^{-1}, a sharp peak with a shoulder ~4520 cm^{-1}, an absorption band in the 4000–3250 cm^{-1} region, a weak shoulder at 2652 cm^{-1}, and complete absorption of wavelengths below 2400 cm^{-1} (Bhandari and Choudhary, 2010).

While Mexifire synthetic opal is very similar to natural opal in many respects, careful RI and SG measurements should give a strong indicator of its synthetic origin. When identifying gem materials in this property range, it should be noted that manufactured glass is also a possibility.

UNUSUAL SYNTHETICS

Experimentation and failed laser development sometimes result in unusual synthetic gem materials. Such was the case with two materials reported in the 2000s.

A synthetic apatite (figure 23) with a color change from purple pink in incandescent light to violetish blue in fluorescent light was reported by McClure (2001). While most of the gemological properties were consistent with natural apatite, suspicion arose from an unusual spectrum (seen with a desk-model spectroscope) that was different from natural material. EDXRF analysis showed that the synthetic

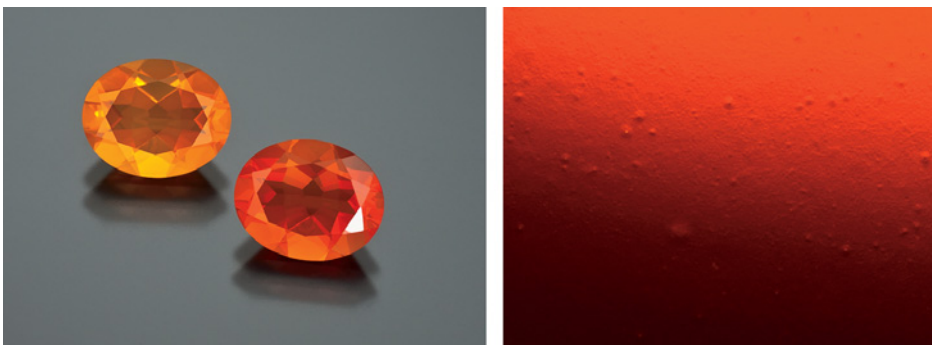

Figure 22. At 1.47 and 1.56 ct (left), these two Mexifire synthetic opals show the color range and transparency of this nonphenomenal material. These synthetics commonly have a turbid appearance and minute pinpoints (right). Left photo by Robert Weldon; right photomicrograph by J. I. Koivula, magnified 60×.

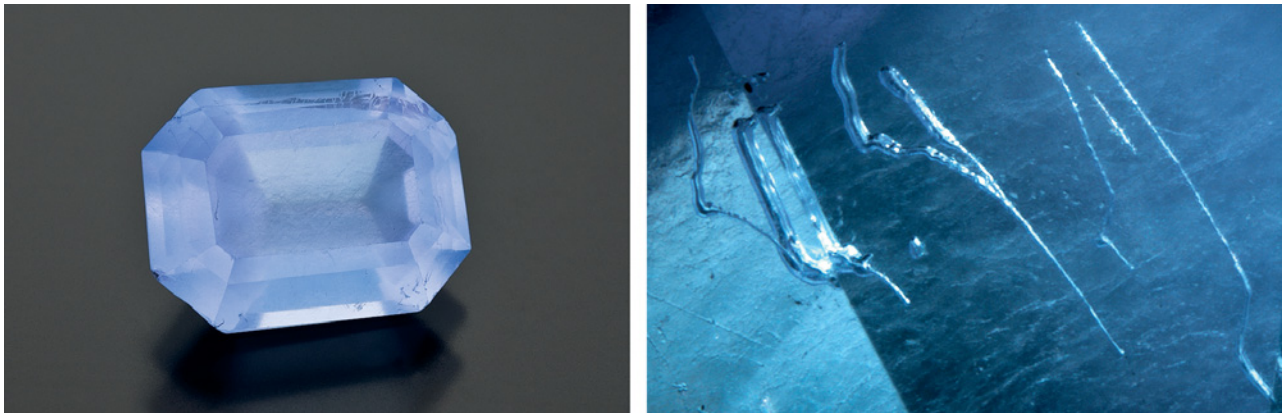

Figure 23. Significant amounts of neodymium and strontium were detected in this unusual 3.03 ct color-change synthetic apatite. Magnification (right) revealed features that indicated synthetic origin, such as these elongated gas bubbles. Left photo by Robert Weldon; right photomicrograph by J. I. Koivula, magnified 30×.

apatite contained a significant amount of neodymium and a small amount of strontium. Magnification revealed chevron-type growth and elongated gas bubbles, features that strongly supported a synthetic origin (figure 23, right). While synthetic apatite is an oddity in the gem world, it has previously been reported for laser applications (Koivula et al., 1992).

Another oddity reported in the early 2000s was the growth of synthetic topaz crystals up to 20 g (100 ct) in size (Lu and Balitsky, 2001). This may strike the reader as particularly unusual given the abundance of natural topaz in large sizes. The stated reason for growing this synthetic was to better understand crystal formation, morphology, and causes of color in natural pegmatitic topaz. This material was hydrothermally grown using crushed natural quartz and topaz dissolved in an aqueous fluoride-bearing fluid. Light gray to colorless crystals were produced as overgrowths on a natural topaz seed plate suspended in the nutrient solution. Experiments were then conducted to modify the color of the as-grown crystals. As is also the case with treated-color natural topaz, reddish brown was produced by ionizing irradiation (Balitsky et al., 2004) and blue was produced by high-energy electron irradiation with subsequent heat treatment (Lu and Balitsky, 2001). The gemological properties and Raman and FTIR spectra were within the ranges for natural material. Chemical analysis by EDXRF showed traces of germanium, nickel, and iron.

CONCLUSION: PREDICTIONS FOR THE NEXT DECADE

It is safe to predict that technology will continue to advance, and with that will come improvements in existing synthesis techniques and products. As with synthetic apatite and topaz, there will always be unusual materials produced with what appear—now—to have limited commercial potential. Such synthetics will surely arise from time to time and present their own unique gemological challenges. We believe, however, that the greatest advances in synthesis will continue to be focused on the most commercially important gems: diamond, emerald, ruby, and sapphire.

Currently, the vast majority of gem-quality synthetic diamonds are melee-size HPHT-grown material (Quinn, 2005; Kitawaki et al., 2008), which require care to identify. Eventually, the trade will have to decide at what point it is no longer economic to identify such small synthetic diamonds, especially if swift, accurate, and inexpensive testing methods are not developed.

Will the jewelry industry be ready for these developments? When you consider that many synthetic growth processes are more than a century old and still plague the trade, our preparedness must be questioned. If tradespeople continue to submit flame-fusion synthetic rubies, sapphires, and spinels to gem laboratories for identification, then one must ask: How are they handling the thousands of carats of more technologically advanced flux-grown, hydrothermal, and Czochralski-pulled synthetics? We believe the answer will be found through gemological education. Over the next decade, every jeweler's goal should be to gain gemological expertise on a par with their "computer age" business skills. It is vital to have a sound working knowledge of the identifying characteristics for all synthetics, past and present. Such knowledge will also help the gemologist prepare for future developments.

Figure 24. Purchased over the internet, these were advertised as heat-treated natural sapphires, but all turned out to be flame-fusion synthetics (4.5–7.0 ct). Photo by G. Roskin.

New treatment processes were by far the big news of the past decade. Because of that, today's experts too often expect sapphires to be beryllium treated, or diamonds to be HPHT treated. In Las Vegas in June 2010, a 1977 GIA classmate of one of the authors (GR) handed him a parcel of seven stones purchased over the Internet as heated natural sapphires (figure 24). Since they were advertised as heated, he assumed when he purchased them that the worst case scenario would be that they turned out to be beryllium diffused. After examination, worse news was evident: They all were flame-fusion synthetic sapphires, with not a heat-treated natural stone in the group.

ABOUT THE AUTHORS

Mr. Renfro (nathan.renfro@gia.edu) is staff gemologist, and Mr. Koivula is chief gemologist, at the GIA Laboratory in Carlsbad, California. Dr. Wang is director of research at the GIA Laboratory in New York. Mr. Roskin is based in Downingtown, Pennsylvania, and is editor of the online magazine Roskin Gem News Report.

ACKNOWLEDGMENTS

The authors are indebted to Dr. Ilaria Adamo, of the Università degli Studi di Milano, and Robert Weldon, of GIA Carlsbad, for help in preparing certain sections and for performing archival research for this article.

REFERENCES

Adamo I., Pavese A., Prosperi L., Diella V., Merlini M., Gemmi M., Ajò D. (2005) Characterization of the new Malossi hydrothermal synthetic emerald. *G&G*, Vol. 41, No. 4, pp. 328–338.

Adamo I., Pavese A., Prosperi L., Diella V., Ajò D., Gatta G.D., Smith C.P. (2008) Aquamarine, Maxixe-type beryl, and hydrothermal synthetic blue beryl: Analysis and identification. *G&G*, Vol. 44, No. 3, pp. 214–226.

Angus J.C. (1994) Development of low-pressure diamond growth in the United States. In K.E. Spear and J.P. Dismukes, Eds., *Synthetic Diamond: Emerging CVD Science and Technology*, John Wiley & Sons, New York, pp. 21–39.

Badzian A., Badzian T. (1993) Diamond homoepitaxy by chemical vapor deposition. *Diamond and Related Materials*, Vol. 2, No. 2/4, pp. 147–157.

Balitsky V.S., Balitskaya O.V. (2009) The genetic approach for identification of varieties of crystalline and amorphous silica. *Australian Gemmologist*, Vol. 23, No. 11, pp. 500–508.

Balitsky V.S., Balitsky D.V., Bondarenko G.V., Balitskaya O.V. (2004) The 3543 cm^{-1} infrared absorption band in natural and synthetic amethyst and its value in identification. *G&G*, Vol. 40, No. 2, pp. 146–161.

Balitsky V.S., Balitsky D.V., Balitsky S.D., Aurisicchio C., Roma M.A. (2006) Silica and alumina transfer in supercritical aqueous fluids and growing of topaz monocrystals in them. *Geochemistry International*, Vol. 44, No 2, pp. 175–181.

Bates R. (2003) *Wired* cover spotlights synthetics. *JCK*, Vol. 174, No. 11, p. 46.

Bhandari R., Choudhary G. (2010) Update on Mexifire synthetic fire opal. *G&G*, Vol. 46, No. 4, pp. 287–290.

Bundy F.P., Hall H.T., Strong H.M., Wentorf R.H. (1955) Man-made diamonds. *Nature*, Vol. 176, p. 51.

Butler J.E., Woodin R.L. (1993) Thin film diamond growth mechanisms. *Philosophical Transactions of the Royal Society of London A*, Vol. 342, pp. 209–224.

Butler J.E., Mankelevich Y.A., Cheesman A., Ma J., Ashfold M.N.R. (2009) Understanding the chemical vapor deposition of diamond: Recent progress. *Journal of Physics: Condensed Matter*, Vol. 21, Art. 364201 (20 pp.).

Cao S.-M., Qi L.-J.,Guo Q.-H., Zhong Z.-Q., Qiu Z.-L., Li Z.-G. (2008) Study on the vibrational spectra characterization of synthetic jadeite jade made by General Electric Company. *Spectroscopy and Spectral Analysis*, Vol. 28, No. 4, pp. 847–851.

Chadwick K. (2008) Lab Notes: HPHT-treated CVD synthetic diamond submitted for Dossier grading. *G&G*, Vol. 44, No. 4, pp. 365–367.

Chadwick K.M., Breeding C.M. (2008) Lab Notes: First CVD synthetic diamond submitted for Dossier grading. *G&G*, Vol. 44, No. 1, pp. 67–69.

Choudhary G. (2005) Gem News International: Yellow hydrothermal synthetic sapphires seen in India. *G&G*, Vol. 41, No. 2, p. 182.

——— (2008) Gem News International: Purplish blue synthetic quartz. *G&G*, Vol. 44, No. 4, pp. 377–379.

Choudhary G., Bhandari R. (2008) A new type of synthetic fire opal: Mexifire. *G&G*, Vol. 44, No. 3, pp. 228–233.

Davis J. (2003) The new diamond age. *Wired*, Vol. 11, No. 9, pp. 96–146.
Davis R.F. (1993) *Diamond Films and Coatings: Development, Properties, and Applications*. Noyes Publications, Park Ridge, NJ, 421 pp.
Doering P.J., Linares R.C. (1999) Large area single crystal CVD diamond: Properties and applications. *Proceedings of Applied Diamond Conference/Frontier Carbon Technology Joint Conference 1999*, Tsukuba, Japan, pp. 32–35.
Fumagalli M., Prosperi L., Pavese A., Bordiga S. (2003) Natural versus hydrothermal synthetic Russian red beryl: Chemical composition and spectroscopic measurements. *Journal of Gemmology*, Vol. 28, No. 5, pp. 291–301.
Grahm D.D. (2003) A company called LifeGem gives memorials for the dead a high-tech twist. *Colored Stone*, Sept./Oct., pp. 50, 52–53.
Gübelin E.J., Koivula J.I. (1986) *Photoatlas of Inclusions in Gemstones*. ABC Edition, Zurich, Switzerland.
——— (2005) *Photoatlas of Inclusions in Gemstones*, Vol. 2. Opinio Publishers, Basel, Switzerland.
——— (2008) *Photoatlas of Inclusions in Gemstones*, Vol. 3. Opinio Publishers, Basel, Switzerland.
Henn U., Wehr K., and Milisenda C.C. (2010) Synthetischer Feueropal—"Mexifire." *Gemmologie: Zeitschrift der Deutschen Gemmologischen Gesellschaft*, Vol. 59, No. 1/2, pp. 47–50.
Jang-Green H., Befi R. (2007) Lab Notes: Glass-filled synthetic ruby. *G&G*, Vol. 43, No. 3, pp. 250–251.
Kane R.E. (2009) Seeking low-cost perfection: Synthetic gems. *Elements*, Vol. 5, No. 3, pp. 169–174.
Karampelas S., Fritsch E., Zorba T., Paraskevopoulos K.M., Sklavounos S. (2005) Distinguishing natural from synthetic amethyst: The presence and shape of the 3595 cm^{-1} peak. *Mineralogy and Petrology*, Vol. 85, No. 1/2, pp. 45–52.
Kiefert L., Hänni H.A., Schmetzer K. (2004) Gem News International: Synthetic Verneuil corundum with unusual color zoning. *G&G*, Vol. 40, No. 4, pp. 354–355.
Kiffer A.D. (1956) Synthesis of diamond from carbon monoxide. Tonawanda Laboratories, Linde Air Products, June 6.
Kitawaki H., Abduriyim A., Okano M. (2008) Identification of melee-sized synthetic yellow diamonds in jewelry. *G&G*, Vol. 44, No. 3, pp. 202–213.
Kitawaki H., Abduriyim A., Kawano J., Okano M. (2010) Gem News International: Treated CVD-grown pink synthetic diamond melee. *G&G*, Vol. 46, No. 1, pp. 68–69.
Koivula J.I., Kammerling R.C. (1988) Gem News: Unusual synthetic beryls from the Soviet Union. *G&G*, Vol. 24, No. 4, p. 252.
Koivula J.I., Kammerling R.C., Fritsch E. (1992) Gem News: Update on crystal growth. *G&G*, Vol. 28, No. 4, p. 277.
——— (1993) Gem News: Color-zoned synthetic blue quartz. *G&G*, Vol. 29, No. 2, pp. 140–141.
Koivula J.I., Tannous M., Schmetzer K. (2000) Synthetic gem materials and simulants in the 1990s. *G&G*, Vol. 36, No. 4, pp. 360–379.
Koivula J.I., Inns A., Shen A.H.-T. (2008) Lab Notes: Green synthetic sapphire with vibrant blue inclusions. *G&G*, Vol. 44, No. 1, pp. 72–73.
Laurs B.M., Overton T.W. (2003) Gem News International: LifeGem synthetic diamonds. *G&G*, Vol. 39, No. 1, p. 62.
Linares R.C., Doering P.J. (1999) Properties of large single crystal diamond. *Diamond and Related Materials*, Vol. 8, No. 2/5, pp. 909–915.
Lu T., Balitsky V.S. (2001) Gem News International: Synthetic topaz crystals. *G&G*, Vol. 37, No. 4, pp. 339–341.
Martineau P.M., Lawson S.C., Taylor A.J., Quinn S.J., Evans D.J.F., Crowder M.J. (2004) Identification of synthetic diamonds grown using chemical vapor deposition (CVD). *G&G*, Vol. 40, No. 1, pp. 2–25.
Mayerson W.M., Kondo D. (2005) Lab Notes: Unusual synthetic alexandrite. *G&G*, Vol. 41, No. 3, pp. 256–257.
McClure S.F. (2001) Lab Notes: Synthetic apatite. *G&G*, Vol. 37, No. 1, p. 57.
Miyatake H., Arima K., Maida O., Teraji T., Ito Y. (2007) Further improvement in high crystalline quality of homoepitaxial CVD diamond. *Diamond and Related Materials*, Vol. 16, No. 4/7, pp. 679–684.
Moses T. (2002) Lab Notes: High-quality synthetic jadeite from General Electric. *G&G*, Vol. 38, No. 2, pp. 166–167.
Nassau K. (1990) Synthetic gem materials in the 1980s. *G&G*, Vol. 26, No. 1, pp. 50–63.
Nassau K., Shigley J.E. (1987) A study of the General Electric synthetic jadeite. *G&G*, Vol. 23, No. 1, pp. 27–35.
Quinn E.P. (2005) Lab Notes: Small synthetic diamonds. *G&G*, Vol. 41, No. 4, pp. 345–346.
Roskin G. (2003) Identifying CVD synthetic diamond. *JCK*, Vol. 174, No. 11, pp. 46–49.
——— (2004) Tucson 2004: A gemstone cornucopia. *JCK*, Vol. 175, No. 4, pp. 102–108.
Schmetzer K., Bernhardt H.-J., Schwarz D. (2007) Vanadium- and copper-bearing Tairus hydrothermally-grown synthetic emerald: An update on microscopic properties. *Journal of the Gemmological Association of Hong Kong*, Vol. 28, pp. 71–75.
Shigley J.E., McClure S.F., Cole J.E., Koivula J.I., Lu T., Elen S., Demianets L.N. (2001) Hydrothermal synthetic red beryl from the Institute of Crystallography, Moscow. *G&G*, Vol. 37, No. 1, pp. 42–55.
Shigley J.E., Abbaschian R., Clarke C. (2002) Gemesis laboratory-created diamonds. *G&G*, Vol. 38, No. 4, pp. 301–309.
Shigley J.E., McClure S.F., Breeding C.M., Shen A.H.-T., Muhlmeister S.M. (2004) Lab-grown colored diamonds from Chatham Created Gems. *G&G*, Vol. 40, No. 2, pp. 128–145.
Stockton C.M., Kane R.E. (1988) The distinction of natural from synthetic alexandrite by infrared spectroscopy. *G&G*, Vol. 24, No. 1, pp. 44–46.
Spear K.E., Dismukes J.P. (1994) *Synthetic Diamond: Emerging CVD Science and Technology*. John Wiley & Sons, New York, 663 pp.
Tallaire A., Achard J., Sussmann R.S., Silva F., Gicquel A. (2005) Homoepitaxial deposition of high-quality thick diamond films: Effect of growth parameters. *Diamond and Related Materials*, Vol. 14, No. 3/7, pp. 249–254.
Wang W. (2009) Lab Notes: Diamond—Fancy red, irradiated and annealed. *G&G*, Vol. 45, No. 3, p. 208.
Wang W., Johnson P. (2010) Lab Notes: Red CVD synthetic diamond with multiple treatments. *G&G*, Vol. 46, No. 1, pp. 52–54.
Wang W., Moe K.S. (2010) Lab Notes: CVD synthetic diamond over one carat. *G&G*, Vol. 46, No. 2, pp. 143–144.
Wang W., Moses T.M. (2010) Lab Notes: Large yellow-orange HPHT synthetic diamond. *G&G*, Vol. 46, No. 4, pp. 299–300.
Wang W., Moses T., Linares R.C., Shigley J.E., Hall M., Butler J.E. (2003) Gem-quality synthetic diamonds grown by a chemical vapor deposition (CVD) method. *G&G*, Vol. 39, No. 4, pp. 268–283.
Wang W., Tallaire A., Hall M.S., Moses T.M., Achard J., Sussmann R.S., Gicquel A. (2005) Experimental CVD synthetic diamonds from LIMHP-CNRS, France. *G&G*, Vol. 41, No. 3, pp. 234–244.
Wang W., Hall M.S., Moe K.S., Tower J., Moses T.M. (2007) Latest-generation CVD-grown synthetic diamonds from Apollo Diamond Inc. *G&G*, Vol. 43, No. 4, pp. 294–312.
Wang W., Doering P., Tower J., Lu R., Eaton-Magaña S., Johnson P., Emerson E., Moses T.M. (2010) Strongly colored pink CVD lab-grown diamonds. *G&G*, Vol. 46, No. 1, pp. 4–17.
Yan C.-S., Mao H.-K., Li W., Qian J., Zhao Y.S., Hemley R.J. (2004) Ultrahard diamond single crystals from chemical vapor deposition. *Physica Status Solidi (a)*, Vol. 201, No. 4, pp. R25–R27.

YELLOW SCAPOLITE FROM IHOSY, MADAGASCAR

Margherita Superchi, Federico Pezzotta, Elena Gambini, and Emanuela Castaman

Attractive yellow to light greenish yellow gem scapolites have been mined from a skarn deposit near the town of Ihosy, in southern Madagascar, since the late 1990s. Chemical analysis indicates that the scapolites have a mostly meionite content, with lesser amounts of marialite and a small percentage of silvialite. These results are agreeable with the RI measurements and IR spectra. Inclusions were identified as diopside, garnet (andradite-grossular), and mica (probably phlogopite), consistent with the minerals accompanying scapolite in Ihosy skarns. The samples' UV fluorescence appears to be distinctive from that of commercially available scapolites from other localities.

Scapolite is a silicate mineral that occurs in crystals often characterized by good transparency, significant size, and a wide variety of colors: greenish yellow, yellow, pink, purple, dark pinkish purple, and violet. Colorless crystals also exist. Despite its relatively low hardness (Mohs 6), it has interest as a collector's gem. The most important localities for gem-quality scapolite are Afghanistan (Badakhshan), China (Xinjiang-Uygur Autonomous Region), Myanmar (Mogok), Pakistan, Sri Lanka, Tajikistan, Kenya, Madagascar, Mozambique, Tanzania, and Brazil.

The scapolite group consists of two main end members: marialite ($Na_4[Al_3Si_9O_{24}]Cl$) and meionite ($Ca_4[Al_6Si_6O_{24}]CO_3$). Intermediate compositions in the solid-solution series are named after the closest end member (Deer et al., 1992). Meionite (Me) possesses higher RI and SG values than marialite. The meionite end member has refractive indices of n_o = 1.600 and n_e = 1.564, and an SG of 2.78; the marialite end member has RIs of n_o = 1.539 and n_e = 1.531 and an SG of 2.50 (Deer et al., 1992). A third end member of the group, silvialite, is characterized by an SO_4 anionic group ($Ca_4[Al_6Si_6O_{24}]SO_4$; Teertstra et al., 1999); however, silvialite has not been considered in previous gemological studies of gem scapolite.

It has not yet been systematically established whether the different colors of scapolite correspond to different compositions. Likewise, it is also unclear if properties such as RI and SG are related to specific colors. However, Couper (1991), reporting on a study of scapolite from Myanmar, noted that violet-to-pink samples plotted in the marialite field, and yellow and colorless samples fell in the meionite field. Because of the uncertainties concerning minerals of this group, a better knowledge is needed of the composition of gem-quality scapolites and the methods for their identification.

This study characterizes yellow scapolite from the Ihosy deposit in Madagascar, and investigates the suitability of previously established methods for calculating scapolite composition so it can be properly identified.

BACKGROUND

Yellow gem scapolite has been known from Madagascar since the beginning of the 20th century (Lacroix, 1922). In the past, production was sporadic and large gem crystals were rare. In the late 1990s, however, a new discovery was made about 35 km south of the town of Ihosy, in veins associated with skarn rocks typical of southern Madagascar (Martelat et al., 1997). The high-grade gneiss host

See end of article for About the Authors and Acknowledgments.
GEMS & GEMOLOGY, Vol. 46, No. 4, pp. 274–279.

Figure 1. The largest of these rough scapolites from Ihosy weighs about 10 g and measures 2.7 cm in diameter. A standard penlight is shown for scale. Photo by F. Pezzotta.

rocks contain a network of narrow granular scapolite veins associated with calcite, apatite, diopside, and minor spinel.

Local miners equipped with hand tools have worked the veins close to the surface in partially weathered horizons, and in fresh rock to a depth of a few meters. In 2007, occasional finds of good-quality scapolite caused them to work the deposits more actively, and there was a significant increase in production. The material showed an attractive yellow color (figure 1), and several kilograms of gem-quality rough—including clean, well-formed crystals up to 90 g—began to reach the local market. The faceted scapolites usually range from 4 to 12 ct, with some pieces as large as 30 ct (e.g., figure 2).

MATERIALS AND METHODS

Five cut stones (4.14–7.50 ct) and 16 pieces of rough (0.74–2.15 g) scapolite were analyzed (figure 3). Samples were selected from a large parcel of rough purchased from local miners in Ihosy by author FP. The studied samples are representative of the quality range produced from this locality. The five faceted stones were cut in Antsirabe (Madagascar) by a local

Figure 2. These faceted scapolites from Ihosy weigh 22.5 ct (left) and 29.7 ct (right). Courtesy of Giovanni Bossi and Riccardo Caprilli, respectively; photos by Roberto Appiani.

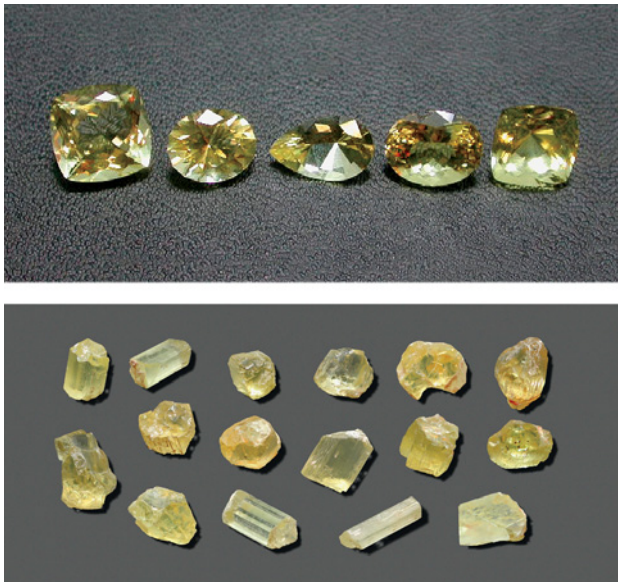

Figure 3. These five faceted scapolites (4.14–7.50 ct) and 16 rough crystals (0.74–2.15 g) from Ihosy were studied for this report. Photos by E. Castaman.

gem cutter; they were examined by standard gemological methods to determine their refractive indices, hydrostatic specific gravity, and microscopic features (using 20×–60× magnification). Long-wave (365 nm) and short-wave (254 nm) ultraviolet fluorescence was observed using a standard UV lamp.

Semiquantitative analyses of all 21 samples were performed with energy-dispersive X-ray fluorescence (EDXRF) spectroscopy using a Philips 9100 instrument operated with a voltage of 35 kV and a current of 100 μA. We also performed quantitative analyses of two representative pieces of rough (S2-P and S4-P), which were mounted in resin and polished, using a Cameca SX50 wavelength-dispersive spectroscopy (WDS) electron microprobe with an accelerating voltage of 15 kV and a current of 15 nA. Minerals used as standards for each element were apatite (F), albite (Na), olivine (Mg), corundum (Al), wollastonite (Si, Ca), sphalerite (S), vanadinite (Cl), orthoclase (K), synthetic $MnTiO_3$ (Ti, Mn), hematite (Fe), and celestite (Sr).

Infrared absorption spectroscopy of the scapolite was performed, but the spectra were not useful because the thickness of the whole samples resulted in total saturation in the 1600–400 cm^{-1} region (obscuring the diagnostic area for scapolite at 610.4 cm^{-1}). Accordingly, we used the KBr disc method on powder from one of the pieces of rough, and analyzed it with a Jasco FTIR 410 spectrometer (64 scans and a resolution of 4 cm^{-1}).

The few inclusions we observed in both the rough and faceted samples were analyzed by Raman spectroscopy (Renishaw 1000 instrument equipped with a 514 nm laser). One surface-reaching inclusion was analyzed by electron microprobe.

TABLE 1. Properties of five cut scapolites from Ihosy, Madagascar.[a]

Sample	Weight (ct)	RI (n_e–n_o)	SG	Me (%)[b]
1	4.13	1.555–1.575	2.68	60.0
2	4.32	1.555–1.580	2.71	64.9
3	5.70	1.554–1.581	2.72	64.9
4	7.23	1.555–1.581	2.72	65.9
5	7.50	1.552–1.574	2.68	56.0

[a] *All samples fluoresced pale yellow to long-wave UV radiation and strong purplish red to short-wave UV.*
[b] *Calculated from refractive indices following the formula reported in Deer et al. (1992).*

NEED TO KNOW

- Gem scapolite is a solid-solution series consisting of two main end members, marialite and meionite, and a third end member, silvialite.
- RI, SG, and IR spectral features vary with chemical composition.
- Gem-quality yellow scapolite has been produced sporadically from the Ihosy area since the late 1990s.
- Unlike most other gem scapolite, which is primarily marialite, Ihosy scapolite is mostly meionite with lesser marialite and minor silvialite components.

RESULTS AND DISCUSSION

The samples were yellow to light greenish yellow (Munsell 10Y 9/4 to 10Y 9/6), with moderate light yellow to light yellow-green pleochroism. Standard gemological data for the five cut stones are reported in table 1. The refractive indices were n_o= 1.574–1.581 and n_e=1.552–1.555, with a birefringence of 0.022–0.027; the SG ranged from 2.68 to 2.72. These values are consistent with meionite-dominant scapolites (Deer et al., 1992). All the samples fluoresced pale yellow to long-wave UV radiation and

strong purplish red to short-wave UV. The fluorescence of Ihosy scapolite is similar only to that of the rare crystals found in Switzerland (table 2).

Semiquantitative EDXRF data from all samples suggested a limited compositional range. Therefore, we believe the two rough pieces chosen for quantitative WDS electron microprobe analysis (table 3) are representative for all these samples. The data revealed they were mainly meionite (54.7–62.0%) with lesser marialite (29.9–37.8%) and minor silvialite components (7.5–8.1%; see also figure 4). The chemical composition had significant influence on the physical properties of the gem material.

Ulbrich (1973), Arem (1987), and Deer et al. (1992) related scapolite's refractive indices to its meionite content. Their methodology for calculating composition from RI values does not take into account the silvialite component (a rather new addition to the scapolite group). Moreover, Deer et al. (1992) pointed out the uncertainty of the method for specimens containing relatively large amounts of K, S, or Cl, and suggested a typical error of ±6.5% in the Me value. Nevertheless, in view of the rather consistent and relatively low silvialite component of our samples, we applied the method proposed by Deer et al. (1992), represented by the equation $(n_e+n_o)/2 = 1.5346 + 0.000507(Me\%)$. The results, shown in table 1, indicate a meionite content of 56.0–65.9%, assuming a two-component composition. These results are in good agreement with the microprobe data obtained from the two crystals. Moreover, the SG values of the samples generally agreed with their meionite content, per Deer et al. (1992).

Wehrenberg (1971) proposed an indirect method for

TABLE 2. UV fluorescence of yellow scapolite from various geographic origins.

Locality	UV fluorescence	
	Long-wave (365 nm)	Short-wave (254 nm)
Madagascar[a]	Pale yellow	Strong purplish red
Tanzania[a]	Pale purple	Strong purple
Tanzania[b]	Strong yellow	Strong yellow
Myanmar[a,b]	Pale yellow to orange	Moderate yellow-orange to pink
Brazil (Espirito Santo)[a]	Inert to pale "lilac"-pink	Strong red to purple
Switzerland (Lake Tremorgio)[a]	Pale yellow	Strong purplish red

[a] *Samples from the Natural History Museum of Milan.*
[b] *Data from Arem (1987).*

TABLE 3. Quantitative electron microprobe analyses of two rough scapolite samples from Ihosy, Madagascar.

Oxide (wt.%)	S2-P[a]	S4-P[b]
SiO_2	44.71	49.29
TiO_2	0.01	0.01
Al_2O_3	26.83	25.77
Fe_2O_3	0.06	0.04
MnO	0.01	0.01
MgO	0.03	0.02
CaO	16.24	14.41
Na_2O	3.82	4.95
K_2O	0.66	0.80
SO_3	0.71	0.70
Cl	1.24	1.86
F	0.01	0.02
Total	94.34	97.88
Calculated components (%)[c]		
Meionite	62.0	54.7
Marialite	29.9	37.8
Silvialite	8.1	7.5

[a] *Average of 16 point analyses.*
[b] *Average of 18 point analyses.*
[c] *Calculated using Mincalc software; CO_2 used for the meionite component was calculated to obtain the best stoichiometry.*

Figure 4. This ternary diagram shows the composition of the two scapolite samples analyzed by electron microprobe. The oval field illustrates the compositional variation (from EDXRF semiquantitative analyses) of all 21 samples.

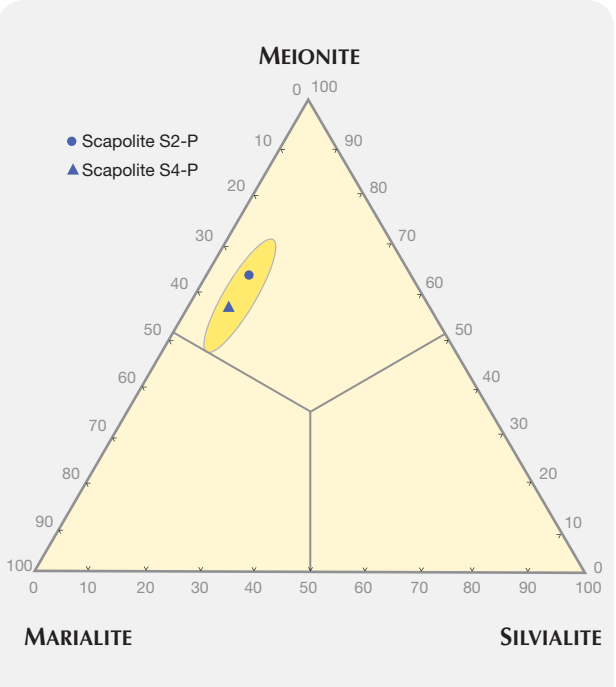

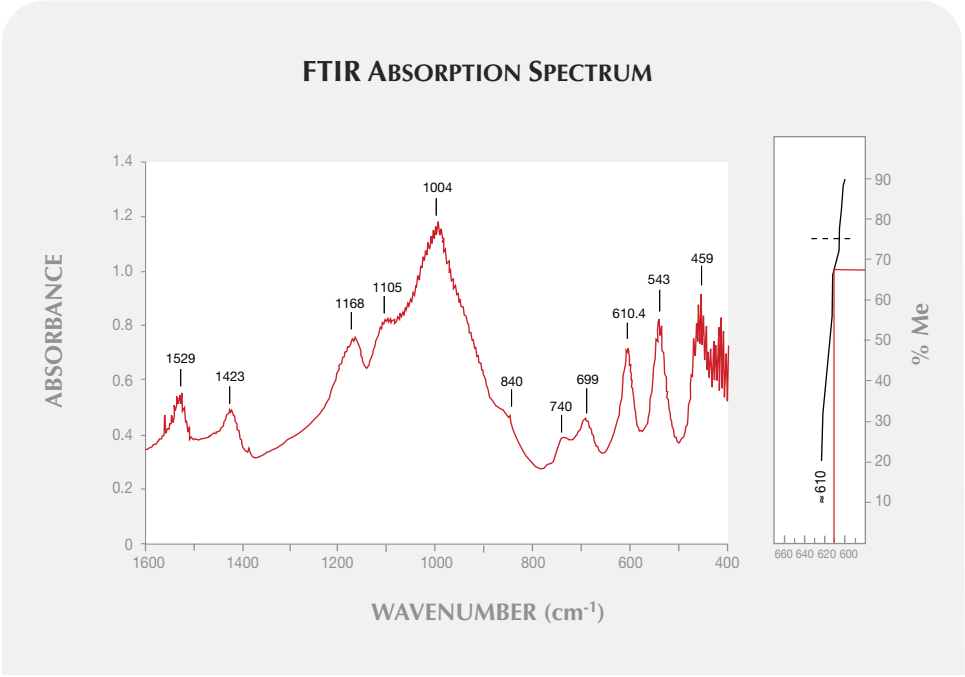

Figure 5. The FTIR spectrum on the left and the diagram on the right (after Wehrenberg, 1971) illustrate the correlation between the absorption peak at 610.4 cm^{-1} and Me content.

determining meionite content based on the position of the IR band located at ~610 cm^{-1}, which is directly related to meionite content in scapolites containing 20–90% Me. Sample S2-P's diagnostic peak was centered at 610.4 cm^{-1}, which corresponds to 67% ± 5% meionite (figure 5). This is somewhat similar to the 62.0% Me obtained by microprobe analysis if we consider that the latter value was calculated for a three-component system (i.e., accounting for silvialite, in addition to marialite and meionite). On the same sample, the refractive indices obtained on a polished area before mounting in epoxy correlated to 62.9% Me.

Inclusions were rare in all samples, and most consisted of hollow channels, probably related to growth structures that were affected by late-stage corrosion. The few mineral inclusions observed in the samples (e.g., figure 6) were identified by Raman spectroscopy as garnet (andradite-grossular), mica (very likely phlogopite, the most abundant mica in the host rock), and calcic pyroxene. Microprobe analysis of the (surface-reaching) pyroxene identified it as diopside. All of these inclusions correspond with minerals present in the skarn host rocks at the Ihosy deposit.

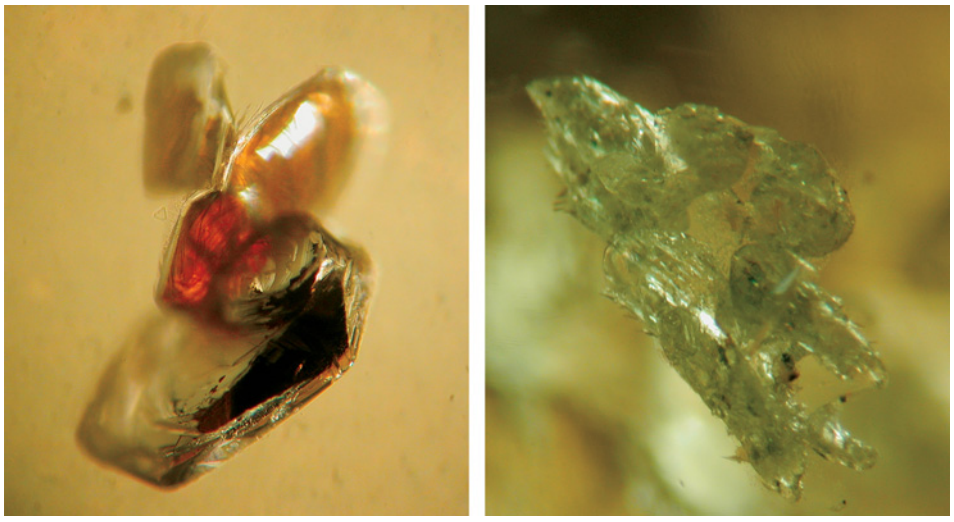

Figure 6. Microscopic examination revealed inclusions of tabular hexagonal mica and brownish orange garnet (left), as well as diopside (right). Photomicrographs by E. Castaman; fields of view 0.5 mm (left) and 0.8 mm (right).

CONCLUSIONS

Various analytical techniques allowed us to establish the meionite-dominant composition of Ihosy scapolites, in the approximate range of 55–65% Me. The results obtained from different samples using the three methods applied (electron microprobe, RI, and FTIR) were generally in good agreement. Moreover, the electron microprobe analyses showed the silvialite content of the Ihosy scapolite was ~8%. To our knowledge, this is the first gemological study in which the silvialite content of scapolite has been reported. We have yet to make compositional comparisons with scapolites from other sources. Nevertheless, it is interesting to note that these scapolites fell in the meionite field, while the majority of commercial gem scapolite from other localities are marialite (see, e.g., Graziani and Gübelin, 1981 [Tanzania]; Peili, 1992 [China]; Kammerling et al., 1995 [Tajikistan]; Gomes et al., 2004 [Mozambique]; Zwaan, 1996 [Sri Lanka]; and McClure et al., 2005 [Afghanistan]).

Although only limited mining for Ihosy scapolite is being conducted, there is strong potential for future production from this deposit.

ABOUT THE AUTHORS

Margherita Superchi is scientific gemological consultant, and Elena Gambini and Emanuela Castaman are staff members, at the Gemmological Centre of the Milan Chamber of Commerce (CISGEM), Milan, Italy. Federico Pezzotta (fpezzotta@yahoo.com) is mineral curator of the Natural History Museum of Milan, Italy.

ACKNOWLEDGMENTS

The authors thank Antonello Donini and Andrea Marzola of CISGEM for their help in collecting and analyzing the data. We also thank Alessandro Guastoni of the University of Padua for the electron microprobe analyses and Alberto Paleari of the University of Milan-Bicocca for helpful discussions. This study is based in part on the diploma thesis of Barbara Gorini (2006).

REFERENCES

Arem J.E. (1987) *Color Encyclopedia of Gemstones*, 2nd ed. Van Nostrand Reinhold, New York, pp. 166–167.

Couper A.G. (1991) Colour as a guide to the composition of scapolite from Burma. *Journal of Gemmology*, Vol. 22, No. 5, pp. 259–263.

Deer W.A., Howie R.A., Zussman J. (1992) *An Introduction to the Rock-Forming Minerals*. Longman Scientific & Technical, London, 696 pp.

Gomes C.L., Quinn E.P., Koivula J.I. (2004) Gem News International: Scapolite from Mozambique. *G&G*, Vol. 40, No. 2, pp. 172–173.

Gorini B. (2006) Caratterizzazione della scapolite di Ihosy, Madagascar. Unpublished B.S. thesis, Università degli Studi di Milano-Bicocca, 128 pp.

Graziani G., Gübelin E. (1981) Observations on some scapolites of central Tanzania. *Journal of Gemmology*, Vol. 17, No. 6, pp. 395–405.

Kammerling R.C., Koivula J.I., Johnson M.L., Alitsch E. (1995) Purple scapolite from Tajikistan. *G&G*, Vol. 31, No. 3, pp. 211–212.

Lacroix A. (1922) *Minéralogie de Madagascar*, Vol. 1–3. A. Challamel, Paris.

Martelat J.E., Nicollet C., Lardeaux J.M., Vidal G., Rakotondrazafy R. (1997) Lithospheric tectonic structures developed under high-grade metamorphism in the southern part of Madagascar. *Geodinamica Acta*, Vol. 10, pp. 94–114.

McClure S.F., Rossman G.R., Shigley J.E. (2005) Gem News International: Tenebrescent scapolite from Afghanistan. *G&G*, Vol. 41, No. 3, pp. 269–271.

Peili Z. (1992) Gem-quality scapolite from Sinjiang region, west China. *Australian Gemmologist*, Vol. 18, No. 4, pp. 115–117.

Teertstra D.K., Schindler M., Sherriff B.L., Hawthorne F.C. (1999) Silvialite, a new sulfate-dominant member of the scapolite group. *Mineralogical Magazine*, Vol. 63, pp. 321–329.

Ulbrich H. (1973) Crystallographic data and refractive indices of scapolites. *American Mineralogist*, Vol. 58, pp. 81–92.

Wehrenberg J.P. (1971) The infrared absorption spectra of scapolite. *American Mineralogist*, Vol. 56, pp. 1639–1654.

Zwaan P.C. (1996) Enstatite, cordierite, kornerupine, and scapolite with unusual properties from Embilipitiya, Sri Lanka. *G&G*, Vol. 32, No. 4, pp. 262–269.

A MICROSTRUCTURAL STUDY OF PIETERSITE FROM NAMIBIA AND CHINA

Kaifan Hu and Peter J. Heaney

Pietersite has been described as a brecciated variety of tiger's-eye. This study examined pietersite specimens from Namibia and China (the main sources) using powder X-ray diffraction, optical microscopy, environmental scanning electron microscopy, and conventional gemological methods. On the basis of the results, quantitative approaches were developed to distinguish pietersite samples from the two localities. It is also proposed that the petrogenesis of this gem material is quite different from that of South African tiger's-eye.

Pietersite is named after its discoverer, Sid Pieters, a well-known gem and mineral dealer who first described it in 1962 from a locality in Namibia (Thomas, 2008). The term is now used generally to describe brecciated varieties of tiger's-eye. Tiger's-eye *sensu stricto* occurs within Precambrian banded iron formations as seams that run parallel to layers of jasper. It is characterized by lustrous "golden" brown bands that exhibit a radiant chatoyancy when polished due to the inclusion of crocidolite fibers within a microcrystalline silica host (Heaney and Fisher, 2003). (Crocidolite is an asbestiform variety of an amphibole called riebeckite.) Although Namibian pietersite exhibits the same mineralogy as tiger's-eye, the chatoyant field is not observed as a continuous band. Rather, pietersite contains angular fragments that are cemented as an irregular patchwork of "bundles," some of which exhibit sheen (Koivula et al., 1992). Thus, pietersite offers a chaotic chatoyancy, with a brecciated texture that has been likened to bold paint strokes that flow in many directions (see, e.g., figure 1).

Pietersite has been found at two main sources: Kuraman, Namibia; and Xichuan, Henan Province, China. Mr. Pieters discovered the Namibian pietersite within round dolostone cobbles while prospecting some farmland in the neighborhood of Outjo, in the Kuraman district. He registered the gem in the mineral records of Great Britain in 1964 and brought it to market in the 1970s (Koivula et al., 1992; Thomas, 2008). In 1996, Zeitner reported that much of the minable stock in Namibia was depleted and that material was becoming scarce. Chinese pietersite was discovered in 1966 while geologists were prospecting for crocidolite. It was mined in the 1970s and 1980s, but it did not come to market until the 1990s (Zhong, 1994). Although it appears that both mining areas are still closed, material from these localities continues to appear in the marketplace.

In this article, we compare the properties of pietersite from Namibia and China, identify their distinguishing characteristics, and propose mechanisms for their formation that account for differences in their appearance and phenomena. A comparison to South African tiger's-eye is also provided.

MATERIALS AND METHODS

The specimens examined included five samples from China and six from Namibia (e.g., figure 2). The Chinese specimens consisted of two flat polished oval slabs from the GIA Collection (no. 32394, donated by the late Hannes Kleynhans) and three cabochons labeled as Chinese and purchased at the 2008 Tucson Gem and Mineral Show. The Namibian specimens consisted of three polished pieces and

See end of article for About the Authors and Acknowledgments.
GEMS & GEMOLOGY, Vol. 46, No. 4, pp. 280–286.

Figure 1. China and Namibia are the only known sources of gem-quality pietersite. Studied for this report, this Chinese sample (left, 39.85 g) displays an overall brownish red color, whereas the polished specimen of Namibian pietersite (right, 80.76 g) is dominated by blue-gray,"golden" yellow, and white hues. Photos by K. Hu.

three flat unpolished slabs from author PJH's personal collection (purchased at the 2008 and 2009 Tucson gem shows). Two of the six Namibian samples contained traces of the original host rock. The specimens ranged from 7 to 85 g.

Standard gemological tests were performed on all samples. RI values were measured from the five Chinese and three Namibian polished specimens with a GIA Duplex refractometer. We obtained hydrostatic SG values using a Scout Pro SP 602 electronic balance. UV fluorescence was observed with standard long-wave (366 nm) and short-wave (254 nm) UV lamps.

Figure 2. These are some of the Namibian pietersite specimens that were investigated for this report (3.3–6.0 cm in maximum dimension). Photo by K. Hu.

Eight doubly polished petrographic thin sections were prepared from both the Chinese and the Namibian material (four from each), and these were examined with an Olympus SZ-CTV microscope and an Olympus BX40 petrographic microscope. Photomicrographs were obtained with a Nikon DS-5M camera. Powder X-ray diffraction (XRD) patterns were collected using a Rigaku DMAX-Rapid microdiffractometer. Environmental scanning electron microscope (ESEM, in which the sample does not need an electrically conductive coating) analysis of all eight thin sections was performed using an FEI Quanta 200 microscope operating at 20 kV, and chemical analyses were obtained using an Oxford INCA energy-dispersive spectroscopy system. All work was conducted in the Pennsylvania State University Mineralogy Laboratory in the Department of Geosciences, and in the Materials Characterization Laboratory at the Pennsylvania State University Materials Research Institute.

RESULTS

The gemological properties of the samples are described below and summarized in table 1.

Visual Appearance. The Chinese pietersite specimens were intensely brecciated, with individual fields measuring 2–8 mm in diameter. The overall color was a jasper-like brownish red hue, but regions of chatoyant blue and yellow were discernible, with white flecks from calcite. The chatoyant effect was best developed in the yellow regions, but it was noticeably less vibrant than is typically observed in Namibian pietersite.

The color of the Namibian specimens was not as

TABLE 1. Gemological properties of pietersite from China and Namibia.

Property	China	Namibia
Color	Brownish red, "golden" yellow to brown, rarely blue	Blue-gray, "golden" yellow to brown, rarely red
Diaphaneity	Opaque	Semitranslucent to opaque
Refractive index	1.54–1.55	1.54–1.55
Specific gravity	2.67–2.74	2.50–2.58
UV fluorescence		
Long-wave	Inert	Moderate-to-weak light green
Short-wave	White in calcite areas	Moderate-to-strong bright green
XRD analysis	Quartz, minor calcite	Quartz, minor calcite
Textural features observed by optical microscopy and ESEM	Brecciated clasts measuring 2–8 mm in diameter; fibrous crocidolite intensely coated by hematite and chlorite; quartz veins cross-cutting crocidolite; calcite inclusions	Brecciated clasts measuring 5–10 mm in diameter; fibrous crocidolite occasionally coated by goethite and hematite; chalcedony spherulites; inclusions of calcite, dolomite, barite, and pyrite

varied as that of the Chinese material. Blue-gray and "golden" yellow fibrous regions predominated, with rare secondary brownish red fields, and the overall bodycolor of the Namibian specimens was blue-gray. The brecciated clasts ranged from 5 to 10 mm in diameter, but on average they were larger than those seen in the Chinese specimens. Chatoyancy was particularly well developed in the blue fields. Three of the Namibian specimens had ~2-mm-thick veins of colorless translucent chalcedony. Chalcedony was observable in the Chinese specimens only with the aid of light microscopy.

Refractive Index. The RI values, around 1.54, were consistent with quartz for all samples. There was no difference in RI values between the Chinese and Namibian specimens.

Specific Gravity. The SG values of the Chinese specimens ranged from 2.67 to 2.74. The SG values of the Namibian specimens were notably lower, 2.50–2.58. The SG of quartz is 2.65.

UV Fluorescence. Most of the Namibian specimens luminesced a moderate-to-weak light green to long-wave UV radiation and a moderate-to-strong bright green to short-wave UV. This bright green luminescence is most likely explained by the greater chalcedony content in those sectors. Portions of some of the Chinese specimens luminesced white to short-wave but were inert to long-wave UV; these areas corresponded to calcite.

Powder X-ray Diffraction. Our XRD patterns for the Chinese and Namibian specimens were indistinguishable, producing diffraction peaks only for quartz with minor calcite. No evidence of crocidolite was detected. This result is similar to our experience with many tiger's-eye specimens from Griquatown, South Africa, for which crocidolite was detected only by synchrotron X-ray radiation (Heaney and Fisher, 2003). We infer from these results that despite the intense chatoyancy of pietersite, the mass fraction of crocidolite is on the order of a few weight percent or less.

NEED TO KNOW

- Pietersite, often described as a brecciated variety of tiger's-eye, is known from China and Namibia.
- Pietersite from the two localities has similar RI ranges, but the Namibian material has a lower SG.
- Crocidolite fibers are more densely intergrown (parallel, radial, and disordered textures) in Chinese samples. The fibers in Namibian specimens are generally oriented parallel to one another.
- Namibian pietersite formed under very different geologic conditions from those that produced South African tiger's-eye.

Optical Microscopy. Examination of thin sections of pietersite from both China and Namibia revealed the presence of crocidolite embedded within microcrystalline quartz. The crocidolite could be distinguished on the basis of its moderately high relief, pleochroic grayish blue to greenish blue coloration, and optical extinction of 8–10° in cross-polarized light.

We also noted significant textural differences

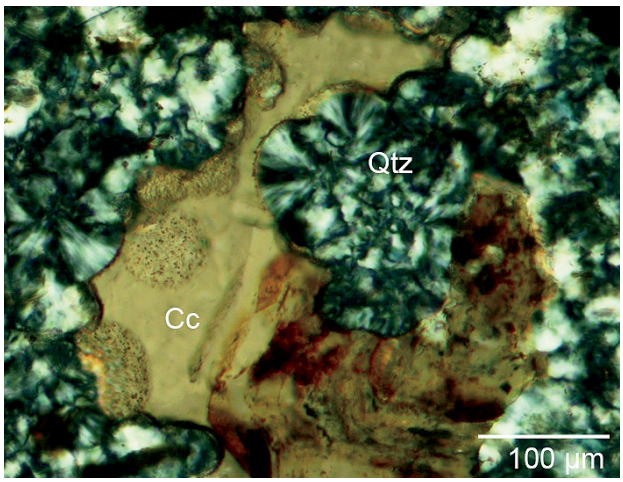

Figure 3. In cross-polarized light, this Namibian pietersite exhibits fibrous chalcedony (Qtz) spherulites that are embaying calcite (Cc) and are surrounded by fine-grained hematite. Photo by K. Hu.

between the Chinese and Namibian specimens. In the Chinese samples, the fibers were more densely intergrown, and they showed a broader variety of fabrics—parallel, radial, and disordered. They ranged from 20 µm to 2 mm long and rarely exceeded 2 µm wide. Both hematite and chlorite coated the fibers of crocidolite. The Chinese pietersite also differed from the Namibian samples in the presence of fibrous chlorite inclusions. The chlorite fibers exhibited strong pleochroism from deep green to yellowish brown.

Unlike the Chinese material, the crocidolite fibers in the Namibian specimens were generally oriented parallel to one another. Fiber lengths were shorter than in the Chinese material, typically 10–50 µm, and they were less than 2 µm wide. The fabric of the microcrystalline quartz also differed significantly; it was commonly fibrous chalcedony and quartzine, whereas in Chinese samples it was uniformly fine-grained and equant, similar to jasper (Heaney and Veblen 1992). Radial spherulites of chalcedony grew within both calcite and hematite in the Namibian pietersite (figure 3).

ESEM Analysis. Consistent with the overall jasper-like red bodycolor of the Chinese pietersite, ESEM imagery showed that the crocidolite fibers were coated with hematite to a much greater degree than in the Namibian specimens (figure 4, right). Both Chinese and Namibian pietersite included calcite as an accessory mineral (figure 4, left), but ESEM revealed that the Namibian pietersite also contained microcrystalline dolomite, barite, and pyrite (figure 5), which we did not observe in the Chinese specimens. In places, these minerals were partly replaced by quartz, with only the edges of crystals visible (figure 6).

Backscattered electron images of the quartz matrix in the Namibian pietersite revealed growth textures that were unusual and instructive. Rims of fine-grained hematite typically enveloped radially fibrous chalcedony spherules, which embayed the precursor dolostone (figure 7, left). The chalcedony spherules displayed concentric, oscillatory spheres of microquartz fibers and open cavities. Crocidolite fibers grew out radially from the hematite-rimmed spherulites into open spaces between them (again, see figure 7, left). In regions marked by a higher degree of overall silicification, the chalcedony spherules appear to have coalesced, and the cores locally contained fibers of crocidolite coated with hematite. In more silicified samples, the crocidolite fibers were seen transecting multiple spherulites (figure 7, right).

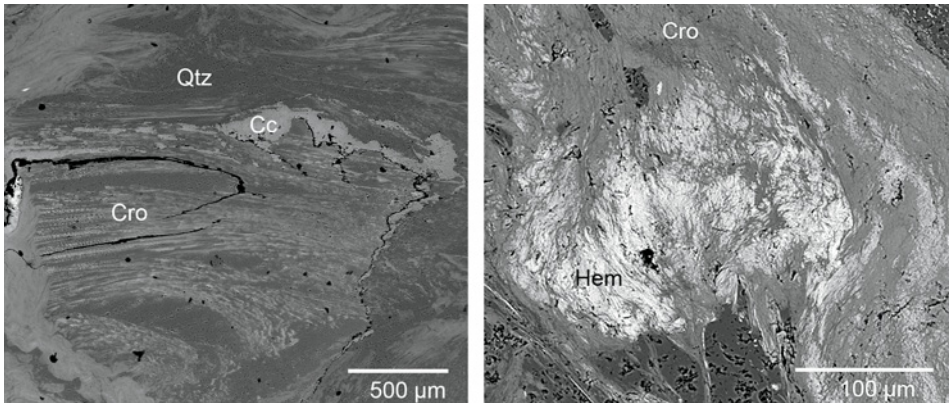

Figure 4. Parallel aggregates of crocidolite (Cro) and intergrowths of calcite (Cc) are evident in the backscattered electron (BSE) image of Chinese pietersite on the left. On the right, the BSE image of a Chinese specimen shows the coating of some crocidolite fibers (dark gray) by hematite (Hem; light gray). Micrographs by K. Hu.

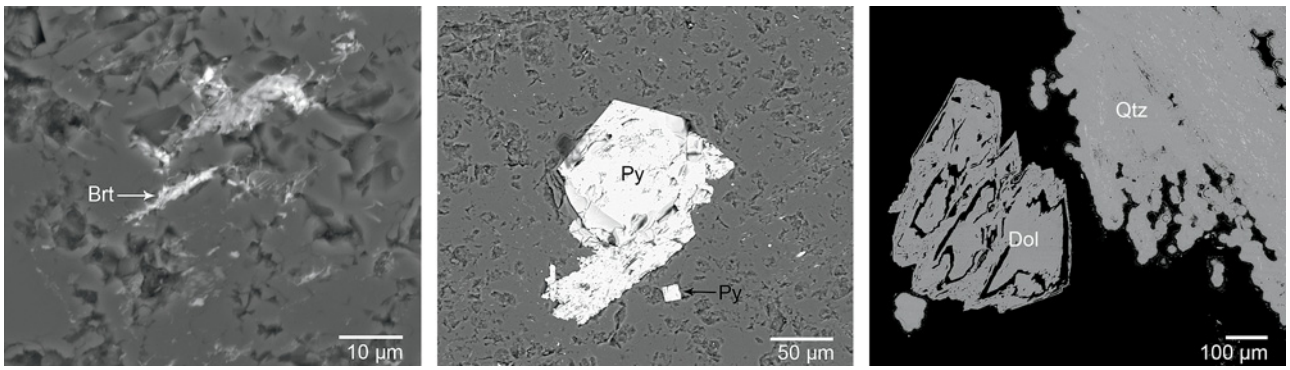

Figure 5. As revealed in BSE images (and identified by energy-dispersive spectroscopy), Namibian pietersite included barite (Brt; left), pyrite (Py; center), and dolomite (Dol; right). Micrographs by K. Hu.

Consistent with a previous report (Leake et al., 1992), energy-dispersive spectroscopy revealed that the crocidolite in both Chinese and Namibian material contains variable amounts of Mg in solid solution with Fe and should be classified as magnesioriebeckite.

DISCUSSION

Pietersite has been described as a "breccia aggregate made up largely of hawk's-eye and tiger's-eye" (Schumann, 2009, p. 320) and as a "disoriented pseudo-crocidolite mass with limonite" (Manutchehr-Danai, 2008, p. 368). Our analyses indicate that pietersite specimens from Namibia and China do share many hallmarks of tiger's-eye. Mineralogically, both tiger's-eye and pietersite contain asbestiform fibers of crocidolite embedded within a fine-grained quartz host, and the included crocidolite is responsible for the chatoyancy of the material. Chatoyancy is degraded where the crocidolite has altered to iron (hydr)oxides. For example, much of the Chinese material that we examined contained nonphenomenal areas in which a jasper-like dullness superseded the original chatoyancy because of this alteration reaction. Finally, like tiger's-eye, the pietersite samples revealed no evidence for pseudomorphism of quartz after crocidolite, despite popular assumptions to the contrary.

Nevertheless, our analyses suggest that the petrogenesis of pietersite is quite different from that of the tiger's-eye found in Griquatown, South Africa. Heaney and Fisher (2003) proposed that South African tiger's-eye formed through a "crack-seal" process: The hydrofracture of banded-iron formations generated flat seams parallel to the jasper bedding planes, and these cracks were sealed by quartz and crocidolite as an antitaxial infilling (i.e., growth from opposing crack walls toward the center of the vein). The quartz crystals in tiger's-eye exhibit a

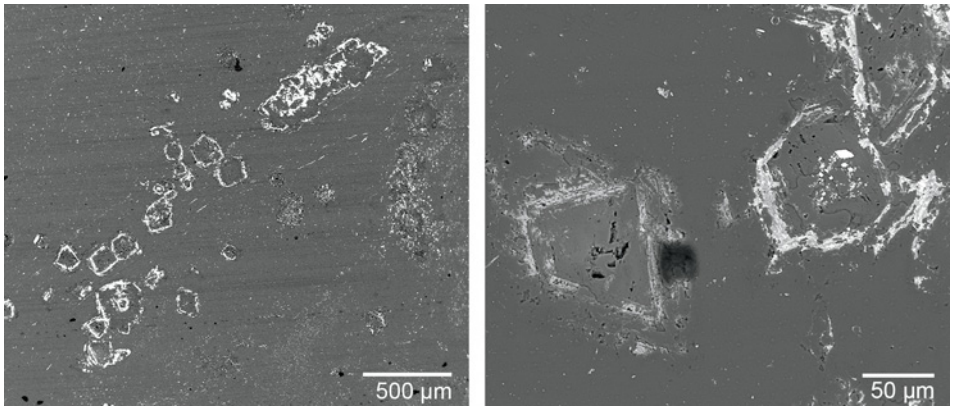

Figure 6. These BSE images of Namibian pietersite show the replacement of barite by quartz, leaving only the outer rims of the crystals. Micrographs by K. Hu.

characteristic columnar habit with an elongation parallel to the c-axis. The crocidolite fibers asymmetrically cross-cut the quartz boundaries, and the ends facing the vein wall are jagged while those facing the vein interior are tapered.

The textures in Namibian pietersite rule out a crack-seal origin. Many lines of reasoning suggest instead that the Namibian (and perhaps the Chinese) pietersites are solution breccias. (Solution breccias form when soluble minerals are partly or wholly removed by circulating groundwater, creating cavities into which overlying rock collapses and fragments. Often, the fragmented material is subsequently welded into a breccia by precipitation of a silica or calcite cement from the groundwater.) Namibian pietersite is developed within dolostone cobbles that underwent fragmentary dissolution and were silicified. During this process, silica-rich fluids partially dissolved the original dolomite and deposited chalcedony spherulites. The presence of hematite crystals at the centers of the spherulites suggests that hematite served as nucleation centers for silica. The growth of chalcedony fibers radially outward from these nuclei "bulldozed" residual hematite to form exterior rims of hematite.

We propose that a later episode of fluid infiltration resulted in the formation of crocidolite (a sodic amphibole) from reactions between chalcedony and hematite in the presence of aqueous Na^+. The formation of crocidolite during the coalescence of chalcedony spherulites generated regions in which the crocidolite fibers grew as parallel thatches. These sheaves of crocidolite are responsible for the spectacular chatoyancy observed in the highest-quality pietersite specimens. As is typical of dissolution breccias, however, the replacement of dolostone by silica was localized, and resulted in distinct patches of crocidolite with differing fiber orientations. This produced the chaotic chatoyancy that differentiates pietersite from South African tiger's-eye. The optical homogeneity that is characteristic of the latter probably can be attributed to the large-scale tectonic forces that exerted a broad control over crack-seal fiber growth. Chemical dissolution, by contrast, is not correlated over long spatial scales.

As is also typical of many South African tiger's-eye specimens, the last stage of pietersite formation involved a back-reaction of crocidolite to hematite and/or goethite. These microcrystalline iron (hydr)oxides initially coated the crocidolite fibers; then, in some instances, they completely replaced the fibers pseudomorphically. This final alteration reaction may have occurred at low temperatures much more recently than the crocidolite reaction, which presumably required low-grade metamorphism (Miyano and Klein, 1983). The breakdown of the crocidolite to iron (hydr)oxides proceeded to a greater extent in the Chinese than in the Namibian material, and it greatly diminished the capacity for chatoyancy.

CONCLUSION

Despite similarities in color, appearance, and mineralogy, we believe pietersite crystallized under very different geologic conditions from those that produced South African tiger's-eye. Whereas South African tiger's-eye probably can be attributed to crack-seal events related to tectonic stress fields, Namibian pietersite (e.g., figure 8) is a brecciated gem material created by fragmentary dissolution of precursor dolomite and replacement by silica. Subsequent reactions between silica and hematite in the presence of aqueous Na^+ formed crocidolite.

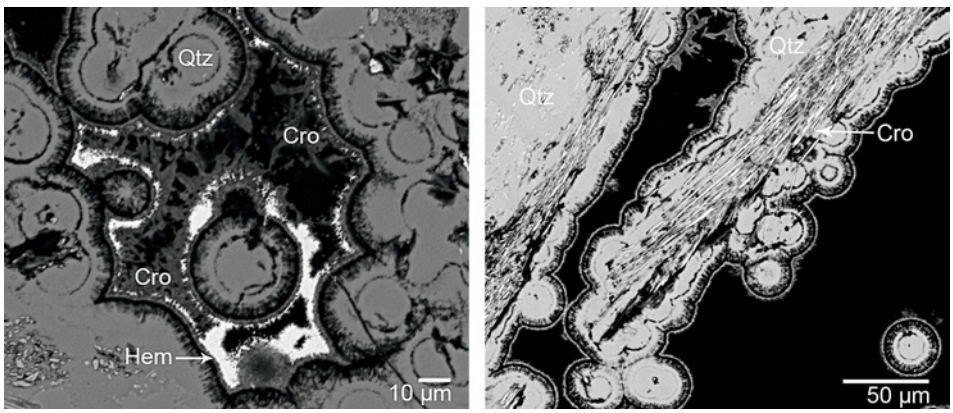

Figure 7. On the left, BSE imaging reveals radially fibrous chalcedony (Qtz) surrounded by white-appearing rims of hematite (Hem). Dark gray fibers of crocidolite (Cro) are present between the chalcedony spherulites. The black areas are empty cavities. The BSE image on the right shows crocidolite fibers transecting chalcedony spherulites in Namibian pietersite. Micrographs by K. Hu.

Figure 8. This slab of pietersite (12 cm across) shows the colorful appearance and brecciated texture that are typical of fine Namibian material. Photo by John Passaneau.

With little published information on the geologic setting of the Chinese pietersite, assigning the same petrogenetic model to the material from Xichuan is less certain. Despite their geographic separation, the microscopic textures of the Namibian and Chinese materials are strikingly similar. Nevertheless, our investigations have revealed that Namibian pietersite can be distinguished from its Chinese counterpart in several ways. Careful microscopic examination along with specific gravity and UV fluorescence characteristics can readily discriminate gems from these different localities.

ABOUT THE AUTHORS

Ms. Hu (hukaifan@gmail.com) is a Ph.D. candidate at the Faculty of Material Science and Chemistry Engineering, China University of Geosciences, Wuhan. Dr. Heaney is professor of mineralogy in the Department of Geosciences, Pennsylvania State University, University Park.

ACKNOWLEDGMENTS

The authors gratefully acknowledge support from NSF grant EAR07-45374 and from the Penn State Schreyer Honors College. One of us (KH) was supported as a visiting scholar at Penn State University by the Joint-Training Research Program sponsored by the Chinese Scholarship Council. The authors are grateful for the insightful reviews of Dr. George Rossman, Dr. James Shigley, and Alan Jobbins.

REFERENCES

Heaney P.J., Fisher D.M. (2003) New interpretation of the origin of tiger's-eye. *Geology*, Vol. 31, No. 4, pp. 323–326.

Koivula J.I., Kammerling R.C., Fritsch E., Eds. (1992) Gem News: Pietersite from Namibia. *G&G*, Vol. 28, No. 1, p. 61.

Leake B.E., Woolley A.R., Arps C.E.S. (1997) Nomenclature of amphiboles: Report of the subcommittee on amphiboles of the International Mineralogical Association, Commission on New Minerals and Mineral Names. *Canadian Mineralogist*, Vol. 35, No. 1, pp. 219–246.

Manutchehr-Danai M. (2008) *Dictionary of Gems and Gemology*, 3rd ed. Springer, New York.

Miyano T., Klein C. (1983) Conditions of riebeckite formation in the iron-formation of the Dales Gorge Member, Hamersley Group, Western Australia. *American Mineralogist*, Vol. 68, pp. 517–529.

Schumann W. (2009) *Gemstones of the World*, 4th ed. Sterling, New York.

Thomas A. (2008) *Gemstones: Properties, Identification and Use*. New Holland Publishers, London.

Zeitner J.C. (1996) *Gems and Lapidary Materials for Cutters, Collectors, and Jewelers*. Geoscience Press, Tucson, AZ.

Zhong H. (1994) Gemstone sources in Henan Province. *China Lapidary*, Vol. 9, No. 3, pp. 43–46.

UPDATE ON MEXIFIRE SYNTHETIC FIRE OPAL

Rajneesh Bhandari and Gagan Choudhary

As a result of changes in the manufacturing process, recent production of the synthetic fire opal marketed as "Mexifire" exhibits some new properties. While the earlier material could be identified on the basis of low RI and SG values, the new synthetics have values that are quite similar to—and partially overlap those of—natural fire opals. With the change in the manufacturing process, the water content has also changed, as reflected in the IR spectra.

In Choudhary and Bhandari (2008), we described a new synthetic fire opal marketed as "Mexifire." The article detailed the material's gemological properties, chemical composition, and infrared spectra, as well as provided a brief outline of the manufacturing process. Since November 2009, this process has been slightly modified. Water content is now controlled in such a manner that the refractive index and specific gravity values are much closer to those of natural fire opal. This article presents the properties of this new generation of Mexifire; the previous generation is no longer being produced, although some material undoubtedly remains in the marketplace.

Materials and Methods. We examined nine faceted ovals (3.40–4.40 ct; figure 1) representative of the new Mexifire production. Standard gemological tests were performed on all samples. Qualitative energy-dispersive X-ray fluorescence (EDXRF) chemical analyses of all samples were conducted using a PANalytical Minipal 2 instrument under two different conditions: Elements with a low atomic number (e.g., Si) were measured at 4 kV tube voltage and 0.850 mA tube current, while transition and heavier elements were measured at 15 kV and 0.016 mA. Spectroscopic measurements of all samples in the infrared range (6000–400 cm^{-1}) were performed with a Shimadzu IR Prestige 21 Fourier-transform infrared (FTIR) spectrometer, operating at room temperature with a diffuse-

Figure 1. These new samples of Mexifire synthetic fire opal (3.40–4.40 ct) were manufactured by a modified process and exhibit properties different from those recorded in the original production in 2008. Photo by G. Choudhary.

See end of article for About the Authors and Acknowledgments.
GEMS & GEMOLOGY, Vol. 46, No. 4, pp. 287–290.

TABLE 1. Properties of Mexifire synthetic opals (new and original products) and natural fire opals.

Properties	New Mexifire synthetic fire opal (this study)	Mexifire synthetic fire opal (Choudhary and Bhandari, 2008)	Natural fire opal
Color	Brownish orange to orangy brown	Brownish orange to orangy yellow	Brownish orange to orangy yellow
Color distribution	Typically even; on rotation, color appeared to concentrate in the center	Typically even	Often color zoned; flow-like or wavy pattern
Diaphaneity	Transparent under normal viewing conditions; translucent/turbid with fiber-optic light	Transparent under normal viewing conditions; translucent/turbid with fiber-optic light	Transparent to translucent
Quality of polish	Good	Good	Dull to good
Refractive index	1.470	1.380–1.405	1.440–1.460 (Simoni et al., 2010); 1.400–1.435 (Choudhary and Bhandari, 2008); and 1.435–1.455 (Webster, 1994)
Specific gravity	2.19	1.63–1.77	2.15–2.38 (Simoni et al., 2010); 1.92–2.06 (Choudhary and Bhandari, 2008); and 1.97–2.06 (Webster, 1994)
Polariscope reaction	Weak strain pattern; no snake-like bands observed	Strong strain pattern with snake-like bands	Weak strain pattern; no snake-like bands observed
Long- and short-wave UV fluorescence	Inert	Inert	Inert
Spectroscope	No features	No features	No features
Internal features	• Zoned turbidity • Scattered pinpoints	• Zoned turbidity • Scattered pinpoints • Whisker-like inclusion in one sample	Choudhary and Bhandari (2008): • Zoned turbidity • Scattered pyrite or some flake-like inclusions • Dendritic inclusions common • Flow patterns, cloudy zones, and fluid inclusions
EDXRF analysis	Si, Fe, and Ca	Si, Fe, and Ca	Si, Fe, and Ca (Choudhary and Bhandari, 2008); Al (Gaillou et al., 2008)
FTIR spectroscopy	Weak hump at ~5440 cm^{-1}; sharp peak with a shoulder at ~4520 cm^{-1}; absorption band in the 4000–3250 cm^{-1} region; weak shoulder at 2652 cm^{-1}; a sharp peak at 2262 cm^{-1} and complete absorption below 2100 cm^{-1}	Absorption band in the 5350–5000 cm^{-1} region; hump from 4600 to 4300 cm^{-1}; detector saturated below 4000 cm^{-1}	Absorption band in the 5350–5000 cm^{-1} region; hump from 4600 to 4300 cm^{-1} (absent from some stones); detector saturated below 4000 cm^{-1} (Choudhary and Bhandari, 2008)

reflectance accessory in transmittance mode. We used a standard resolution of 4 cm^{-1} and recorded 50 scans per sample. In addition to the nine faceted samples, two slices (one from the previous production and one from the new production) with parallel surfaces were prepared for FTIR analysis; both measured 10.06 × 8.06 × 4.75 mm.

Results and Discussion. *Physical and Optical Properties.* The physical and optical characteristics of the new Mexifire synthetic fire opals are given in table 1, together with the Mexifire properties reported in Choudhary and Bhandari (2008) and those of natural fire opal. Most of the samples we examined for the current study were brownish orange; only one was orangy brown (again, see figure 1). The samples exhibited even coloration and good transparency under normal lighting conditions, but (as with the earlier product) they appeared slightly turbid when viewed with a fiber-optic light (figure 2). When the specimens were rotated and viewed from different directions, the color appeared to be concentrated toward the center.

The most significant development with these products was the fact they had higher RI and SG values than the Mexifire synthetics studied previously. All the new samples yielded consistent RI and SG readings of 1.470 and 2.19, respectively, which are closer to those of their natural counterparts (again, see table 1). Simoni et al. (2010) reported RI values for natural fire opal from Bemia, Madagascar, of 1.440–1.460 and SG values of 2.15–2.38. The SG values of these new Mexifire synthetics clearly overlap those of the fire opals from Madagascar, though the RI values, while close to natural fire opals, are sufficiently higher to allow

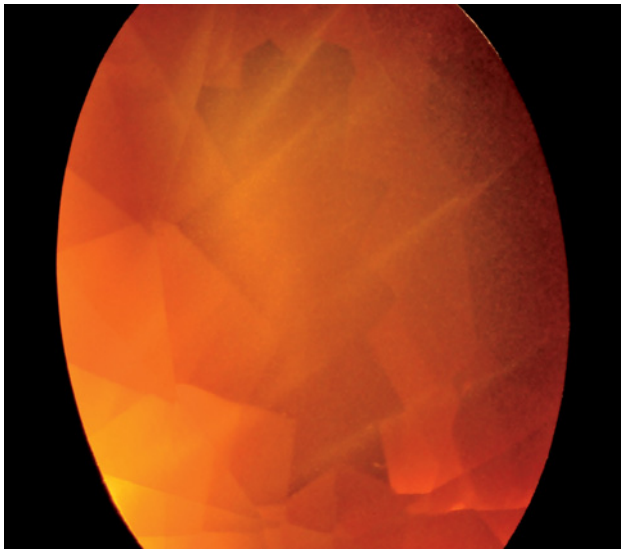

Figure 2. The turbid zones observed in almost every Mexifire sample remain an identifying criterion. Photomicrograph by G. Choudhary, fiber-optic illumination; magnified 15×.

a clear distinction. However, because there are minute variations in the calibration of refractometers of different makes and models, one must be very careful when using RI to separate natural from synthetic fire opals.

Microscopic Features. In addition to the zoned turbidity, these samples displayed fine pinpoints scattered throughout (figure 3), like the earlier product (Choudhary and Bhandari, 2008). These pinpoints were clearly seen with fiber-optic illumination, but they were only weakly visible with darkfield illumination. We could not resolve the exact nature of the pinpoints with the instruments we used. Although similarly scattered flake-like inclusions have been seen previously in natural opals, and Gübelin and Koivula (2005) mentioned tiny grains of pyrite scattered throughout one stone, we did not find any reports of such "pinpoint" inclusions in natural opal.

EDXRF Analysis. As was reported for the earlier material in Choudhary and Bhandari (2008), only Si, Fe, and Ca were detected in the new Mexifire synthetic fire opals. There were no additional elements. Gaillou et al. (2008) reported Al as a major impurity in natural opals; however, we did not detect any Al in the natural samples we studied for the previous article or received for identification at the laboratory over the years. In our samples, we recorded the same results for both the natural and the synthetic opals.

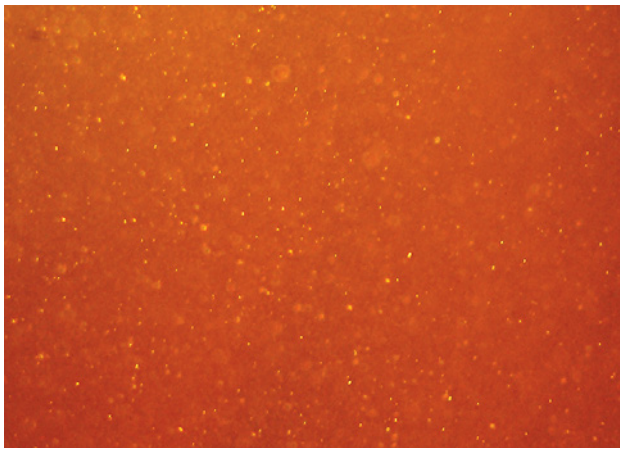

Figure 3. The exact nature of the scattered pinpoints in the Mexifire material could not be resolved at 80× magnification. Photomicrograph by G. Choudhary, fiber-optic illumination.

FTIR Analysis. The IR spectra of the new Mexifire product were quite different from those of either natural fire opal (studied in the previous article or at the Gem Testing Laboratory in Jaipur) or the earlier synthetic product. All nine samples displayed a weak hump at ~5440 cm^{-1}, a sharp peak with a shoulder ~4520 cm^{-1}, an absorption band in the 4000–3250 cm^{-1} region, a weak feature at 2652 cm^{-1}, and complete absorption of wavelengths below 2400 cm^{-1}.

The earlier version of Mexifire had an absorption band in the 5350–5000 cm^{-1} region; this feature also consisted of a series of sharp peaks, depending on the transmission. A hump was observed in the 4600–4300 cm^{-1} range, often with small peaks (a feature absent in some natural opals, including fire opal). The detector was saturated by strong absorption below ~4000 cm^{-1}. The absorption at ~5440 cm^{-1} in the new Mexifire product is attributed to O-H stretching/vibration, the peak at ~4520 cm^{-1} is due to a combination of O-H stretching and Si-O-H bending, and the absorption band in the 4000–3250 cm^{-1} region is due to the presence of O-H groups (Yamagishi et al., 1997).

These differences in the IR spectra reflect the lower water content of the new type of Mexifire opal. Although some of the differences could also have been due to variations in sample thickness (i.e., thicker samples would have greater absorbance and vice versa), the fact that the samples previously studied were smaller (0.23–3.50 ct) than those in the present study (3.40–4.40 ct) negates this possibility. To confirm this, we cut slices of equal thickness (4.75 mm) from one piece each of old and new Mexifire opal and polished two parallel faces; the IR spectra of

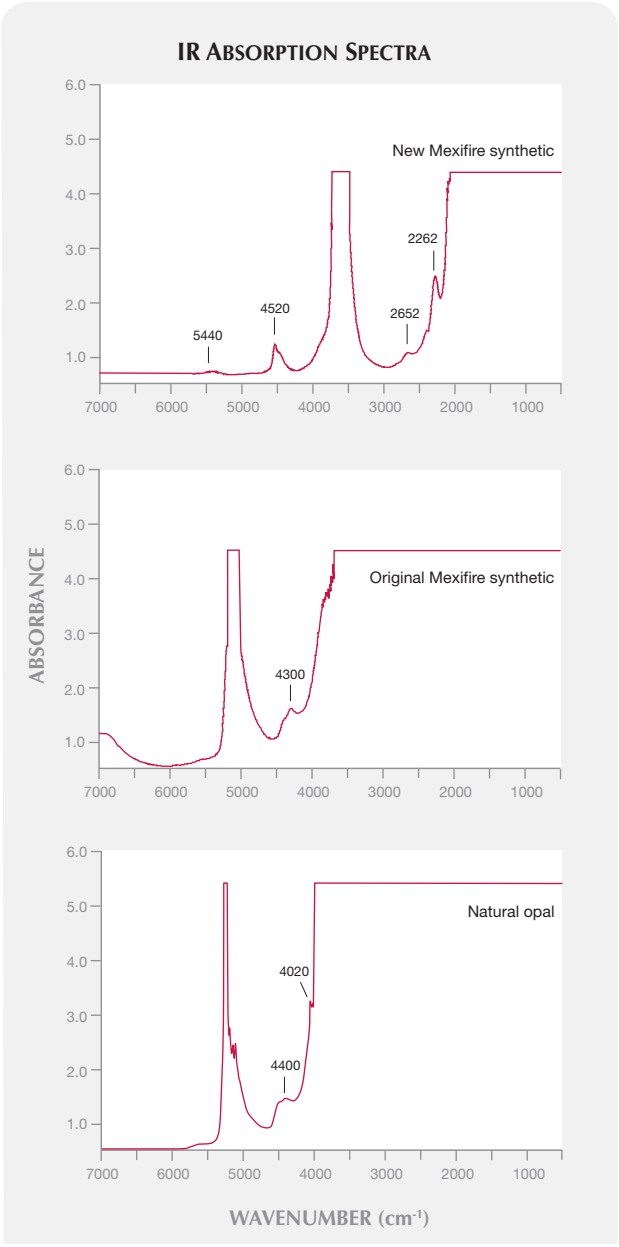

Figure 4. This IR spectrum of a slice of the new Mexifire synthetic opal (top; 4.75 mm thick) is quite different from that of a slice from the previous generation (center; 4.75 mm) and from natural fire opals (bottom; 0.6–4.0 ct) studied by the authors in the past.

both slices were similar to the spectra described above for faceted samples (figure 4). However, for the slice of new Mexifire synthetic opal, a sharp peak at 2262 cm^{-1} was resolved and the area of complete absorption was reduced to 2100 cm^{-1}. The other features and peaks remained unchanged between the slice and faceted samples of the new product.

It should be noted, though, that some natural opals from Ethiopia show absorption features similar to those seen in this new Mexifire product (E. Gaillou, pers. comm., 2010). Therefore, it does not appear that IR spectra provide a conclusive means of differentiating these new Mexifire opals from natural opal.

Conclusions. The higher RI and SG values of these new Mexifire synthetic fire opals will make their identification more difficult. The microscopic features are unchanged, however, and the fine pinpoints scattered throughout remain helpful in identifying the synthetic product. IR spectra, when used carefully, can offer some identification criteria, although similar absorption features have been seen in some natural opals from Ethiopia. The changes in the RI and SG values correlate with changes seen in the IR spectra as a result of a lower water content. Since the water content in these synthetics can be controlled, we anticipate additional changes in the properties of future product. Work is ongoing to further characterize this material.

ABOUT THE AUTHORS

Mr. Bhandari is a chemical engineer and owner of Rhea Industries (Jaipur, India), the manufacturer of Mexifire. Mr. Choudhary (gtl@gjepcindia.com) is deputy director of the Gem Testing Laboratory in Jaipur.

ACKNOWLEDGMENTS

The authors acknowledge Dr. Eloïse Gaillou of the Smithsonian Institution, Washington, DC, for her valuable input on the manuscript.

REFERENCES

Choudhary G., Bhandari R. (2008) A new type of synthetic fire opal: Mexifire. *G&G*, Vol. 44, No. 3, pp. 228–233.

Gaillou E., Delaunay A., Rondeau B., Bouhnik-Le Coz M., Fritsch E., Cornen G., Monnier C. (2008) The geochemistry of opals as evidence of their origin. *Ore Geology Reviews*, Vol. 34, pp. 113–126.

Gübelin E.J., Koivula J.I. (2005) *Photoatlas of Inclusions in Gemstones*, Vol. 2. Opinio Publishers, Basel, Switzerland.

Simoni M., Caucia F., Adamo I., Galinetto P. (2010) New occurrence of fire opal from Bemia, Madagascar. *G&G*, Vol. 46, No. 2, pp. 114–121.

Webster R. (1994) *Gems: Their Sources, Descriptions and Identification*, 5th ed. Edited by P. G. Read, Butterworth-Heinemann, Oxford, UK.

Yamagishi H., Nakashima S., Ito Y. (1997) High temperature infrared spectra of hydrous microcrystalline quartz. *Physics and Chemistry of Minerals*, Vol. 24, pp. 66–74.

The information you need... at a glance!
Perfect for home or office use.

LAMINATED REFERENCE CHARTS

- HPHT-Grown Synthetic Diamonds
- World Gem Localities **NEW!**
- Gem Treatments
- GIA Diamond Cut Grading System
- Pink Diamond Color Chart
- Recognizing Be-Diffused Rubies and Sapphires

Also available:

- Separation of Natural and Synthetic Diamonds
- Identification of Filled Diamonds

Only $16.95 (plus shipping)
Buy two or more and SAVE!

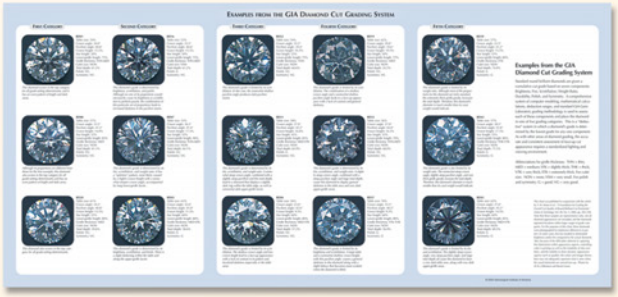

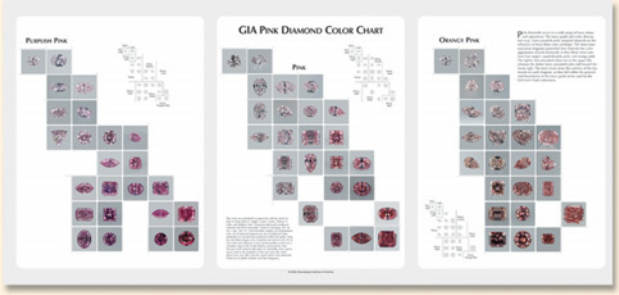

GEMS & GEMOLOGY®

Order Yours Today!

Visit store.gia.edu

Or call 800-421-7250, ext. 7142
(outside the U.S., 760-603-4000, ext. 7142).

Rapid Communications

A Study of the Gems in a Ciborium From Einsiedeln Abbey

Stefanos Karampelas, Marie Wörle, Katja Hunger, Hanspeter Lanz, Danilo Bersani, and Susy Gübelin

The gemstones that adorn a late-16th-century ciborium from Einsiedeln Abbey in Einsiedeln, Switzerland, were investigated by nondestructive gemological methods and EDXRF and Raman spectroscopy at the Collections Center of the Swiss National Museum. The ciborium is decorated with 17 colored stones: 10 almandine garnets, four grossular garnets, and three sapphires. Inclusions in the sapphires and a historic description of the piece suggest a Sri Lankan origin for the gems.

A group of four sacred objects belonging to the treasury of Einsiedeln Abbey, an important Benedictine monastery in Einsiedeln, Switzerland, were recently loaned to the Swiss National Museum in Affoltern am Albis, for identification of the materials used in their construction. This article presents the results of the investigation of the oldest object, a late-16th-century ciborium (a container for storing the consecrated host from a Mass; figure 1).

Einsiedeln Abbey dates from the 10th century. It is dedicated to Our Lady of the Hermits and is a destination on a major Roman Catholic pilgrimage, the Way of Saint James. The ciborium was crafted by Nikolaus Wickart, an established goldsmith, in Zug about 1592. Its construction cost 300 krones (equivalent to 975 g of gold), paid for by donations from Maximilian III of Habsburg and numerous other contributors. The main body of the ciborium depicts the 12 apostles of Jesus Christ, while the lid illustrates the passion of Christ and is where the Christogram *IHS* is engraved. On the underside of the ciborium, there are several stamps, including those of Maximilian III, Wickart, and Einsiedeln Abbey. For more information regarding the history of the ciborium, as well as a stylistic and iconographic description, see Distelberger and Lanz (2009).

The ciborium could not be removed from the Swiss National Museum laboratory for security reasons; thus, all testing took place there. The results were compared with the observations made by Father Eustache Tonassini from 1794 to 1798, during the documentation of the treasures of Einsiedeln Abbey (figure 2). Father Tonassini mentioned that all the stones and the gold had an "oriental" origin.

Materials and Methods. Only nondestructive means could be used to examine this artifact, and all the investigators wore cotton gloves to avoid causing damage. Microscopic examinations were performed on all gems using a Zeiss Stemi 2000-CS binocular microscope equipped with a fiber-optic light source and a camera. However, the object was difficult to handle under the microscope, which impacted the quality of the photos. Fluorescence reactions to standard long-wave (366 nm) and short-wave (254 nm) UV radiation were observed on all stones with an 8 watt UV lamp from System Eickhorst UV. On six stones, where the geometry of the object permitted, we performed semiquantitative chemical analy-

See end of article for About the Authors and Acknowledgments.
Gems & Gemology, Vol. 46, No. 4, pp. 292–296.

sis by energy-dispersive X-ray fluorescence (EDXRF) with an Edax Eagle III XXL micro-analyzer. This instrument has a large sample chamber and is equipped with a lens for micro-measurements (spot size ~50 m). A rhodium tube was used for the analysis, under the following conditions: no filter, 20 kV, 100 µA, a livetime of 200 seconds per measurement point, and 30 points per measurement area.

Conclusive identifications were made by taking Raman spectra of all the gems and comparing them to the Gübelin Gem Lab's reference spectra as well as those in the RRUFF project (http://rruff.info) and other published references. Spectra were obtained with a Horiba Jobin Yvon (LabRam Aramis) spectrometer coupled to an Olympus metallurgical microscope. As all stones were difficult to access, we used an additional L-shaped lens (magnification 30×) to take the spectra (figure 3) and a camera for adequate positioning of the beam. Measurements were carried out using excitation wavelengths of 532 nm (Nd:YAG laser), 633 nm (He:Ne laser), and 785 nm (diode laser). Laser power was 50 mW, with a 60 second acquisition time, at various resolutions (2–4 cm^{-1}) in the range from 200 to 2000 (sometimes up to 4000) cm^{-1}. To confirm the results, we took measurements on at least two different points of each gemstone.

Results and Discussion. The ciborium contains 17 colored stones—10 pinkish red, four orange, and three light blue—mounted in metal settings that are attached to the body and lid. Its total weight is 1,350 g, and its height is 33 cm (about 13 in.). All the gems are held in closed-back settings; thus, their faceting arrangements were identified only from the crown. They were polished in near-round, rectangular, octagonal, and cushion shapes (all the light blue stones had slightly domed tables; e.g., figure 4), with one step of parallel facets on the crown. Table 1 provides a summary of the sizes, colors, and shapes/cuts. No indications of doublets, imitations, glasses, or synthetics were observed with magnification.

Raman spectroscopy demonstrated that all 10 red stones were Al-garnets. Father Tonassini had described these stones as rubies. All four orange stones were Ca-garnets. These were identified by Father Tonassini as "hyacinth" (an archaic term for red-orange-yellow zircon). Although some slight differences in the spectra of the 10 Al- and four Ca-garnets were observed (reflecting differences in composition), all were close to almandine and grossular, respectively (see table DD-1 and figure DD-1 in the *G&G* Data Depository at gia.edu/gandg; for more information regarding the semiquantitative analysis of garnets, see Smith [2005] and Bersani et al. [2009] and references therein).

Figure 1. This gold and gem-set ciborium (33 cm high), which dates from the end of the 16th century, is part of the treasures of Einsiedeln Abbey in Switzerland. Photo by Donat Stuppan, Swiss National Museum.

The blue stones all showed the main characteristic vibration band of corundum at about 415 cm^{-1}. Additionally, bands at 1400 and 1370 cm^{-1} were observed with 633 nm excitation; these are the characteristic Cr photoluminescence emission bands of corundum (see figure DD-2 in the *G&G* Data

Figure 2. The ciborium (left) is mentioned in an 18th century inventory (right) prepared by Father Eustache Tonassini. Photos by Hanspeter Lanz, Swiss National Museum (left), and Franz Kälin, Einsiedeln Abbey (right).

Depository). Father Tonassini correctly identified these stones as sapphires.

The EDXRF results for the six stones analyzed were in agreement with the Raman data. Different points on the metal were also analyzed and found to contain 82–85% gold, 7–8% silver, and 6–9% copper. No evidence was observed that any of the stones had been removed after they were originally set.

All the garnets were inert to UV radiation. The three sapphires fluoresced faint orange-yellow to long-wave UV and faint orange to short-wave UV. With magnification, the almandines showed mainly rutile needle–like inclusions and zircons, while the grossulars contained negative crystals and healed

Figure 3. A Raman spectrometer with an L-shaped lens was used to take spectra on the mounted ciborium gems (inset), which were difficult to access with conventional equipment. All the stones were conclusively identified with this instrument. Photos by Michael Wörle.

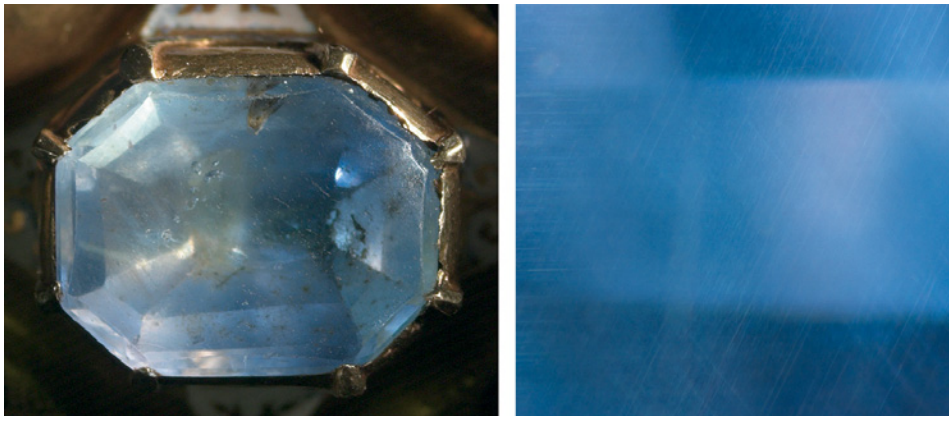

Figure 4. Sapphire KS1 (see table 1), like the other sapphires in the ciborium, has a slightly domed table (left; stone is 10.4 mm wide) and rutile needle-like inclusions (right; field of view ~90 μm). Photos by Marie Wörle.

fissures. In the sapphires we saw mainly rutile needles (figure 4, right), fissures, negative crystals, and black particles. Taking into account when these stones were set and the oriental origin mentioned by Father Tonassini, Sri Lanka is the most probable source. The inclusions in these sapphires are consistent with sapphires from that island nation. At the time, garnets were also known from the same region (as well as from India). However, more research with other methods and reference materials would be necessary to build a comprehensive database with which to compare these samples.

Conclusion. The Einsiedeln ciborium is decorated with 17 colored stones, all of which have old cuts and are natural. We saw no evidence that any were doublets or imitations, contrary to studies on other historical objects (e.g., Hänni et al., 1998, and references therein). Using Raman spectroscopy, we found that 10 were almandine (identified by Father Tonassini as rubies), four grossular (originally identified as hyacinths) and three were sapphires (identified by Father Tonassini as such). Further research would be needed to confirm the geographic origins, though Sri Lanka is possible.

TABLE 1. Characteristics of the colored gems set in the ciborium from Einsiedeln Abbey.

Number[a]	Color	Shape/Cut	Measurements (crown; mm)	Identification	
				This study	Tonassini (1794–98)
CN1S1	Pinkish red	Modified rectangular/step	5.9 × 5.6	Almandine	Ruby
CN1S2	Pinkish red	Near round/step	5.4 × 5.2	Almandine	Ruby
CN1S3	Pinkish red	Near round/step	5.2 × 4.9	Almandine	Ruby
CN1S4	Pinkish red	Modified rectangular/step	3.7 × 3.5	Almandine	Ruby
CN1S5	Pinkish red	Modified rectangular/step	4.4 × 3.4	Almandine	Ruby
CN2S1	Orange	Modified rectangular/step	7.4 × 6.3	Grossular	Hyacinth
CN2S2	Pinkish red	Near round/step	5.5 × 5.2	Almandine	Ruby
CN2S3	Pinkish red	Near round/step	5.2 × 4.7	Almandine	Ruby
CN2S4	Orange	Near round/step	5.5 × 5.4	Grossular	Hyacinth
CN2S5	Pinkish red	Oval/step	5.1 × 4.7	Almandine	Ruby
CN2S6	Pinkish red	Modified rectangular/step	7.6 × 6.0	Almandine	Ruby
KS1	Light blue	Octagonal/step	10.4 × 9.0	Sapphire	Sapphire
KS2	Orange	Modified rectangular/step	10.0 × 7.3	Grossular	Hyacinth
KS3	Light blue	Octagonal/step	10.1 × 8.0	Sapphire	Sapphire
KS4	Orange	Octagonal/step	13.3 × 10.0	Grossular	Hyacinth
KS5	Light blue	Octagonal/step	12.4 × 9.7	Sapphire	Sapphire
KS6	Pinkish red	Oval/cabochon	13.9 × 10.7	Almandine	Ruby

[a]*The numbering of the stones begins from the stamp of Einsiedeln and proceeds clockwise: C indicates the lid, K the body, and S the stone. On the lid, two levels are present: N1 for the upper level and N2 for the lower. For example, stone CN2S5 is in the lid, in the second level, the fifth stone clockwise from the Einsiedeln stamp.*

ABOUT THE AUTHORS

Dr. Karampelas (s.karampelas@gubelingemlab.ch) is a research scientist and Mrs. Gübelin is a gemologist at Gübelin Gem Lab, Lucerne, Switzerland. Dr. Wörle is head of conservation research, Mrs. Hunger is an archeometrist, and Dr. Lanz is a curator at the Swiss National Museum, Zurich. Dr. Bersani is a researcher in the physics department at the University of Parma, Italy.

ACKNOWLEDGMENTS

The authors thank Dr. Rudolf Distelberger (Kunsthistorisches Museum of Vienna, Austria) and the priests of the Benedictine Abbey of Einsiedeln for facilitating access to the ciborium.

REFERENCES

Bersani D., Andó S., Vignola P., Moltifiori G., Marino I.-G., Lottici P.-P., Diella V. (2009) Micro-Raman spectroscopy as a routine tool for garnet analysis. *Spectrochimica Acta Part A*, Vol. 73, No. 3, pp. 484–491.

Distelberger R., Lanz H. (2009) Gold für das seelenheil kostbare weihegeschenke an die Madonna von Einsiedeln aus der Zeit um 1600 [Gold for salvation: Votive offerings to the Madonna of Einsieldeln from around 1600]. *Journal of Swiss Archaeology and Art History*, Vol. 66, No. 4, pp. 193–262 [in German].

Hänni H., Schubiger B., Kiefert L., Häberli S. (1998) Raman investigations on two historical objects from Basel Cathedral: The Reliquary Cross and Dorothy Monstrance. *G&G*, Vol. 34, No. 2, pp. 102–113.

Smith D.C. (2005) The RAMANITA method for non-destructive and in situ semi-quantitative chemical analysis of mineral solid-solutions by multidimensional calibration of Raman wavenumber shifts. *Spectrochimica Acta Part A*, Vol. 61, No. 10, pp. 2299–2314.

Tonassini P.E. (1794–1798) Beschreibung des Kirchenschatzes Teil I [Description of the church treasure Part I]. Archive of Einsiedeln Abbey, Einsiedeln, Switzerland.

What's *missing* from your collection?

Spring–Winter 2009

Spring 2006
"Paraíba"-type Tourmaline from Brazil, Nigeria, and Mozambique: Chemical Fingerprinting by LA-ICP-MS
Identification and Durability of Lead Glass–Filled Rubies
Characterization of Tortoise Shell and Its Imitations

Summer 2006
Applications of LA-ICP-MS to Gemology
The Cullinan Diamond Centennial
The Effects of Heat Treatment on Zircon Inclusions in Madagascar Sapphires
Faceting Transparent Rhodonite from New South Wales, Australia

Fall 2006—Special Issue
Proceedings of the 4th International Gemological Symposium and GIA Gemological Research Conference

Winter 2006
The Impact of Internal Whitish and Reflective Graining on the Clarity Grading of D-to-Z Diamonds at the GIA Laboratory
Identification of "Chocolate Pearls" Treated by Ballerina Pearl Co.
Leopard Opal from Mexico
The Cause of Iridescence in Rainbow Andradite from Japan

Spring 2007
Pink-to-Red Coral: Determining Origin of Color
Serenity Coated Colored Diamonds
Trapiche Tourmaline from Zambia

Summer 2007
Global Rough Diamond Production since 1870
Durability Testing of Filled Diamonds
Chinese Freshwater Pearl Culture
Yellowish Green Diopside and Tremolite from Tanzania
Polymer-Impregnated Turquoise

Fall 2007
The Transformation of the Cultured Pearl Industry
Nail-head Spicule Inclusions in Natural Gemstones
Copper-Bearing Tourmalines from New Deposits in Paraíba State, Brazil
Type Ia Diamond with Green-Yellow Color Due to Ni

Winter 2007
Latest CVD Synthetic Diamonds from Apollo Diamond Inc.
Yellow Mn-Rich Tourmaline from Zambia
Fluorescence Spectra of Colored Diamonds
An Examination of the Napoleon Diamond Necklace

Spring 2008
Copper-Bearing (Paraíba-type) Tourmaline from Mozambique
A History of Diamond Treatments
Natural-Color Purple Diamonds from Siberia

Summer 2008
Emeralds from Byrud (Eidsvoll), Norway
Creating a Model of the Koh-i-Noor Diamond
Coated Tanzanite
Coloring of Topaz by Coating and Diffusion Processes

Fall 2008
Identification of Melee-Size Synthetic Yellow Diamonds
Aquamarine, Maxixe-Type Beryl, and Hydrothermal Synthetic Blue Beryl
A New Type of Synthetic Fire Opal: Mexifire
The Color Durability of "Chocolate Pearls"

Winter 2008
Color Grading "D-to-Z" Diamonds at the GIA Laboratory
Rubies and Sapphires from Winza, Tanzania
The Wittelsbach Blue

Spring 2009
The French Blue and the Hope: New Data from the Discovery of a Historical Lead Cast
Gray-Blue-Violet Hydrogen-Rich Diamonds from the Argyle Mine
Hackmanite/Sodalite from Myanmar and Afghanistan
Pink Color Surrounding Growth Tubes and Cracks in Tourmalines from Mozambique
Identification of the Endangered Pink-to-Red Stylaster Corals by Raman Spectroscopy

Summer 2009
Celebrating 75 Years of *Gems & Gemology*
The "Type" Classification System of Diamonds
Spectral Differentiation Between Copper and Iron Colorants in Gem Tourmalines
Andalusite from Brazil
Peridot from Sardinia, Italy

Fall 2009
Characterization of "Green Amber"
Crystallographic Analysis of the Tavernier Blue
"Fluorescence Cage": Visual Identification of HPHT-Treated Type I Diamonds
Ammolite Update
Polymer-Filled Aquamarine
Yellow-Green Haüyne from Tanzania
Aquamarine from Masino-Bregaglia Massif, Italy

Winter 2009
Ruby and Sapphire Production and Distribution: A Quarter Century of Change
Cutting Diffraction Gratings to Improve Dispersion ("Fire") in Diamonds
Chrysoprase and Prase Opal from Haneti, Central Tanzania
Demantoid from Val Malenco, Italy

For a complete list of articles from 1981 forward, visit www.gia.edu/gandg.

GEMS & GEMOLOGY®

The Quarterly Journal That Lasts A Lifetime

Now Available Online:

All Articles and Issues 1981–2010

Get PDF Articles
gia.metapress.com
Electronic (PDF) versions of all articles from Spring 1981 forward are available as part of *Gems & Gemology* Online.

Order Print and PDF Back Issues at store.gia.edu
or Call Toll Free 800-421-7250 ext. 7142
or 760-603-4000 ext. 7142
Fax 760-603-4070

E-Mail gandg@gia.edu
or write to
Gems & Gemology
PO Box 9022, Carlsbad, CA
92018-9022, USA

Complete volumes of 1992–2010 print back issues are available, as are limited issues from 1985–1991.

10% discount for GIA Alumni and active GIA students.

Order Your BACK ISSUES CHARTS & BOOKS Today!

DIAMOND

Lab Sees Increasing Number of Large HPHT-Treated Type IIa Diamonds

It is well known that natural type IIa brown diamonds can be decolorized through annealing under high pressure and high temperature (HPHT). Recent studies have shown that the annealing process removes vacancy clusters, which are the cause of brown coloration. While not all brown diamonds are suitable for decolorization, gem labs frequently see colorless to near-colorless HPHT-treated type IIa diamonds, with most under 5 ct. In recent weeks, however, the New York lab has examined an increasing number of relatively large HPHT-treated type IIa diamonds, many of them over 5 ct and some 10+ ct.

One example is the round-cut 18.12 ct (17.11 × 17.04 × 10.24 mm) diamond in figure 1, which was color graded F. While many HPHT-treated diamonds have no observable internal features except for some graining, this stone contained a tiny hexagonal graphite inclusion surrounded by a tension fracture (figure 1, right). It is very likely that this inclusion was formed due to graphitization of the host diamond; its presence and the tension fracture are good indications that this stone was HPHT treated. Careful spectroscopic analysis provided confirmation of HPHT treatment.

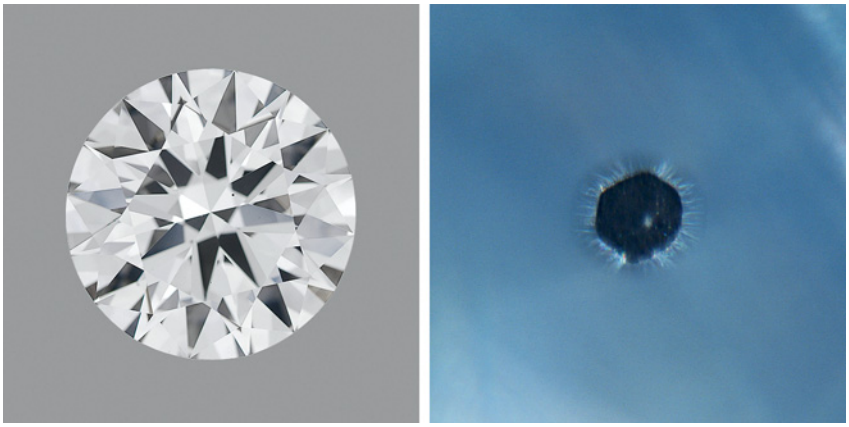

Figure 1. The New York lab has been seeing a greater number of relatively large HPHT-treated type IIa diamonds, such as this 18.12 ct round brilliant (left). The hexagonal graphite inclusion it contained (right, magnified 112×) is a good indication of this treatment.

HPHT annealing involves a higher risk of damaging the diamond than other treatment techniques, so it is somewhat unusual to see it applied to such large stones. It is not clear if this increase in the number of large treated diamonds is a short-term phenomenon or the beginning of a trend. One possible explanation is that more of the suitable starting material has become available in the market.

Wuyi Wang

One Dapper Diamond

Gemological microscopy occasionally reveals unusual inclusions that stimulate the imagination and remind the viewer of landscapes, insects, flowers, and the like. An unlikely new source for playful imagery is the DTC DiamondView, which reveals a diamond's growth patterns by exposing the stone to intense short-wave ultraviolet (UV) radiation.

The Carlsbad laboratory recently examined an ~1 ct Fancy Deep brownish greenish yellow round brilliant to determine its origin of color. Initial examination with a microscope revealed only a few small clouds, and Fourier-transform infrared (FTIR) spectroscopy indicated that the diamond

Editors' note: All items were written by staff members of the GIA Laboratory.

GEMS & GEMOLOGY, *Vol. 46, No. 4, pp. 298–307.*

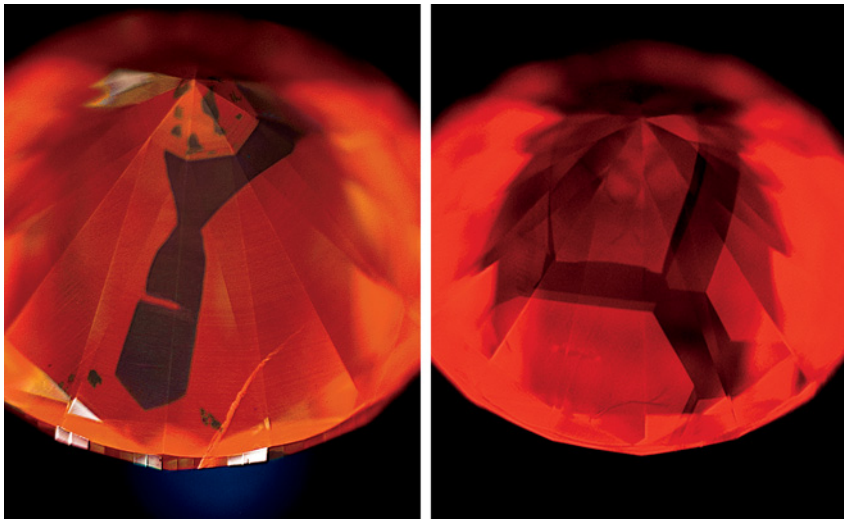

Figure 2. The DiamondView image at left, which depicts a pattern reminiscent of a necktie, reveals a pseudo-cuboctahedral growth structure unique to some natural type Ib diamonds. HPHT-grown synthetic diamonds can show similar structures (right), but the patterns are more angular and symmetrical due to their controlled artificial growth conditions. Fields of view ~7 mm.

was type Ib. Since almost all HPHT-grown synthetic diamonds are type Ib, the laboratory often examines the fluorescence patterns of type Ib stones with the DiamondView when other gemological testing proves insufficient to establish natural or synthetic origin. However, when this stone was placed in the DiamondView, we were amused to see a fascinating geometric growth pattern that resembled a man's necktie worn around the culet, complete with tie clip (figure 2, left).

This fluorescence image reveals a pseudo-cuboctahedral growth structure that is unique to some natural type Ib diamonds and is proof that this stone is natural. It is similar to, but not to be confused with, the cuboctahedral growth structure seen in synthetic diamonds (figure 2, right), which is more structured and has a predictable symmetry and geometry.

DiamondView imagery is becoming more widely published because of the intriguingly complex and even beautiful compositions of pattern and color that can be seen in both natural and synthetic diamonds. Such images offer yet another perspective on the fascinating micro-world of gems.

Laura L. Dale

Figure 3. A pink coating was detected on this Very Light pink heart shape (1.50 ct) and Faint pink pear shape (1.68 ct). The diamonds initially appeared equivalent to Fancy pink and Fancy Light pink, respectively (see insets for approximate color representations).

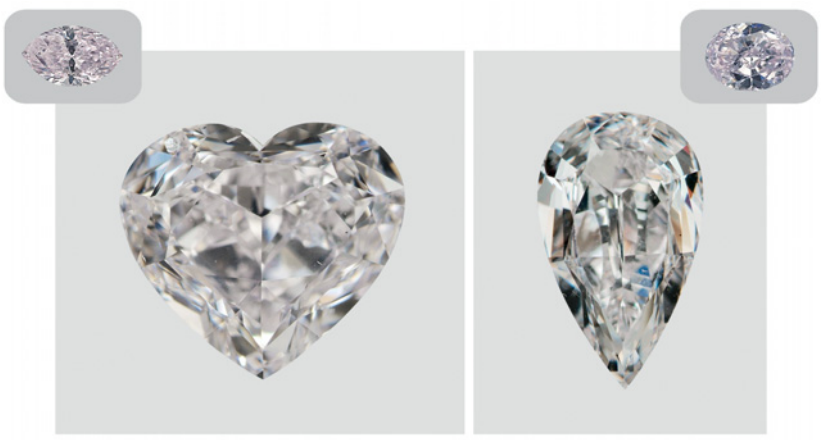

Pale Pink Diamonds, Coated Fancy Pink

Numerous reports have described diamonds that were coated pink, by techniques ranging from the ancient practice of "painting" a stone (e.g., Summer 1983 Lab Notes, pp. 112–113) to sophisticated thin-film coatings (e.g., A. H. Shen et al., "Serenity coated colored diamonds: Detection and durability," Spring 2007 *G&G*, pp. 16–34). Recently, the Carlsbad lab received a 1.50 ct heart shape and a 1.68 ct pear shape (figure 3) that initially appeared the equivalent of Fancy pink and Fancy Light pink, respectively. Their FTIR and photoluminescence (PL) spectra were consistent with type IIa pink diamonds. However, their Vis-NIR spectra (taken at low temperature) were anomalous for such stones, which show a broad band centered at 550 nm. Instead, the spectra of both displayed peaks centered at ~505 and 540 nm (e.g., figure 4, top trace). Additional exposure to the liquid-nitrogen bath decreased the intensity of these absorption peaks (e.g., figure 4, middle trace).

Microscopic observation revealed a nearly imperceptible trace of reddish residue on a natural of one of the diamonds. After both were thoroughly cleaned in soapy water and, ultimately, acetone, they were noticeably lighter in color, indicating they had been treated with a coating that was removed by such a solvent.

The cleaned diamonds now

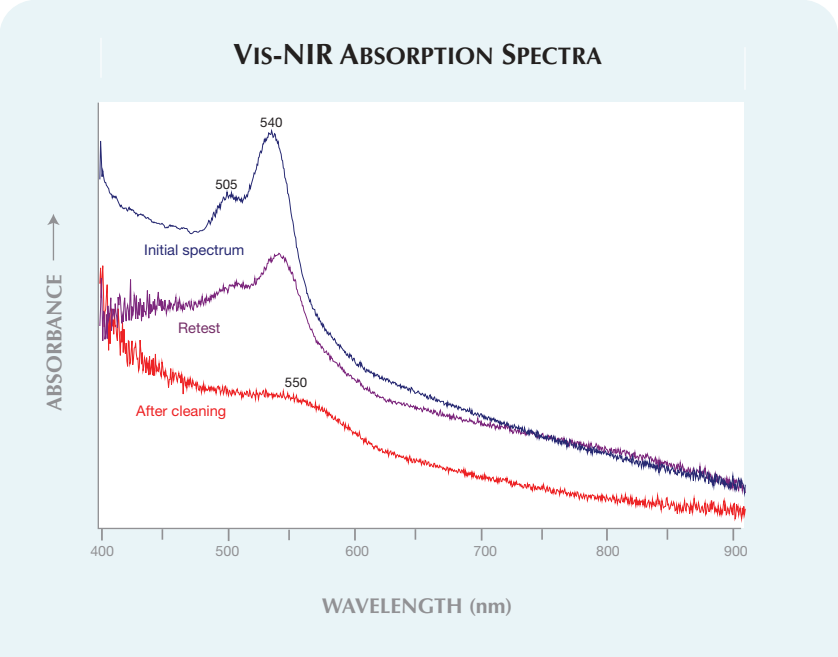

Figure 4. The initial Vis-NIR spectrum for the 1.68 ct pear shape (top) was not consistent with a type IIa pink diamond and was weaker when retested after additional exposure to a liquid-nitrogen bath (center). After all traces of the coating were removed with soapy water and acetone, the spectrum showed the expected 550 nm band (bottom). Per standard procedure, all Vis-NIR spectra were collected at liquid-nitrogen temperature.

showed the expected Vis-NIR spectra (e.g., figure 4, bottom trace). When they were color graded a second time, without the coating, the heart shape was Very Light pink and the pear shape Faint pink—a decrease of several color grades for both. Despite a slight reduction in some broad fluorescence bands, the PL spectra showed no changes. This was not surprising, as surface treatments are usually not detectable with analytical methods that penetrate deep into the diamond, such as FTIR and PL (again, see Shen et al., 2007).

The treatment was undoubtedly meant to intensify the color of these pale pink diamonds, likely with the knowledge that the coating would not be permanent but the hope it would at least last through the grading process. The coating generally withstood normal handling with tweezers and cleaning with a gem cloth, and some was still present after exposure to the liquid-nitrogen bath. However, a simple but thorough cleaning with soapy water removed most of the coating, and acetone removed the rest.

Sally Eaton-Magaña

SYNTHETIC DIAMOND

Intense Purplish Pink HPHT-Grown/Treated Synthetic Diamond

Many of the pink-to-red diamonds currently in the jewelry market owe their color to artificial treatment. This usually involves natural starting material and multiple treatment processes, including HPHT annealing combined with irradiation and annealing at relatively low temperatures. HPHT annealing can be used to create isolated nitrogen, followed by irradiation to create vacancies, and low-temperature annealing to create suitable concentrations of nitrogen-vacancy (NV) centers, which are responsible for the pink-to-red color (e.g., Winter 2005 Lab Notes, pp. 341–343). This technique has also been applied to HPHT-grown synthetic diamonds since the 1990s (e.g., T. M. Moses et al., "Two treated-color synthetic red diamonds seen in the trade," Fall 1993 *G&G*, pp. 182–190). However, it appears that some HPHT-grown synthetic diamonds can be produced with very low controlled nitrogen concentrations for a more intense color appearance with after-growth treatments.

The 0.20 ct round brilliant in figure 5 was color graded Intense purplish pink at the New York laboratory. Although there were few internal inclusions, it had a large surface-reaching fracture with a cavity on the table and crown facets. It displayed strong color zoning, with zones of intense pink color, and fluoresced strong orangy red to both long- and short-wave UV radiation.

Our initial observations suggested that this might be one of the multiply treated natural diamonds described above. The mid-IR spectrum showed a type Ia diamond with a very low nitrogen concentration. The UV-Vis spectrum, taken with a custom-made high-resolution UV-Vis spectrometer, indicated that the pink color was caused by strong NV centers at 575

Figure 5. This 0.20 ct Intense purplish pink round brilliant proved to be a treated synthetic diamond.

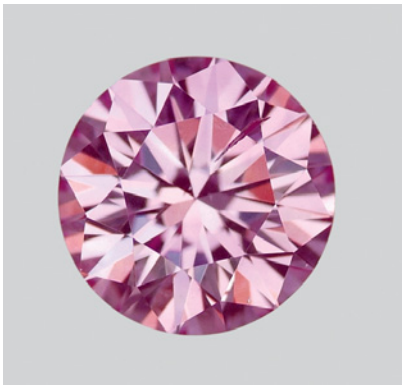

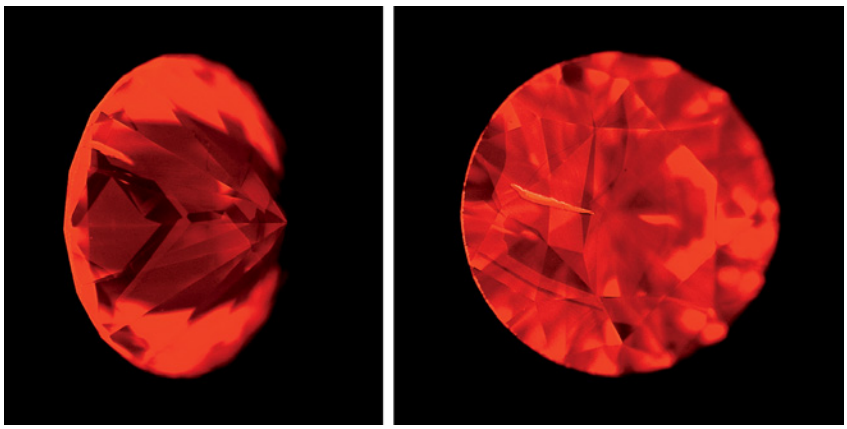

Figure 6. In the DiamondView, the round brilliant in figure 5 showed a subtle synthetic growth structure, which was more obvious on the pavilion (left).

and 637 nm. These strong vacancy centers can be produced by HPHT treatment, and their intensity is related to the amount of nitrogen in the diamond. Other features in the visible spectrum, such as a strong peak at 595 nm, were indicative of artificial irradiation. All these observations confirmed that an irradiation/annealing treatment was involved in introducing the NV centers, which are responsible for the attractive pink color. These features are very similar to those observed in natural diamonds that have undergone multiple treatments.

However, careful examination with the DTC DiamondView revealed a subtle growth structure that was indicative of an HPHT-grown synthetic diamond. Seen face-up, the unusual growth zoning was suspicious but not definitive, while the pattern seen on the pavilion showed obvious multi-sectoral synthetic growth (figure 6). It appeared that this synthetic diamond was carefully grown with a very low concentration of nitrogen (~1 ppm), but enough to induce the high concentration of NV centers during post-growth treatments.

Care is needed to separate these types of synthetic pink-to-red diamonds from treated natural diamonds.

Paul Johnson

Large (4+ ct) Yellow-Orange HPHT-Grown Synthetic Diamond

Lab-grown diamonds have improved dramatically in recent years. In the Summer 2010 *G&G*, W. Wang and K. S. Moe reported on the first near-colorless chemical vapor deposition (CVD)-grown synthetic diamond over 1 ct identified by the New York laboratory (Lab Notes, pp. 143–144). Now we have examined a yellow-orange HPHT-grown synthetic diamond (figure 7) that is also notable for its large size and high quality.

The rectangular sample (9.07 × 8.54 × 5.98 mm) weighed 4.09 ct, making it the largest faceted synthetic diamond submitted to the GIA Laboratory for testing and grading to date. It was color graded Vivid yellow-orange and had notably even color distribution (color zoning is common in HPHT synthetic diamonds). Some strings of black pinpoint inclusions were seen with the microscope, and the clarity grade was VS_1, which is remarkable for a large synthetic diamond. Fluorescence images collected using the DiamondView showed typical synthetic growth sectors, with patterns of varying intensity and color. These features were more obvious when viewed through the pavilion than through the table.

The mid-IR absorption spectrum revealed a high concentration of predominantly A-form nitrogen. Also observed was a weak absorption at 1344 cm^{-1} from isolated nitrogen, which was responsible for the yellow-orange color. The UV-Vis absorption spectrum showed a gradual increase in absorption from ~570 nm to higher energies, a typical feature caused by isolated nitrogen. A moderately strong, sharp absorption at 793.6 nm, attributed to a Ni-related defect, was also recorded, and we observed a weak peak at 986.2 nm from the H2 defect.

The predominantly A-form nitrogen and the occurrence of the H2 optical center strongly suggested growth at a relatively high temperature. An advantage to high-temperature growth is that it limits the development of growth sectors other than {111}. As a result, the color appears more evenly distributed. This sample's size, clarity, and vivid, evenly distributed yellow-orange color were exceptional and demonstrate continued improvements in the HPHT growth technique.

Subsequently, Gemesis president and CEO Stephen Lux stated that this was the largest cut stone the company had produced (M. Graff, "Gemesis to sell lab-grown whites to consumers," *National Jeweler*, Nov. 24, 2010).

Wuyi Wang and Tom Moses

Figure 7. This 4.09 ct HPHT-grown synthetic diamond was clarity graded VS_1 and color graded Vivid yellow-orange.

Figure 8. This 0.30 ct Vivid blue round brilliant (left) was identified as an HPHT-grown synthetic diamond by the growth pattern displayed in the DiamondView (right). It contained a Si-related defect that usually occurs only in CVD synthetic diamonds and is believed to result from post-growth treatment.

Silicon-Vacancy Defect Found in Blue HPHT-Grown Synthetic Diamond

Gem-quality type IIb synthetic diamonds, which contain traces of boron and usually have a blue color, can be created by both HPHT and CVD growth processes. The Si-related lattice defect is widely considered an identifying feature of CVD synthetic diamond. At the New York lab, however, we recently tested an HPHT-grown synthetic type IIb diamond that contained this defect.

The 0.30 ct round brilliant (4.43 × 4.33 × 2.67 mm) was color graded Vivid blue (figure 8, left). Like other HPHT-grown synthetic diamonds, it contained some pinpoint inclusions and showed uneven color distribution along growth sectors that were clearly revealed in DiamondView fluorescence images (figure 8, right). These were the only internal features seen. The mid-IR absorption spectrum showed a relatively high concentration of boron, consistent with the intense blue coloration. However, PL spectroscopy at liquid-nitrogen temperature using 514 nm laser excitation revealed clear Si-related emission lines. The sharp peaks at 736.7 and 737.0 nm (figure 9), attributed to a $[Si\text{-}V]^-$ lattice defect, closely matched those observed in CVD synthetic diamonds.

This is the first documented $[Si\text{-}V]^-$ defect in an HPHT-grown synthetic gem diamond. Its occurrence strongly suggests some post-growth treatment process. During treatment, an existing Si impurity could have combined with other optical centers such as a vacancy and formed the $[Si\text{-}V]^-$ defect. As always, care is required in identifying synthetic diamonds, particularly when post-growth treatment is involved.

Kyaw Soe Moe and Wuyi Wang

Three Melee-Size Synthetic Diamonds

Small synthetic diamonds pose a special concern in the trade, since they are often mixed in parcels with loose natural melee and are less likely to be sent for a lab report. A Fall 2008 *G&G* article, H. Kitawaki et al.'s "Identification of melee-size synthetic yellow diamonds in jewelry" (pp. 202–213), described the identification of very small synthetic diamonds by combining analytical techniques with standard gemological testing. The GIA Laboratory in New York recently examined three melee-size yellow

Figure 9. Sharp emissions at 736.7 and 737.0 nm were detected in the 0.30 ct HPHT-grown synthetic diamond's PL spectrum. These lines, assigned to the $[Si\text{-}V]^-$ lattice defect, correspond closely to those observed in CVD synthetic diamonds.

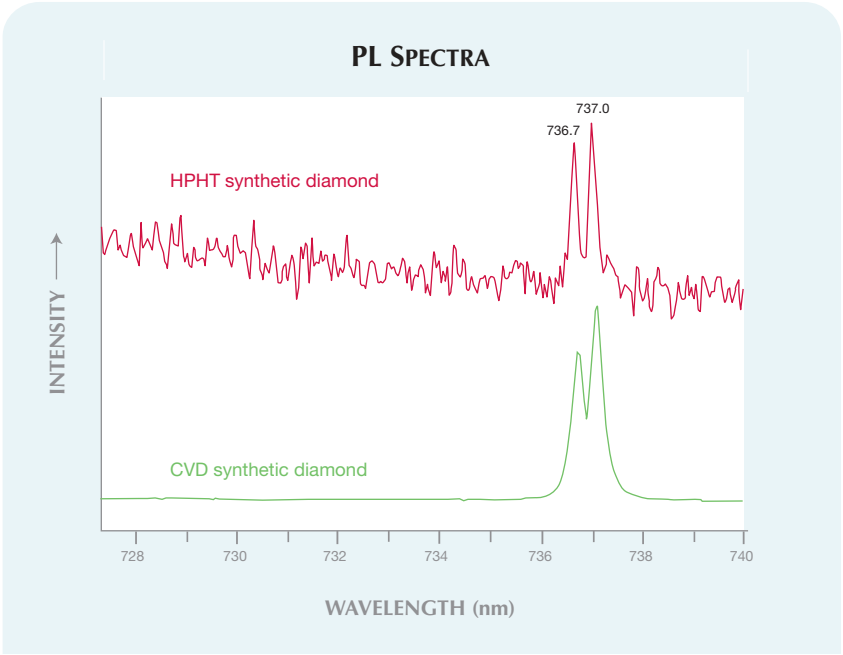

Figure 10. Melee-sized synthetic diamonds such as these (0.009, 0.010, and 0.080 ct) are usually set in jewelry as accent stones, making them difficult to identify without careful examination.

round brilliants (0.009, 0.010, and 0.080 ct) submitted for color origin reports (figure 10) that confirmed how challenging the identification of small diamonds can be.

Microscopic examination at high magnification revealed that two of the round brilliants contained metallic flux inclusions (that were attracted to a magnet) and pinpoints, which are characteristic of synthetic diamond. The third sample showed no inclusions indicative of a synthetic. All three displayed even color zoning, without the hourglass growth structure typical of synthetic diamond. The three samples were inert to long-wave UV radiation and exhibited a weak-to-moderate chalky yellow reaction to short-wave UV. None showed the cross-shaped green luminescence typically seen in synthetic diamonds when exposed to long- and short-wave UV. With only limited evidence that these were synthetics, we turned to advanced testing.

Infrared absorption spectroscopy revealed that all three samples were type Ib, as expected for HPHT synthetic diamonds, with moderate concentrations of isolated nitrogen. Examination with the DTC DiamondView showed growth structures that confirmed they were synthetics, with much weaker fluorescence in the {110} and {113} growth sectors (figure 11).

It is important for the trade to be aware of the presence of melee-size synthetic diamonds, which are normally used as accent stones in jewelry. They may require careful examination to identify. When standard gemological testing proves inconclusive, advanced laboratory analysis is needed.

Jason Darley, Sally Chan, and Michelle Riley

Artificial Metallic Veining in MANUFACTURED GEM MATERIALS

The Carlsbad laboratory recently examined one purple and one greenish blue cabochon (26.24 and 6.11 ct) manufactured from turquoise, plastic, and metal flakes (figure 12). While composite turquoise is becoming increasingly common in the gem trade, this was the first time we had encountered artificial metallic veining in this material.

Figure 11. This DiamondView image of the 0.010 ct sample displays a typical synthetic diamond growth structure, with much weaker fluorescence in the {110} and {113} growth sectors.

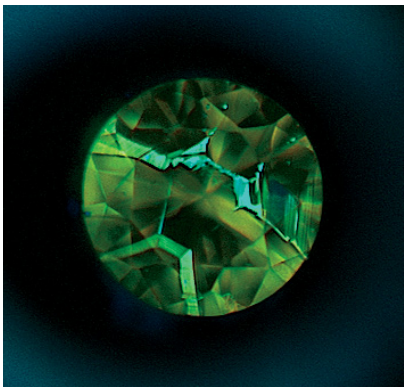

The gemological properties of the cabochons—especially the spot RIs of 1.58 (the purple cab) and 1.60 (the greenish blue)—were consistent with those of impregnated turquoise, which can have a refractive index lower than that of untreated material (1.61–1.65) due to the plastic impregnation. When exposed to long-wave UV radiation, the purple cabochon fluoresced moderate-to-strong orange and the greenish blue cabochon fluoresced weak blue. Microscopic examination of the purple cabochon showed obvious veins of red plastic. Plastic veining was also observed in the greenish blue cabochon, but those veins appeared colorless. With the exception of the metallic veining, this purple material was similar to that reported earlier this year (Spring 2010 Lab Notes, pp. 56–57).

Closer inspection of the metallic veining in both stones revealed that these veins were actually composed of fine flattened particles of metal suspended in a plastic. These flakes typically were aligned parallel to the walls of the veins (figure 13) and showed a

Figure 12. Artificial metallic veining is prominent in both of these composite turquoise cabochons (6.11 and 26.24 ct).

finely foliated structure. Similar-appearing material was recently reported by G. Choudhary (Summer 2010 *G&G*, pp. 106–113), but the metallic veining was not identified. By contrast, natural turquoise occasionally contains black or brown veins of limonite and also grains of pyrite.

With client approval, small samples were collected from the purple and greenish blue host material for advanced testing. Mid-IR spectroscopy confirmed that they were turquoise. To identify the metallic component, we removed small areas of those veins and analyzed them using energy-dispersive X-ray fluorescence (EDXRF) spectroscopy. The yellow metal from the greenish blue cabochon was identified as copper; also present in the turquoise host were fragments of pyrite. The only element detected in the white metal from the purple cabochon was zinc.

Figure 13. The metallic veins in this composite turquoise cabochon are composed of tiny copper flakes suspended in a plastic resin. Note the fine foliation of the flakes. Magnified 60×.

This type of artificial metallic veining has also been seen recently in imitation lapis lazuli. Diane Hankinson loaned GIA a 36.43 ct pierced carving of what she assumed to be natural lapis lazuli (figure 14). The testable gemological properties were in the range of those published for the natural material, but magnification revealed a manufactured structure of finely ground blue fragments punctuated by small areas of brassy metallic veining. Magnification of the veins revealed the same finely foliated structure as in the turquoise veining described above. EDXRF testing of the vein material confirmed the presence of both copper and zinc, the major components of brass. This veining was obviously used to simulate pyrite in natural lapis lazuli, and was quite convincing without magnification.

As the popularity of turquoise and other affordable ornamental gem materials grows, there will be an ever-increasing number of treatments to make a competitive saleable product. Adding metallic veining is surprisingly effective at creating interesting and sometimes natural-appearing manufactured gem materials. Although we have only seen this technique in composite turquoise and imitation lapis, it could be readily applied to other materials, such as gold-veined quartz or composite coral. The structure of the vein, characterized by fine metal flakes in a plastic suspension, provides visual evidence that the item has been manufactured.

Nathan Renfro and Phil Owens

A Rare Natural Green PEARL

Natural pearls are quite rare, and those with a natural green color are rarer still. Even then, the color tends to be greenish gray, where gray is the dominant hue. The Bangkok laboratory recently examined a green-gray round pearl (figure 15) that measured 10.35 × 9.98 × 9.18 mm (6.72 ct). The pearl was mounted with a 0.70 ct D-color SI_1 diamond in a yellow and white metal pendant suspended from a linked chain interspersed with natural "seed" pearls.

Figure 14. This 36.43 ct pierced carving of imitation lapis also showed artificial metallic veining caused by microscopic metallic flakes suspended in a plastic resin (inset, magnified 60×). The metal is a brass alloy composed of copper and zinc.

Figure 15. This 10.35 × 9.98 × 9.18 mm (6.72 ct) natural pearl had a rare untreated green-gray color.

Microscopic examination of the pearl revealed overlapping platelets of aragonite that varied from green to blue-green, with none of the artificial color concentrations at the platelet edges that would indicate dye (figure 16). It fluoresced a dull, mottled green to long-wave UV radiation and was inert to short-wave UV. Microradiography revealed the concentric growth structures characteristic of natural origin. We used EDXRF to determine the Mn and Sr concentrations and thereby establish whether the pearl formed in a saltwater or freshwater mollusk. EDXRF detected 77 ppmw Mn and 2148 ppmw Sr, indicating a saltwater origin.

Figure 16. The surface structure of the green-gray natural pearl revealed serrated black lines against a green background, denoting the edges of overlapping platelets of nacre. Magnified 180×.

The pearl's Raman spectrum contained a major peak at 1087 cm^{-1} and a doublet situated at 703.6 and 706.9 cm^{-1}, confirming that the outer platelet layer was composed of aragonite, the norm for natural saltwater pearls. The pearl's UV-Vis reflectance spectrum showed troughs at 229, 282, 343, 489, and 834 nm, extending from the near-infrared through the visible and UV regions. These features are not found in typical spectra for *Pinctada margaritifera* pearls, which have a reflectance trough at 700 nm. Because the reaction to long-wave UV did not match that expected for pearls from *Pteria sterna*, the most likely mollusk host is *Pinctada mazatlanica*, the black-lipped oyster from Baja California, Mexico.

Kenneth Scarratt

Rock Containing RICHTERITE and SUGILITE

In the laboratory, where we typically examine homogeneous materials, it is interesting to encounter a combination of minerals in a single stone. The Carlsbad laboratory recently received such a specimen, a 5.59 ct translucent dark blue and purple modified triangular step cut that was submitted for identification (figure 17). In addition to its purple and blue sections, the stone contained a brown accessory mineral; overall, it had a slightly layered structure (figure 18).

Figure 17. This 5.59 ct modified triangular step cut proved to be a rock composed primarily of richterite and sugilite.

The blue and purple sections had spot RIs of 1.62 and 1.61, respectively. In the handheld spectroscope, the blue portion displayed a weak 540–580 nm band and a strong 650–680 nm band, while the purple section showed a 550 nm band. Raman spectra yielded good matches with richterite for the blue mineral, sugilite for the purple mineral (consistent with the 550 nm absorption band), and aegirine for the brown accessory mineral.

Richterite ($Na[CaNa]Mg_5Si_8O_{22}[OH]_2$) belongs to the amphibole group; blue richterite is a potassium-bearing version of the mineral. Sugilite ($KNa_2[Fe,Mn,Al]_2Li_3Si_{12}O_{30}$) is from the milarite group, while aegerine ($NaFeSi_2O_6$) is in the pyroxene group. All three minerals have commonalities in their chemical composition and mode of formation, so finding them together in one rock is not too surprising. The client suggested that the rock might be from the Wessels mine in South Africa, which is known for yielding potassian richterite and sugilite.

Alethea Inns

Lead Glass–Filled RUBY Damaged During Jewelry Repair

Ruby filled with lead glass has been the source of much concern in the jewelry industry for several years. One of the main reasons is that the filler material is not durable—tests have shown that it is highly susceptible to damage from solvents, even relatively mild ones such as lemon juice. The initial study of the durability of these stones (S. F. McClure et al., "Identification and durability of lead glass–filled rubies," Spring 2006

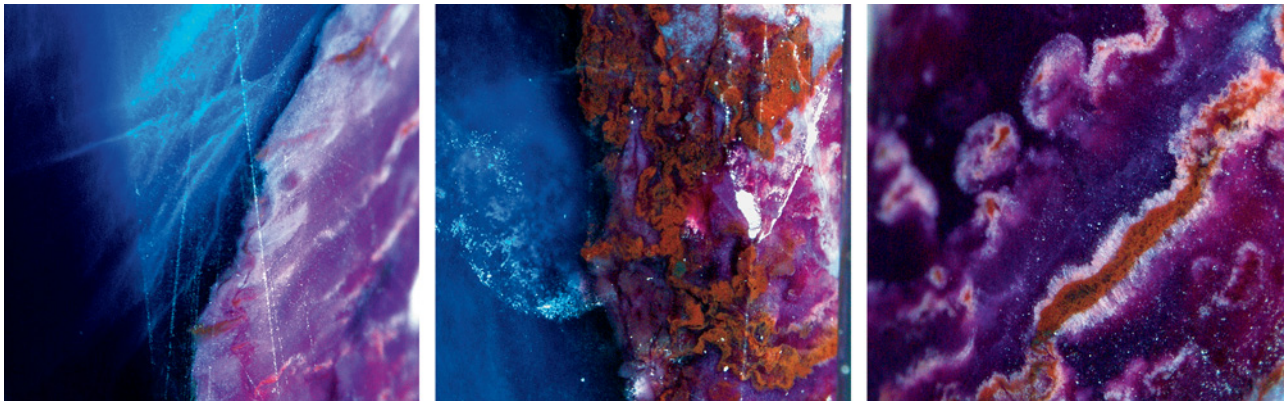

Figure 18. The stone in figure 17 showed a sharp boundary between the blue richterite and purple sugilite in some areas (left), and an intergrowth (center) or layered structure (right) with brown aegirine in others. Magnified 15×.

G&G, pp. 22–34) found that jeweler's pickling solution rapidly etched the lead glass filler at the surface. To prevent such damage, we recommended that jewelers remove all rubies treated in this way from their settings before undertaking repair procedures.

Of course, to follow that advice one would first need to know a ruby has been treated by this method. It is unfortunate that sometimes a jeweler will not examine a stone thoroughly enough or will depend on what the client says about it. Inevitably, this practice leads to problems.

One such case is illustrated in figure 19. This ~6 ct ruby was sent to the Carlsbad lab because it had been damaged during repair procedures and the jeweler wanted to know what had happened. While the exact circumstances were not revealed to us, the appearance of the stone suggested it was left in the setting during soldering or retipping and subsequently placed in a pickling solution for cleaning. This is standard procedure and usually will not harm a ruby. As outlined above, however, rubies filled with lead glass are certain to be damaged, causing a significant change in the stone's appearance and a very unhappy client. As far as we know, these stones cannot be retreated once they are damaged; in this case, it appears that someone tried to hide the damage by applying a red substance (possibly ink) to the surface, hoping it would penetrate into the fractures (figure 20) and make them less visible. If that was the intent, it did not succeed.

Figure 19. This ~6 ct lead glass–filled ruby appears to have been damaged by immersion in jeweler's pickling solution.

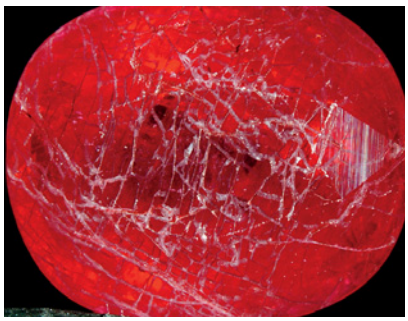

Figure 20. A red substance applied at the surface of the fractures may have been intended to disguise the damage to the ruby. Field of view ~1.1 mm.

Shane F. McClure

Natural SAPPHIRE with a Sapphire Inclusion

Of the many sapphires submitted to the Bangkok laboratory for identification, a 43.05 ct blue cushion cut received recently proved to be particularly unusual. The RIs of 1.760 and 1.769, together with a hydrostatic SG of 3.99, identified it as corundum. But microscopic observation revealed a very interesting inclusion.

Under the crown and just below the girdle, we found a crystal with the hexagonal shape typical of sapphire. And this inclusion had inclusions of its own (figure 21). The area where the crystal reached the surface (part had been removed during cutting) showed a uniform luster with the host, supporting its identification as sapphire. Further examination of both the host and the included crystal using Raman microspectroscopy confirmed both were corundum. The included sapphire crystal contained exsolved needles, many colorless crystals, and some secondary fluid inclusions (figure 22). By contrast, the host sapphire was relatively free of internal features.

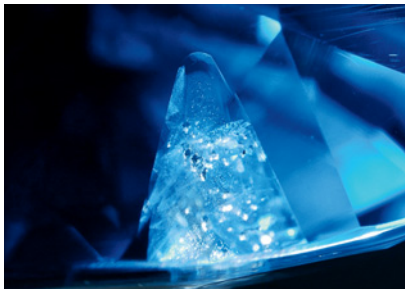

Figure 21. This sapphire crystal is included in a 43.05 ct blue sapphire (magnified 20×).

A variety of inclusions are common in sapphires, but included crystals with their own inclusions are seldom encountered. This is the first sapphire in sapphire this contributor has seen.

Garry Du Toit

SYNTHETIC SPINEL and SYNTHETIC RUBY Doublet

The Carlsbad lab has seen a number of corundum doublets over the years, most with natural corundum crowns and synthetic corundum pavilions. We have also encountered colorless spinel crowns attached to a variety of materials.

We recently received a 4.85 ct red specimen for identification. Standard gemological testing produced refractive indices of 1.725 on the crown and 1.760–1.770 on the pavilion. Viewed face-up with magnification, the sample revealed a single plane of transparent, colorless glue with planar gas bubbles (figure 23). The glue layer separated a blue crown from a red pavilion. The separation plane was easily visible in reflected light (figure 24). These results indicated an assembled stone.

Figure 23. These gas bubbles are trapped in a colorless, transparent layer of glue along the separation plane between the doublet's two layers. Curved striae from the synthetic ruby pavilion are also visible. Magnified 22.5×.

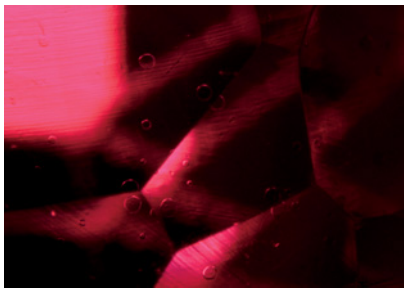

Figure 22. At 50× magnification, needles, crystals, and secondary fluid inclusions can be seen inside the included sapphire crystal.

The crown showed a slightly different luster from the pavilion when viewed with reflected light. Combined with the properties mentioned above, the curved striae indicated synthetic spinel. The pavilion had a large fracture that terminated at the crown, making the doublet even more apparent. Also evident in the pavilion were gas bubbles and curved striae, both typical of flame-fusion synthetic ruby. When viewed with immersion, the two components of the doublet were obvious (figure 25).

Figure 24. In reflected light, the separation plane between crown and pavilion is obvious. Magnified 40×.

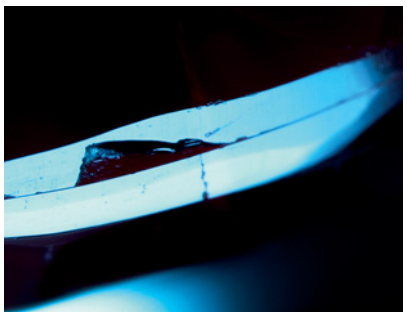

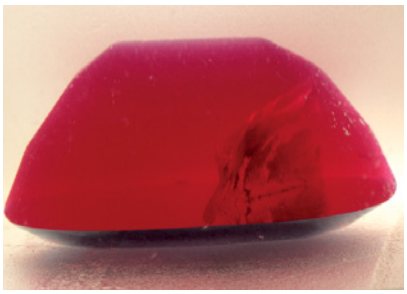

Figure 25. Immersed in water, the 4.85 ct doublet displays different colors in the crown and pavilion, and an abrupt termination of the fracture at the crown.

The two components also reacted differently to UV radiation. The crown was inert, while the pavilion showed moderate red fluorescence when exposed to long-wave UV radiation. With short-wave UV, the crown showed moderate chalky green fluorescence, typical of synthetic spinel, while the pavilion had a weak-to-moderate red reaction.

It was unclear what gem this doublet was intended to imitate—perhaps red spinel. We were surprised to see a doublet with a synthetic crown *and* pavilion, since it is unlikely to pass for a natural material.

Alethea Inns

PHOTO CREDITS
Jian Xin (Jae) Liao—1 (left), 5, and 7; Wuyi Wang—1 (right) and 8 (right); Laura L. Dale—2; Robinson McMurtry—3 and 17; Paul Johnson—6; Sood-Oil (Judy) Chia—8 (left) and 10; Jason Darley—11; C. D. Mengason—12, 14, and 17; Nathan Renfro—13 and 14 (inset); Adirote Sripradist—15; Ken Scarratt—16; Alethea Inns—18 and 23–25; Shane F. McClure—19 and 20; Pantaree Lomthong—21 and 22.

OUR EDUCATION.
YOUR WORLD OF OPPORTUNITY.

Almost anywhere you go, someone is using education acquired from GIA. Our international campuses, traveling classes, corporate seminars and online courses help individuals define and refine vital skills.

And GIA supports that learning with credentials valued throughout the gem and jewelry world.

WWW.GIA.EDU

GIA®

CARLSBAD ANTWERP BANGKOK DUBAI FLORENCE GABORONE HONG KONG
JOHANNESBURG LONDON MOSCOW MUMBAI NEW YORK OSAKA SEOUL TAIPEI TOKYO

GEM NEWS International

COLORED STONES AND ORGANIC MATERIALS

Amber with mineral inclusions. Besides its use as a gem material, amber has scientific value because of the wide variety of inclusions it contains. However, most such inclusions are organic in nature. Inorganic inclusions are rare, though pyrite and quartz have been reported (e.g., E. J. Gübelin and J. I. Koivula, *Photoatlas of Inclusions in Gemstones*, 2nd ed., ABC Edition, Zurich, 1992, pp. 212–228).

Recently, two transparent yellow samples (189.35 and 115.33 ct) with an unusually wide variety of inclusions—including some with a metallic appearance (figure 1)—were submitted to the NGTC Gem Laboratory for identification reports. Among the internal features were trapped insects, gas bubbles, reddish brown flow lines, plant debris, and minerals. Those with a metallic luster occurred in various sizes and shapes, and two were large enough to be seen with the unaided eye (again, see figure 1). With magnification, we observed a large number of round metallic inclusions, measuring several microns to several hundred microns, in one piece; a few reached the surface of the host and showed a "golden" metallic luster (figure 2). In the other sample, the metallic inclusions were interspersed with other minerals and organic material.

Figure 1. In addition to a variety of organic materials, these two samples of Baltic amber (189.35 and 115.33 ct) contain inclusions of pyrite and other minerals. Photo by Li Haibo.

The specimens fluoresced chalky blue to both long- and short-wave UV radiation, while the surface-reaching metallic inclusions were inert. Both samples had unpolished areas, making it easy to remove a minute amount of material for FTIR analysis. The spectra showed two characteristic peaks, at 1735 and 1157 cm^{-1}, indicating that the specimens were Baltic amber. Energy-dispersive X-ray fluorescence (EDXRF) spectroscopy of the metallic inclusions suggested pyrite, as both Fe and S were identified. The inclusions' Raman spectra showed two strong, sharp peaks at 372 and 339 cm^{-1}, with a weak peak at 425 cm^{-1}; these features are also characteristic of pyrite. Analysis of the other mineral inclusions in the 189.35 ct sample by Raman spectroscopy and microscopic examination between crossed polarizers identified them as feldspar, quartz, and jet (figure 3).

Editor's note: Interested contributors should send information and illustrations to Brendan Laurs at blaurs@gia.edu or GIA, The Robert Mouawad Campus, 5345 Armada Drive, Carlsbad, CA 92008. Original photos will be returned after consideration or publication.

Gems & Gemology, Vol. 46, No. 4, pp. 309–335.

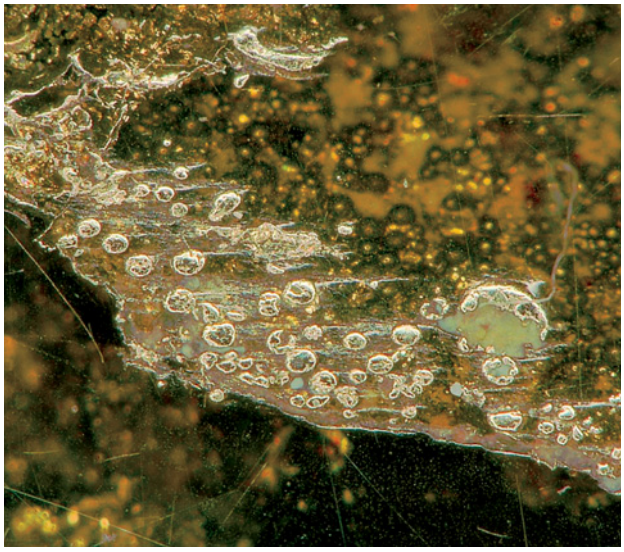

Figure 2. Where they reach the surface of the samples, the pyrite inclusions show a "golden" metallic luster. Photomicrograph by Li Haibo; magnified 100×.

In November 2010, a Burmese amber sample submitted to our laboratory displayed similar pyrite inclusions.

Li Haibo (lhb@ngtc.gov.cn), Lu Taijin, Shen Meidong, and Zhou Jun
National Gemstone Testing Center Gem Laboratory
Beijing, China

Additional field research on Tibetan andesine. In late September 2010, an international group investigated andesine occurrences in Tibet in an effort to resolve the controversy over the origin of red andesine from China. The group was organized by coauthor AA and hosted by miner Li Tong and his wife, Lou Li Ping. It also included Richard Hughes (Sino Resources Mining Corp., Hong Kong), Flavie Isatelle (geologist, France), Christina Iu (M. P. Gem Corp., Kofu, Japan), Thanong Leelawatanasuk (Gem & Jewelry Institute of Thailand, Bangkok), Young Sze Man (*Jewellery News Asia*, Hong Kong), and coauthor BML. The group flew from Guangzhou, China, to Lhasa, Tibet, and then drove west for ~7 hours (350 km) to Shigatse, Tibet's second-largest city. The andesine mining area is located about 1.5 hours' drive from Shigatse. Paved roads lead to within 1–3 km of all three reported Tibetan andesine localities: Bainang, Zha Lin, and Yu Lin Gu (see table 1 for GPS coordinates).

Figure 3. Microscopic examination of the larger amber sample between crossed polarizers reveals additional inclusions, composed of feldspar, quartz, pyrite, and jet. Photomicrograph by Li Haibo; magnified 100×.

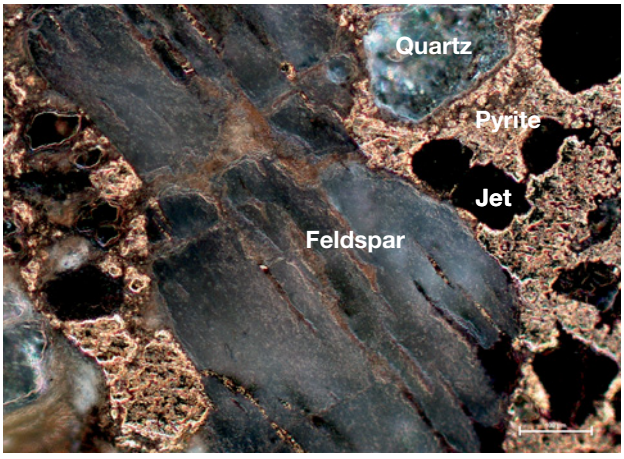

The Bainang mine, allegedly Tibet's principal source of andesine, was visited by one of us in 2008 (see Winter 2008 Gem News International, pp. 369–371; A. Abduriyim, "The characteristics of red andesine from the Himalaya highland, Tibet," *Journal of Gemmology*, Vol. 31, No. 5–8, 2009, pp. 283–298). The deposit is located ~2.2 km southwest of Nai Sa village, where we saw ~10 kg of material that local people claimed to have collected and stockpiled over the past three years. We were told most of the mining at Bainang took place in 2005–2008 and was organized by Li Tong. Unfortunately, we were forbidden from visiting the deposit by a powerful local lama, despite having official permission from the Chinese government and police escorts.

The Zha Lin deposit is located adjacent to a village of the same name. Reportedly it was mined by local people in 2006–2008 using simple hand tools, and ~2 tonnes of andesine were produced there. (Author AA did not visit the deposit in 2008 because Li Tong was not yet aware of it.) We saw a series of shallow pits in the mining area, but there was no evidence of recent digging. The deposit is hosted by medium-gray silty soil (figure 4, left) that underlies alluvial material consisting mainly of shale and mudstone with less-common quartz vein material. The authors dug two small pits (~0.7–1.2 m maximum depth) where we saw pieces of andesine on the surface, and many pieces were found at depth in both of them. We also dug three pits in random areas of alluvium (under thorn bushes) located 30–50 m upslope from the mining area where there was no surface evidence of andesine or prior digging (figure 4, right). These pits ranged up to 0.3 m deep, and andesine was found below the surface in two of them.

TABLE 1. Location of reported Tibetan andesine occurrences.

Location	GPS coordinates	Elevation
Bainang	29°02.48′N, 89°22.25′E (south mine)	4,100 m (13,452 ft.)
	29°02.72′N, 89°22.11′E (north mine)	4,076 m (13,373 ft.)
Zha Lin	29°03.95′N, 89°20.88′E	3,929 m (12,891 ft.)
Yu Lin Gu	29°03.08′N, 89°20.76′E	4,102 m (13,460 ft.)

Figure 4. Shallow pits dug in silty soil appear to be the source of andesine at the Zha Lin deposit (left). The site of one of the random test pits near Zha Lin from which the authors recovered andesine is shown on the right. Photos by B. M. Laurs.

As seen previously in andesine allegedly of Tibetan origin, all the rough material appeared waterworn and ranged from pale to deep red, with a few pieces containing bluish green areas.

At Yu Lin Gu, we found andesine scattered across an alluvial fan (figure 5) located ~2 km up-valley from Zha Lin. Reportedly ~200 kg of andesine have been collected there by local people since 2006, with no organized mining; the andesine has only been picked up from the surface. We collected several pieces that were locally concentrated in patches consisting of 4–10+ pieces per square meter. Most were found on raised portions of the dissected alluvial fan, and also in an active intermittent creek on one side of the fan. We recovered andesine from the surface or slightly below the surface in loose silty soil, but no stones were found when we dug pits into the alluvial fan. The range of color and degree of rounding in these pieces were similar to what was seen in the material from Zha Lin, but many were less saturated (figure 6).

We were unable to verify whether Yu Lin Gu is a true andesine deposit because we could not find samples at depth. At Zha Lin, our discovery of andesine within pits dug in random, previously unexplored areas near the reported mining area is consistent with what we would expect for a genuine Tibetan andesine deposit. The original source rock for the andesine was not evident in the area, and it may have eroded away. Our final conclusion regarding the controversies surrounding Tibetan andesine will depend on the laboratory analyses of samples obtained on this expedition.

Ahmadjan Abduriyim (ahmadjan@gaaj-zenhokyo.co.jp)
Gemmological Association of
All Japan – Zenhokyo, Tokyo
Brendan M. Laurs

Aquamarine and heliodor from Indochina. In June 2010, Jack Lowell (Colorado Gem & Mineral Co., Tempe, Arizona) informed GIA about some attractive gem-quality crystals of aquamarine and heliodor from Indochina (figures 7 and 8). According to his supplier (Tan Pham, Vietrocks.com, Philadelphia), good-quality aquamarine was mined in 2008 from northern Vietnam, from separate areas in the neighboring provinces of Thanh Hoa and Nghe An. The Thanh Hoa finds are located in Thuong Xuan District, while the Nghe An deposits are in Que Phong District. Aquamarine from Nghe An was also produced in 2003–2004; the more recent crystals range up to

Figure 5. At Yu Lin Gu, andesine was found on the surface of this alluvial fan. Photo by B. M. Laurs.

Figure 6. These andesines were recovered by the authors from the Zha Lin (left, 0.10–1.14 g) and Yu Lin Gu (right, 0.25–1.55 g) localities in Tibet. Photos by Robert Weldon.

Figure 7. Fine aquamarine crystals such as these (up to 8.9 cm long) have been produced from a relatively new deposit in Thanh Hoa Province, Vietnam. Photo by Jack Lowell.

20 cm long. Matrix specimens (associated with smoky quartz) have been recovered only rarely (from Thanh Hoa) due to the weathering of the pegmatite host rocks. Mr. Lowell indicated that the Thanh Hoa deposit has yielded substantially more production than Nghe An (specific data were unavailable), and that crystals from the latter deposit are a darker blue. Clean gemstones up to ~35 ct have been faceted from the Vietnamese aquamarine.

Well-formed crystals of heliodor (e.g., figure 8) were recently produced from another area in Southeast Asia, which Mr. Pham suspects is Cambodia. The crystals were first noted on the Vietnamese market with a third-party source in 2007; those seen by Mr. Pham ranged up to 7.5 cm long. This heliodor, as well as the aquamarine described above, has been popular with Chinese buyers.

Brendan M. Laurs

Dark blue aquamarine from Tsaramanga, Madagascar. In July 2009, 300 kg of dark blue aquamarine were recovered from a pegmatite at Tsaramanga, in central Madagascar.

Figure 8. These gem heliodor crystals (up to 7.5 cm long) are from Southeast Asia. Photo by Jack Lowell.

Figure 9. The Tsaramanga pegmatite mine in central Madagascar has produced notable finds of dark blue aquamarine in recent years. Photo by De Rosnay.

The mine (figure 9) is located 5 km from the village of Mahaiza, in the Betafo district. Tsaramanga was first mined by the Germans in the 1920s for tourmaline (black, yellow, and green), pink beryl, and other gem minerals. Today the main production is rose quartz from the pegmatite's core zone (figure 10, left), but occasional concentrations of large (up to 1.5 m long and 40 cm in diameter) dark blue aquamarine crystals are uncovered (e.g., figure 10, right). Some beryls showing multiple colors have also been discovered, though not of gem quality.

The geology of the area consists of gabbros that are intruded by feldspar-rich pegmatites and some large veins of quartz. There are two types of pegmatites, defined by their mica content: muscovite bearing (with aquamarine) and biotite-phlogopite bearing. The main open pit at Tsaramanga measures ~70 × 20 m, and is worked by a team of 10–12 miners using pneumatic drills and hand tools such as hammers and steel bars.

About 10% of this recent aquamarine production was facetable, while 60% was cabochon and carving grade, and the remaining material was fractured and opaque. The unusually dark color of the aquamarine makes this mine noteworthy. Although the kilogram-size beryl crystals (e.g., figure 11) are highly fractured due to their formation within quartz and feldspar rather than open pockets, they typically contain substantial gemmy areas (figure 11, inset) that can yield attractive faceted stones up to ~6–7 ct.

Flavie Isatelle (flavie.isatelle@gmail.com)
Avignon, France

Diopside from Pakistan. In 2007, gem dealer Farooq Hashmi (Intimate Gems, Jamaica, New York) obtained a parcel of pale yellowish green rough in Peshawar, Pakistan. The seller indicated that it was from a new find in the Northern Areas of Pakistan (now called Gilgit-Baltistan), but he did not know the identity of the material. The 200 g parcel contained pieces weighing ~1–5 g. Mr.

Figure 10. The main pit at Tsaramanga (left) is mined primarily for rose quartz, but occasional concentrations of large dark blue aquamarine crystals (right) have been discovered. Photos by F. Isatelle

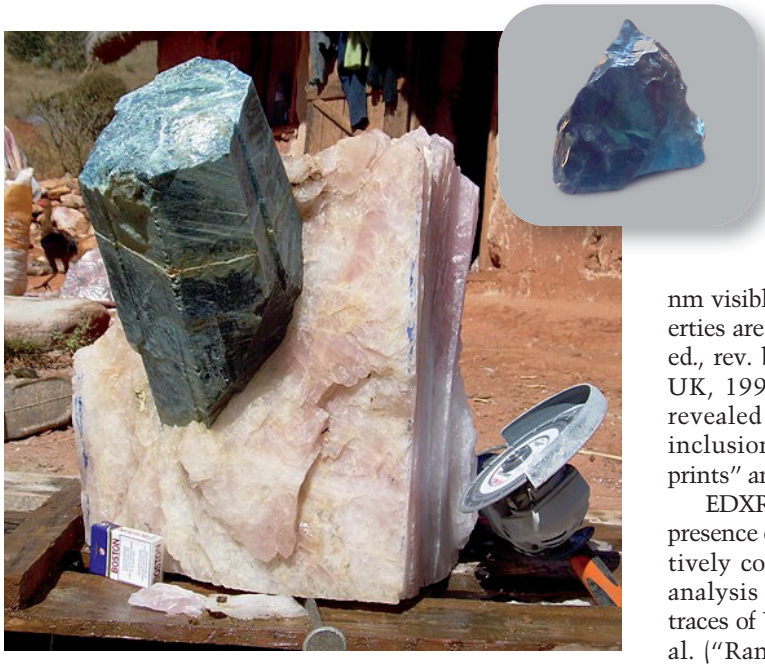

Figure 11. This specimen of aquamarine in rose quartz matrix shows the unusually dark color of the material from Tsaramanga. Such crystals typically contain abundant fractures with small gem-quality areas (see inset). Photos by De Rosnay.

Hashmi saw another parcel of this material with the same dealer during a subsequent trip in mid-2008, but it was of inferior quality.

Mr. Hashmi loaned GIA two well-formed crystals and a 1.97 ct round brilliant, faceted by Robert Buchannan (Hendersonville, Tennessee; see the *G&G* Data Depository at gia.edu/gandg for faceting notes), which are shown in figure 12. Standard gemological testing gave the following properties: color—light yellowish green to yellowish green; pleochroism—none; RI—n_α = 1.670–1.675 and n_γ = 1.695–1.698; birefringence—0.025–0.028; hydrostatic SG—3.27; Chelsea filter reaction—none; fluorescence—inert to long- and short-wave UV radiation; and a fine absorption line at 505 nm visible with the desk-model spectroscope. These properties are consistent with diopside (R. Webster, *Gems*, 5th ed., rev. by P. G. Read, Butterworth-Heinemann, Oxford, UK, 1994, pp. 330–331). Microscopic examination revealed strong doubling in the faceted stone (and no inclusions), while the two crystals contained "fingerprints" and iron-stained fractures.

Figure 12. These three samples (the round brilliant weighs 1.97 ct), reportedly from northern Pakistan, proved to be diopside. Photo by Robert Weldon.

EDXRF spectroscopy of the three samples showed the presence of Si, Mg, Ca, Fe, Al, and Cr. Laser ablation–inductively coupled plasma–mass spectrometry (LA-ICP-MS) analysis indicated a similar composition and revealed traces of V. Previous research on pyroxenes by E. Huang et al. ("Raman spectroscopic characteristics of Mg-Fe-Ca pyroxenes," *American Mineralogist*, Vol. 85, 2000, pp. 473–479) confirmed that Raman spectroscopy can differentiate diopside from other minerals in the (Mg,Fe,Ca)-pyroxene group, such as enstatite, ferrosilite, hedenbergite, and wollastonite. The Raman spectra of these three samples showed diopside vibration modes similar to those published in Huang et al. (spectra are available in the *G&G* Data Depository). We therefore identified the material as diopside.

Pamela Cevallos (pcevallo@gia.edu)
GIA Laboratory, New York

Record-breaking emerald discovered in Hiddenite, North Carolina. Although the area around Hiddenite, North Carolina, has historically produced some exquisite mineral specimens, gem-quality emeralds from this localitiy are exceedingly rare and highly sought-after by collectors. Until recently, the largest known faceted example was an 18.88 ct pear shape, named the Carolina Queen. The ~14 g rough from which it was cut was found in the fall of 1998 at the Rist mine, now called the North American Emerald mine. This same crystal also produced a 7.85 ct oval named the Carolina Prince, which sold for $500,000 to a collector with family ties to the town of Hiddenite.

In August 2009, a 62.01 g gem-quality emerald crystal was discovered in decomposed soil at the Adams Farm (figure 13), previously known primarily as a source of hiddenite (green Cr-bearing spodumene). Miner Terry Ledford and landowner Renn Adams unearthed the emerald from a depth of 4.3 m while pursuing the seams that occasionally lead to pockets containing hiddenite. The discovery occurred in an open field near an overgrown exploration site originally developed by Dr. William Hidden, who was reportedly dispatched to the area by Thomas Edison to procure platinum for his light bulb filaments. Together Dr. Hidden and Dr. George Frederick Kunz—the well-known late 19th/early 20th century gemologist-author—identified

Figure 13. Miner Terry Ledford displays the large emerald crystal next to the pocket where it was found in August 2009 in Hiddenite, North Carolina. The crystal (inset) was well formed and weighed 62.01 g. Photos courtesy of Terry Ledford.

63 different gems and minerals in the Hiddenite area.

The rough emerald exhibited rutile crystals on some faces, a classic signature of North Carolina emerald. After several weeks of study, the owners decided to cut the largest gem possible and enlisted the services of Jerry Call, an experienced cutter who had also faceted the 13.14 ct pear-shaped Carolina Emerald acquired by Tiffany & Co. in the 1970s. The result was a free-form step cut that weighed an impressive 74.66 ct, a new North American record.

Figure 14. The recut emerald, named the Carolina Emperor, is shown with an enlarged image of the 60+ ct Catherine the Great Emerald brooch on the cover of this Christie's catalog dated April 22, 2010. Photo by C. R. Beesley.

Soon after, Christie's announced the sale of a 60+ ct Colombian emerald brooch that belonged to Russia's Catherine the Great in the 18th century. Because of the size and quality similarities between the two emeralds, Adams and Ledford agreed with the suggestion to recut their stone into a hexagonal mixed cut emulating the Catherine the Great Emerald (figures 14 and 15). After three days of meticulous recutting by Ken Blount of Nassi & Sons, in New York City, the recut gem weighed 64.83 ct and showed a significant improvement in appearance. Dubbed the Carolina Emperor, it is the largest cut emerald from North America and has set a new benchmark for size and quality of North Carolina emeralds.

C. R. "Cap" Beesley (capbeesley@yahoo.com)
Gemstone Standards Commission, New York City

Figure 15. At 64.83 ct, the Carolina Emperor is the largest cut emerald from North America. Photo by C. R. Beesley.

Figure 16. Attractive cabochons of emerald-in-matrix (here, 15.27 and 34.37 ct) have recently been produced from material mined in Bahia, Brazil. Photo by Robert Weldon.

Emerald-in-matrix from Bahia, Brazil. At the 2009 Tucson gem shows, Joseph Rott (Tropical Imports, Belo Horizonte, Brazil) informed GIA about polished samples of emerald-in-matrix that were sourced from a long-known emerald deposit in Bahia, Brazil. This material consists of euhedral translucent emerald crystals embedded in white (or rarely pale pink) feldspar. Similar material has been reported from the Big Crabtree mine in Mitchell County, North Carolina (Summer 1993 Gem News, p. 132), and from the Nova Era area of Minas Gerais, Brazil (Summer 2002 GNI, pp. 176–177).

Mr. Rott donated two square cabochons of the Bahia material to GIA (figure 16), and they were studied for this report. The white matrix was confirmed to be feldspar and quartz by Raman analysis. EDXRF spectroscopy indicated that chromium (rather than vanadium) was the chromophore in the emerald. The cause of color in the pale pink feldspar was explored with EDXRF but could not be determined conclusively. Examination of the samples with magnification revealed inclusions of feldspar and dark brown mica (identified by Raman analysis as biotite); the emeralds also showed fracturing throughout. As with many emeralds, these samples were clarity enhanced by oiling. The oil was easily visible when tested with a hot point, as the fractures began to sweat slightly. The fractures in the samples fluoresced moderate blue to long- and short-wave UV radiation, which also provides evidence of clarity enhancement.

Mr. Rott indicated that ~100 kg of this material has been mined and over 2,000 carats of cabochons have been cut in sizes ranging from 8 × 10 mm to 20 × 25 mm. This emerald-in-matrix offers another option for designers, collectors, or anyone else who appreciates new and unusual gem materials.

Nathan Renfro (nrenfro@gia.edu)
GIA Laboratory, Carlsbad

5th century garnet jewelry from Romania. In 2007, nine gold pendants were discovered in an ancient tomb excavated at a shopping center 5 km west of Cluj-Napoca, Romania. Archeologists determined that the pieces belonged to a princess of the 5th century Gepids, a Gothic tribe (contemporaneous with the Merovingians) who lived in the Transylvania region of central Romania. Each pendant measured ~3.85 cm long and contained five tablet-cut red stones (about 1.5 mm thick) in a closed-back setting (figure 17). Their initial appearance suggested they were rubies. The jewels were studied on a single day using nondestructive techniques, and the results were initially presented at the XIX Congress of the Carpathian-Balkan Geological Association in Thessaloniki, Greece, in September 2010.

The stones were isotropic, with a refractive index of ~1.78 (using the spot method on the edge of one slab that protruded from the mounting), and had an almandine-like spectrum. Each plate contained crystallographically oriented rutile needles, and some of the plates contained pinpoints, negative crystals, and small crystals with the appearance of apatite. Most prominent were black, sometimes hexagonal, platy crystals (figure 18) that were nearly identical to ilmenite inclusions seen previously in almandine (see, e.g., E. J. Gübelin and J. I. Koivula, *Photoatlas of Inclusions in Gemstones*, 3rd ed., ABC Edition, Zurich, 1997, p. 289). Raman spectroscopy confirmed the stones were garnet with a high almandine content, with main bands at ~915, 550, 500, and 350 cm^{-1}.

EDXRF spectroscopy showed the metal was nearly pure gold, with only traces of Ag and Cu. A crisscross waffle-like pattern was stamped into gold foil mounted in the gold setting behind the garnet slices (see figure 19). This texture was visible through the transparent stones, producing an effect reminiscent of modern guilloché enamel, in which a pattern is engraved in the metal before the enamel is applied. A similarly stamped foil configuration has been observed in garnet, silver, and gold jewelry from nearby Potaissa, also a Gepid site (C. Ionescu and V. Hoeck, "Zusammensetzung und Herkunft der Granate der Ohrringe und einer Gürtelschnalle aus dem Grab der Franziska aus Potaissa [Turda, Rumänien] [About the composition and origin of garnets mounted in the earrings and buckle from the tomb of Franziska in Potaissa (Turda, Romania)]," in M. Barbulescu, Ed., *Das Germanische Furstengrab von Turda* [*The Germanic Princess Tomb from Turda*], Tribuna, Cluj-Napoca, Romania, 2008, pp. 295–310).

The almandine-rich composition of this garnet would be expected to have an overdark appearance if such material was faceted into stones of typical size for jewelry. Its use in these pendants was possible only because the plates are so thin. Generally, red gem garnets are a mixture of pyrope and almandine, with typically >40% pyrope (see figure 7 of D. V. Manson and C. M. Stockton, "Gem garnets in the red-to-violet color range," Winter 1981 *G&G*, pp. 191–204). The flat morphology of the garnet plates may have resembled the shape of the original rough if the crys-

Figure 17. These 5th century gold and garnet pendants (~3.85 cm long) were discovered near Cluj-Napoca, Romania. Photo by C. Ionescu.

tals had developed "fracture cleavage," as described by J. Ganguily et al. ("Reaction texture and Fe-Mg zoning in granulite garnet from Søstrene Island, Antarctica: Modeling and constraint on the time-scale of metamorphism during the Pan-African collisional event," *Proceedings of the Indian Academy of Sciences, Earth and Planetary Sciences*, Vol. 110, No. 4, 2001, pp. 305–312). Although our research is ongoing, we believe the garnet originated from European deposits that were known at the time, possibly the Austrian localities of

Figure 18. Several inclusions were visible in the garnet slices, including black platy crystals of what appeared to be ilmenite. Photomicrograph by C. Ionescu; field of view ~2.7 mm.

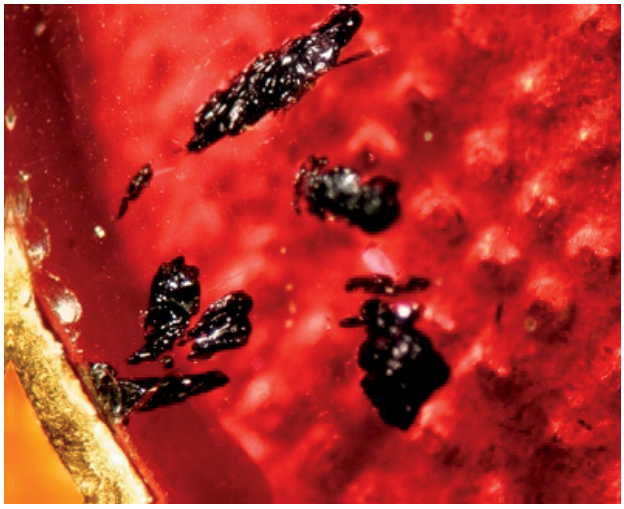

Figure 19. Each flat almandine slice is set above a crisscross-stamped piece of gold foil. The appearance is reminiscent of guilloché enamel. The foil contains a few square holes that were probably produced during the stamping process. Photomicrograph by C. Ionescu; field of view ~2.7 mm.

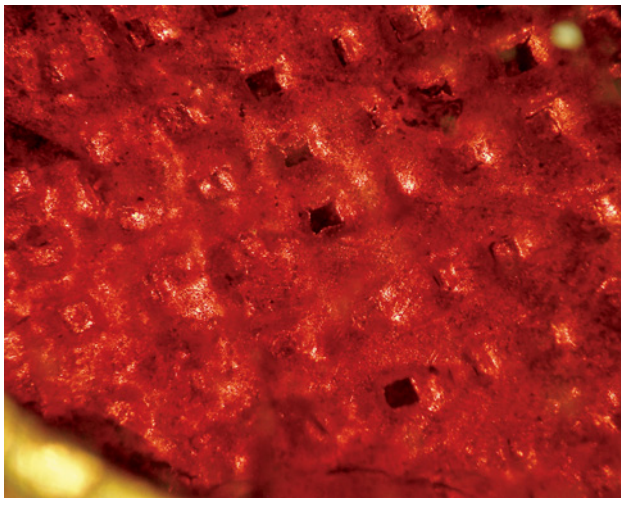

Figure 20. Shown here are some of the Pinctada radiata *and pen shells collected during a recent dive off the coast of Bahrain. The largest shell is ~50 cm long. Photo by A. Al-Attawi.*

Dunkelsteinerwald or Zillertal.

Acknowledgment: This study was funded by the Romanian Ministry of Education and Research, ID-2241/2008.

Emmanuel Fritsch

Corina Ionescu (corina.ionescu@ubbcluj.ro), Viorica Simon, Szabolcs Nagy, Katalin Nagy-Póra, and Mihai Rotea
Babes-Bolyai University, Cluj-Napoca, Romania

Natural pearl diving off the coast of Bahrain. In June 2010 while visiting Manama, Bahrain, these contributors had an opportunity to experience pearl diving in a manner similar to that used in the past. Although our methods were not completely authentic in a historic sense—that is, no nose clip (*Al Fetam*), no stone weight (*Al Kher*) to take us to the sea bed, no person on deck to pull the rope attached to the net basket and accompanying diver to the surface (*Al Seib*), no net bags (*Al Deyeen*) to contain the shells collected on the sea bed, and no traditional fishing vessel (e.g., dhow)—we did search for mollusks without using compressed air.

Our first stop was an area southeast of Manama's Marina Club (~45 minutes by boat) that had been recommended by local contacts. The water was just over 2 m deep, and the sea bed was liberally scattered with specimens of *Pinctada radiata* and some Pinnidae ("pen shell") bivalves (~5–10 shells/m^2). We collected shells of both mollusks before moving to a slightly shallower area nearby. Although that area contained <5 shells/m^2, it did not take long to collect ~200 shells total, mostly *P. radiata* but also some pen shells (e.g., figure 20).

On the boat trip back to Manama, we opened the mollusks with knives and carefully examined their interiors for pearls. Contributor AA-A discovered an ~2 mm cream-colored seed pearl in the mantle region of a *P. radiata*, and contributor AA found a 5.0–5.5 mm near-"golden" pearl within the gonad region of a *P. radiata* (figure 21). Two small blister pearls were also found attached to shells.

Only two whole pearls were found in the 200 or so mollusks recovered. This 1:100 ratio provides some idea of how many Arabian Gulf oysters must be opened to find a pearl worthy of mention, a notion that was reinforced by

Figure 21. A near-"golden" off-round pearl (5.0–5.5 mm) was found in this P. radiata *oyster. Photo by A. Al-Attawi.*

Figure 22. Quantities of fine natural pearls are still being produced in the Arabian Gulf. The largest shown here is ~10 mm. Courtesy of Al-Mahmood Pearls; photo by N. Sturman.

several dealers in Manama. Nevertheless, it is significant that the Arabian Gulf still produces natural pearls (e.g., figure 22).

Nick Sturman (nsturman@gia.edu)
GIA Laboratory, Bangkok
Stefanos Karampelas
Gübelin Gem Lab, Lucerne, Switzerland
Ali Al-Attawi
Gem & Pearl Testing Laboratory of Bahrain, Manama
Ahmadjan Abduriyim

Update on ruby and sapphire mining in Pakistan and Afghanistan. In June–July 2010, this contributor visited two corundum deposits in Pakistan and Afghanistan to collect reference samples for GIA: Basil in Pakistan and Jegdalek in Afghanistan.

In Pakistan, ruby and sapphire have been reported from five deposits: Nangimali (in Pakistan-controlled Azad Kashmir), Hunza (in northern Pakistan along the Karakorum Highway; see, e.g., Fall 2007 GNI, pp. 263–265), Bisil (in northern Pakistan's Basha Valley; see Fall 2007 GNI, pp. 263–265), Basil (in the Kaghan Valley of North-West Frontier Province), and Batakundi (also in the Kaghan Valley, located 30 km from Basil). Regarding the Bisil deposit, this author was unable to confirm its existence or learn any information about the activity there.

The Basil deposit was discovered in 1996. There were three mining sites as of June 2010, operated by Kashmir Gems Ltd. (e.g., figure 23). The first two produce pink, purple, and blue sapphires from graphite veins. At the third site, pink sapphires are found associated with marbles. Mining usually takes place from June to October by small teams using explosives and jackhammers. The output (e.g., figure 24, left) appears to be more significant than that of Nangimali or Batakundi. From this author's field research and conversations with miners/dealers who worked in Batakundi for several months in 2003 and 2004, it turns out that Basil is the source of the pink-to-purple sapphires previously described as coming from Batakundi (see Winter 2004 GNI, pp. 343–344; www.gia.edu/research-resources/news-from-research/batakundi_sapphire.pdf). By contrast, Batakundi is the source of distinctly different material (e.g., figure 24, right) and is more difficult to access. According to Guy Clutterbuck (pers. comm., 2006), Batakundi began producing small dark red rubies from a marble-type deposit in 2000, but several miners apparently died as a result of falls or from altitude sickness. Mining at

Figure 23. Pakistani miners are seen at the entrance of a sapphire mine in Basil, Pakistan. The mine is located at an altitude of 4000 m. Photo by V. Pardieu.

Figure 24. Some rough and faceted (~0.7 ct) sapphires from Basil are shown on the left. On the right are rubies reportedly from Batakundi, Pakistan; the smaller stones are 0.4–1 ct. Photos by V. Pardieu.

Figure 25. The pieces of rough in this parcel of blue sapphires from Badakhshan weigh up to 4 g. Photo by V. Pardieu.

Batakundi is said to have stopped after the devastating earthquake that hit Azad Kashmir in September 2005.

In Afghanistan, there are four ruby and sapphire deposits. Jegdalek, located in the eastern part of Kabul Province near Sorobi, is a well-known source of ruby from a marble-type deposit (G. W. Bowersox et al., "Ruby and sapphire from Jegdalek, Afghanistan," Summer 2000 *G&G*, pp. 110–126). The mining area is about 10 km long by 2 km wide and operates year-round. Approximately 200–300 miners were working the area in July 2010, significantly more than during this contributor's visit in the summer of 2006 (when mining was illegal). Ruby-bearing marble is dug from trenches extending over several hundred meters, and some tunnels are reportedly more than 200 m deep. According to the miners, output is limited by a lack of explosives, and water infiltration is a problem in some deep trenches.

Figure 26. These sapphires were found in 2009 in the Auvergne region of central France. Photo by B. Devouard.

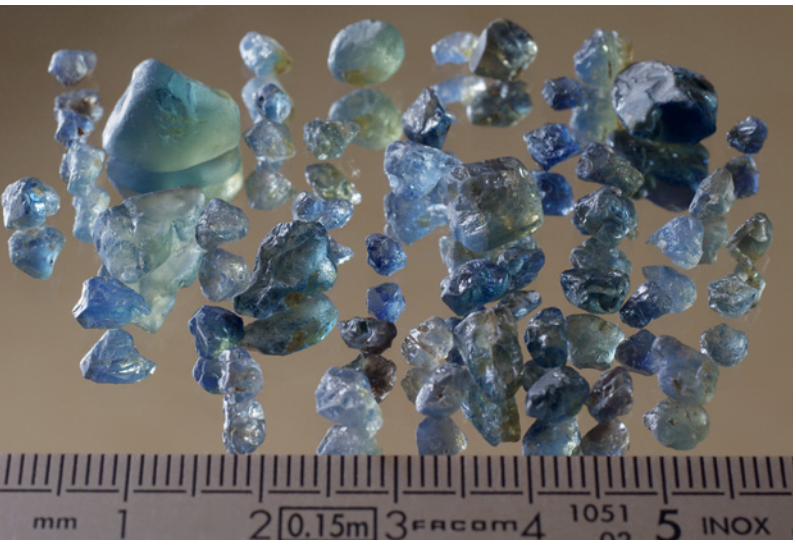

Near Maidan Shar, in Vardak Province, a small blue sapphire deposit was active at the beginning of the 2000s (Winter 2004 GNI, pp. 343–344), but mining reportedly stopped because there was no market for the stones. The material was too gray and included, and treatments were not effective in improving it. The deposit reportedly closed after 2006.

In Badakhshan Province, a small marble-hosted ruby deposit is supposedly located near Khash (see Fall 2007 GNI, pp. 263–265), a small village about two hours west of the village of Bohorak. In July 2010 this author was not allowed to come within 1 km of the reported deposit. Fewer than 10 miners were said to be working in tunnels dug on a hillside overlooking the valley. According to local residents, besides rubies and some low-quality blue sapphires, the area around Bohorak and the village of Jorm produces blue spinel, sphene, aquamarine, green and pink tourmaline, and diopside.

Also in Badakhshan, blue sapphires were reportedly discovered in 2008 near the famous lapis lazuli mines at the village of Sar-e-Sang. The sapphires are associated mainly with mica, and usually form hexagonal bipyramidal crystals that range up to 4 g (figure 25). Dealers in Kabul reported that the main market for these sapphires is Jaipur, India.

Chicken Street, the main gem trading area in Kabul, was much more active in 2010 than in 2006. Rubies were available from Jegdalek as well as Tajikistan, and some parcels also contained synthetics and heated stones (probably of African origin). Lead glass–filled rubies were also common in the Kabul market. Also seen were many parcels of emeralds said to be from Panjshir and Laghman (Afghanistan), Xinjiang (China), Swat (Pakistan), and Zambia. Afghan tourmaline, kunzite, and aquamarine (reportedly from Kunar and Nuristan), and pink spinel from Tajikistan, were also available in a variety of quantities and qualities.

Vincent Pardieu (vpardieu@gia.edu)
GIA Laboratory, Bangkok

Figure 27. These faceted sapphires from the Auvergne discovery range from 0.3 to 5.0 ct. Photo by B. Devouard.

Figure 28. This sapphire washing area lies near the village of Ambalavy, about 50 km southwest of Ilakaka. Photo by V. Pardieu.

Rediscovery of sapphires in central France. The Auvergne region, in France's Massif Central, was an important source of gems from the Middle Ages to the end of the 19th century (F. H. Forestier, "Histoire de l'un des gisements de gemmes le plus anciennement connu d'Europe occidentale: Saphirs, grenats et hyacinthes du Puy-en-Velay [History of one the oldest known gem deposits in western Europe: Sapphires, garnets, and zircons from Puy-en-Velay]," *Cahiers de la Haute Loire*, 1993, pp. 81–152). This region has been affected by several episodes of Cenozoic volcanism that resulted in abundant alkaline basaltic flows. In 2009, a prospector panning a riverbed found several thousand carats of rough sapphires. The stones ranged from 2 to 15 mm and had irregular resorbed shapes, with colors ranging from greenish yellow to greenish blue to saturated blue, as well as dark blue and black. Their moderate-to-strong pleochroism was typical of magmatic sapphires from basaltic terrain.

Approximately 10% (~40 g) of the rough was of gem quality (e.g., figure 26), and a dozen stones have been faceted (e.g., figure 27) by lapidary Jacques Dreher in Clermont-Ferrand, the regional capital. These gems weighed 0.3–5.0 ct and were mostly clean to lightly included. Gem-quality sapphires in such quantity and quality have not been encountered in France, or arguably all of Europe, since the workings at Mont Coupet (also in Auvergne) during the late 19th century.

Bertrand Devouard (b.devouard@opgc.univ-bpclermont.fr) and Etienne Médard
Laboratoire Magma et Volcans, Blaise Pascal University
CNRS (UMR 6524), Clermont-Ferrand, France

Benjamin Rondeau
Laboratoire de Planétologie et Géodynamique
CNRS (Team 6112), University of Nantes, France

Emmanuel Fritsch

Update on sapphire mining in southern Madagascar. In July-August 2010, this contributor visited the Ilakaka-Sakaraha and Andranondambo mining areas in southern Madagascar with several companions (see listing at the end of this report). In addition to collecting reference samples for GIA, our goal was to assess the state of the sapphire industry in the region.

Discovered in 1998, the Ilakaka-Sakaraha deposit (figure 28) extends more than 80 km from the Isalo National Park toward Toliara on the southwest coast. It quickly became one of the world's most important gem deposits, producing an abundance of pink and blue sapphires. Although more than 99% of the blue sapphires require

Figure 29. These blue sapphires are from Andranondambo. Photo by V. Pardieu.

heat treatment to be marketable, several exceptional stones are found daily that do not require heating. The deposit also yields yellow, purple, violet, and pinkish orange "padparadscha" sapphires, as well as chrysoberyl (including alexandrite), zircon, garnet, spinel, and other gems. Mining takes place year-round, mostly by artisanal methods. Many dealers from Thailand and Sri Lanka continue to have buying offices in the area. Most purchases are exported to those two countries for heat treatment and cutting before the gems make their way to the market.

Gem mining in Madagascar, particularly in Ilakaka, has faced many difficulties in recent years. In particular, from February 2008 to July 2009, the Malagasy government banned all gem exports. Compared to previous visits in 2005 and 2008 by this author, the number of foreign buyers has clearly dropped, and digging in the Ilakaka area has waned. As a result, the mining community has suffered shortages of food and other necessities, and security issues are plaguing the region.

In 2010, we found only three small operations (two Thai, one Malagasy) still using machinery. Most of the companies once involved in mechanized mining have withdrawn because of the poor market, fuel costs, and a lack of support from the Malagasy authorities. Because the government tolerates illegal mining, it is very difficult for companies that own mining rights to work legally and responsibly.

At the time of our visit, the main mining area was located near Antsoa, a village on the Taheza River southeast of Sakaraha, where about 1,500 miners were backed by Sri Lankan and local buyers. Antsoa was reportedly producing the best blue sapphires, with fine rough stones up to 10 g. At the more than 20 other sites we visited, we found anywhere from 10 to 500 people working. We estimate that about 50,000 people are now earning a living (directly or indirectly) from sapphire mining in Ilakaka-Sakaraha, half the number reported in 2005.

In the Andranondambo area, blue sapphires are mined from several primary deposits. Société d'Investissement Australien à Madagascar, an Australian company, mined the area for a few years but stopped in 2009. Today, small groups of artisanal miners work sites near Andranondambo, Maromby, Tirimena, and Siva. The most active mining area appeared to be Ankazoabo (north of Andranondambo), where Malaysian company Nantin Ltd. was operating heavy machinery alongside some 200 artisanal miners using hand tools.

While many gems are still produced, particularly fine blue sapphires (e.g., figure 29), the shrinking margins have led to fierce competition between buyers. Meanwhile, the miners' living and working conditions are very difficult. Most mining companies have stopped their activities, and many buyers are considering a switch to ruby dealing in Mozambique.

The author thanks the following for helping with the expedition and editing this report: Nirina Rakotosaona (Société Minière du Cap, Antananarivo, Madagascar), Marc Noveraz (Switzerland), Richard W. Hughes (Bangkok), Tracy Lindwall (San Francisco), Lou Pierre Bryl (Gaspé, Canada), Jazmin Amira Weissgärber Crespo (Mannheim, Germany), and Philippe Ressigeac (Montauban, France).

Vincent Pardieu

A strongly thermoluminescent spodumene. Thermoluminescence is a property of some minerals whereby they glow when heated to a certain temperature. Minerals known to display this property include fluorite (referred to as chlorophane), apatite, calcite, lepidolite, and spodumene (see www.galleries.com/minerals/property/pleochro.htm#thermo). The Gem Testing Laboratory of Jaipur, India, recently examined a spodumene that showed a striking example of thermoluminescence.

The pear-shaped green stone (figure 30) weighed 16.17 ct and measured 19.94 × 11.55 × 10.82 mm. Its color was reminiscent of green beryl or emerald from Nigeria, but the bright luster and liveliness ruled out the possibility of beryl. The following gemological properties were recorded: RI—1.660–1.675; birefringence—0.15; hydrostatic SG—

Figure 30. This 16.17 ct green spodumene was notable for its strong thermoluminescence at low temperature. Photo by G. Choudhary.

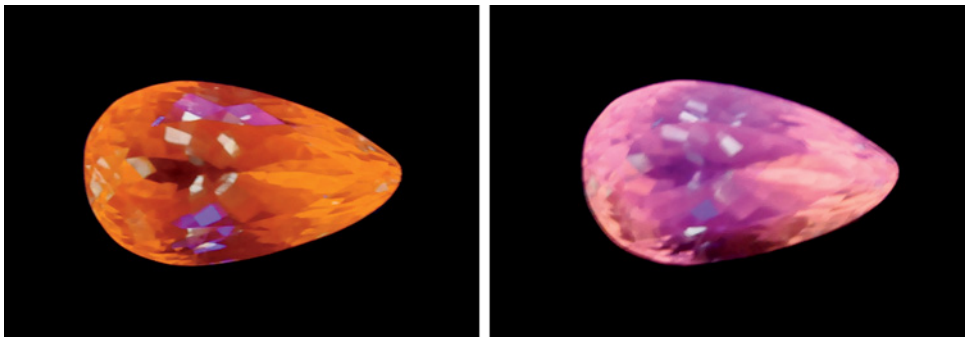

Figure 31. The spodumene in figure 30 fluoresced strong orange when exposed to long-wave UV radiation (left) and strong pink under short-wave UV (right). Photos by G. Choudhary.

3.17; fluorescence—strong orange to long-wave UV radiation and strong pink to short-wave UV (figure 31); and a weak absorption band visible in the blue region at around 440 nm in the desk-model spectroscope (no chromium lines were detected). These properties are consistent with those reported for spodumene (R. Webster, *Gems*, 5th ed., rev. by P. G. Read, Butterworth-Heinemann, Oxford, UK, 1994, pp. 186–189). With magnification, a few liquid "fingerprints" were observed under the table and crown facets. Cleavage planes, a common feature in spodumene, were not evident.

Microscopic examination was conducted with the aid of a fiber-optic lamp. Curiously, when the examination was completed, the green spodumene appeared bright orange (figure 32). Within a few minutes, however, the original green color returned. The orange glow was caused by the heat of the fiber-optic lamp exciting the spodumene's activator elements to produce thermoluminescence. The effect was similar to the stone's fluorescence reaction to long-wave UV radiation (again, see figure 31, left). The stone was reheated with the fiber-optic lamp and glowed orange again after three minutes of exposure, before returning to its original color within two to three minutes after removal of the lamp. These steps were repeated several times with consistent results.

EDXRF analysis revealed the presence of Al, Si, and Fe. Mn, a common constituent in spodumene that is also responsible for its strong fluorescence (see M. Robbins, *Fluorescence: Gems and Minerals Under Ultraviolet Light*, Geoscience Press, Arizona, 1994, pp. 265–266), was not detected in this specimen. Therefore, the cause of the fluorescence and thermoluminescence is unknown.

This is the first time this contributor has seen the heat of a fiber-optic lamp cause thermoluminescence in a gemstone. Webster (1994, p. 187) mentioned this effect occurring in X-ray irradiated kunzite at temperatures around 200°C. The present sample has probably not been laboratory irradiated, as the color was stable even after repeated heating with the fiber-optic lamp. Its thermoluminescence at such a low temperature makes it quite an unusual specimen.

Gagan Choudhary (gtl@gjepcindia.com)
Gem Testing Laboratory
Jaipur, India

"Neon" blue-to-green Cu- and Mn-bearing liddicoatite tourmaline. Four greenish blue faceted oval specimens, 1.29–1.45 ct, were recently submitted to the Gübelin Gem Lab (figure 33). The stones were similar in hue, tone, and saturation to Paraíba-type tourmaline. Standard gemologi-

Figure 32. The heat generated by a fiber-optic lamp caused the spodumene to thermoluminesce bright orange. The original green color returned within three minutes after the stone was removed from the lamp. Photo by G. Choudhary.

Figure 33. These four liddicoatite tourmalines (1.29–1.45 ct) have colors similar to those of some Paraíba-type elbaite tourmaline. Photo by L. Klemm.

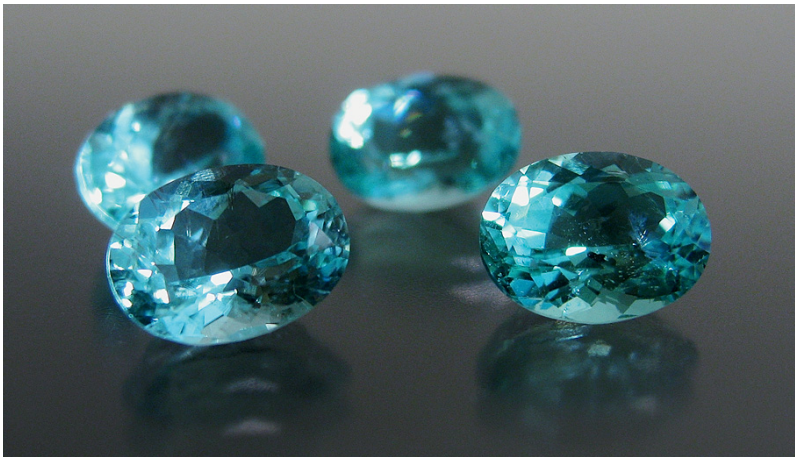

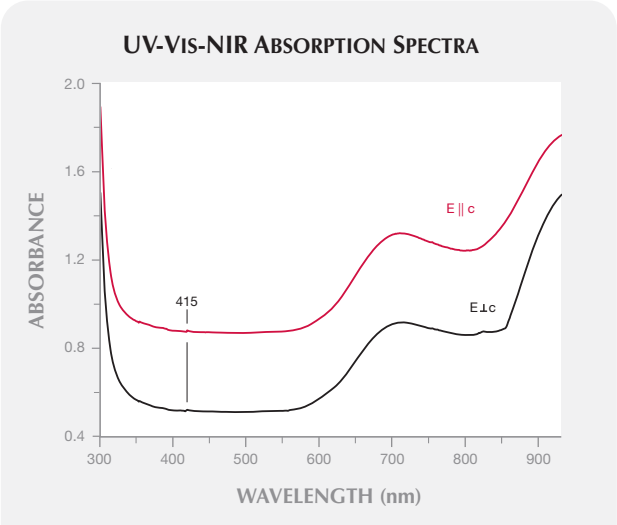

Figure 34. Polarized UV-Vis-NIR spectra of the stones in figure 33 show Cu^{2+} absorptions in the red region (~700 nm), with increasing absorption in the near-IR region (~900 nm). The small, sharp peak at ~415 nm is probably due to Mn^{2+}, and the increasing absorption toward the UV region is likely attributable to Mn^{2+}-Ti^{4+} intervalence charge transfer.

cal examination gave the following properties: RI—n_o = 1.640–1.641 and n_e = 1.621–1.622; birefringence—0.018–0.020; and SG—3.06–3.08; all these are consistent with tourmaline. Microscopic observation revealed parallel tubes, some hollow and others stained yellow to red-brown. Partially healed and unhealed fissures were also seen, and portions of the fissures were either frosted or reflective. Similar patterns have been observed in some heat-treated Paraíba-type tourmaline from Mozambique (B. M. Laurs et al., "Copper-bearing [Paraíba-type] tourmaline from Mozambique," Spring 2008 *G&G*, pp. 4–30). All four samples fluoresced moderate yellowish green to long-wave UV radiation and faint yellowish green to short-wave UV.

The samples' UV-Vis-NIR spectra (figure 34) were also similar to those of Paraíba-type tourmaline (see P. B. Merkel and C. M. Breeding, "Spectral differentiation between copper and iron colorants in gem tourmalines," Summer 2009 *G&G*, pp. 112–119, and references therein). Surprisingly, however, LA-ICP-MS analysis showed that though all of the samples were lithium tourmalines, they contained more Ca than alkalis (Na+K). EDXRF analysis also revealed significantly more Ca than typical of Paraíba-type tourmaline. All samples also contained minor amounts of Mn and Cu.

Elbaite is an Na-rich lithium tourmaline; the other lithium tourmalines are liddicoatite and rossmanite. Identification of tourmaline species is complex, as to date

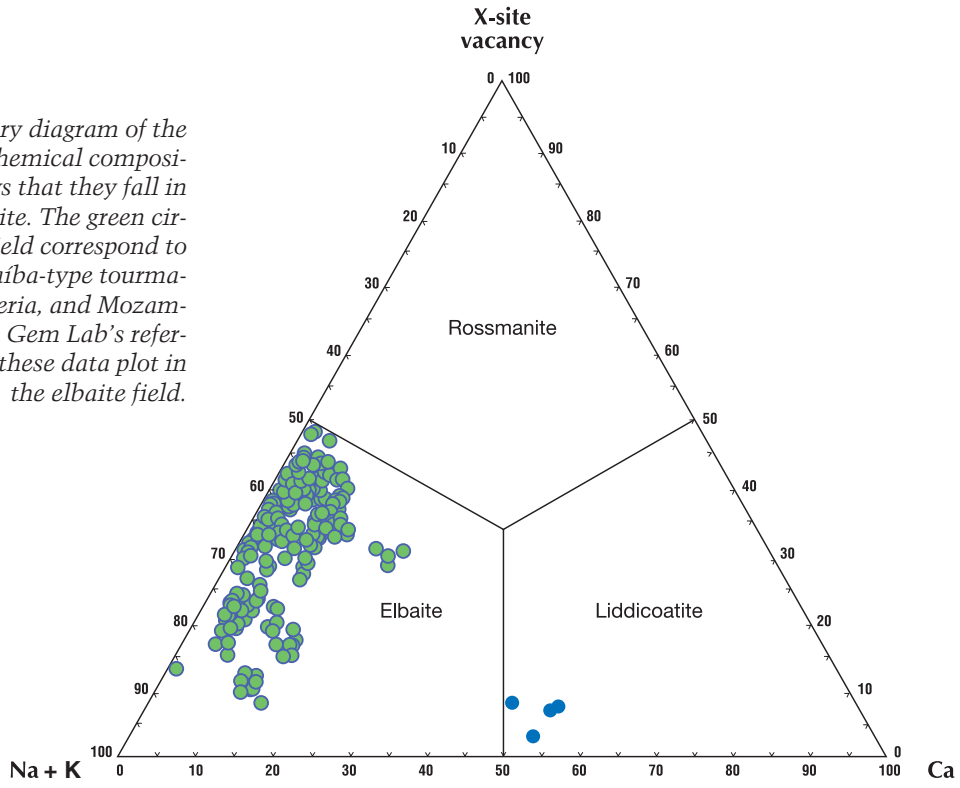

Figure 35. This ternary diagram of the four samples' average chemical composition (blue circles) shows that they fall in the field for liddicoatite. The green circles in the elbaite field correspond to analyses of typical Paraíba-type tourmaline from Brazil, Nigeria, and Mozambique in the Gübelin Gem Lab's reference collection; all of these data plot in the elbaite field.

there are 13 known end members. When plotting the chemical composition of these specimens on a ternary diagram for lithium-rich tourmaline, all four samples fell in the liddicoatite field (figure 35). Based on calculations using a recently developed tool (L. Klemm and P. Hardy, "Determination of tourmaline species by advanced chemical analysis," *Proceedings of the 3rd European Gemmological Symposium*, Berne, Switzerland, June 5–7, 2009, pp. 58–59) and averaging the four chemical analyses obtained on each stone by LA-ICP-MS, the samples contained a 50–57% liddicoatite component; thus, all four were liddicoatite tourmaline.

Some traders we spoke with believe that these stones are from Mozambique, near the mine that produced Paraíba-type elbaite. We also have been told that liddicoatite rough has been found in this area that does not need heat treatment to produce the desirable greenish blue coloration. This is the first report of Cu-Mn bearing liddicoatite tourmalines of such color.

Stefanos Karampelas (s.karampelas@gubelingemlab.ch) and Leo Klemm
Gübelin Gem Lab, Lucerne, Switzerland

INSTRUMENTS AND TECHNIQUES

Use your LCD screen as a gemological tool. Most LCD (liquid crystal display) screens, such as those used for computer or mobile phone displays, are sources of plane-polarized light. We recently tested the possibility of using such screens to observe the pleochroism of faceted gems. When we placed a few gems table-down over the white portion of a mobile phone display, the pleochroism was readily visible (figure 36). Further, by using a handheld polarizer, such as a camera polarizing filter or even polarizing sunglasses, one can create a makeshift polariscope (figure 37).

Given the widespread use of LCD screens in various products, gemologists should keep them in mind as a convenient working tool when traditional instruments are not available, particularly in the field. Note, however, that some displays using new technology (e.g., OLED—organic light emitting diodes) are not a source of polarized light and thus cannot be used as gemological tools. It is therefore advisable to first test a screen with a polarizing filter.

Bertrand Devouard and Rémi Bornet
Laboratoire Magma et Volcans, Blaise Pascal University CNRS (UMR 6524), Clermont-Ferrand, France
Franck Notari, Benjamin Rondeau, and Emmanuel Fritsch

Smartphone photomicrography. Smartphones such as the Apple iPhone, Motorola Droid, and Nokia N8 have become increasingly popular in recent years. Top-end models typically feature good-quality digital cameras that rival some "point-and-shoot" cameras, in addition to having basic photo-editing software.

The popularity of smartphones has also spawned the development of numerous accessories that can expand their functionality even further. One such accessory is a low-power microscope that clips onto the phone over the camera lens. This contributor was interested in seeing if this device could have gemological applications.

The microscope accessory in figure 38 was ordered on the Internet for less than US$20. Its sliding housing offers varying levels of magnification, and illumination is provided by two white LEDs. The lighting assembly can be rotated about 45° to change the angle of illumination.

Although this device is clearly not optimized for gemological use, with some practice it was possible to produce serviceable photomicrographs. The images in figure 39 were taken with an Apple iPhone 4 using the ProCamera photography application, which allows manual adjustment of focus and white balance. As with any photogra-

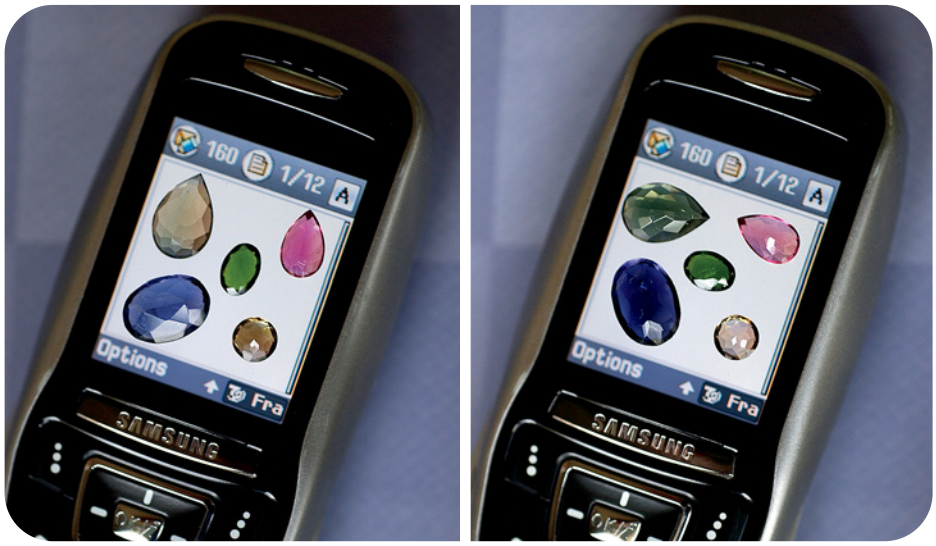

Figure 36. When pleochroic stones are placed table-down on an LCD screen, as on this cell phone, they display pleochroism when rotated 90° (from left to right and top to bottom: kornerupine, tourmaline, chrome diopside, iolite, and smoky quartz). Photo by B. Devouard.

Figure 37. A simple polariscope is created when a polarizer is placed in front of the plane-polarized LCD screen. Here, a colorless topaz has been rotated on the cell phone screen under a camera polarizing filter. Photo B. Devouard.

phy, the biggest challenge was the lighting. The LEDs proved too bright in most situations, and better results were achieved by partially shielding them or turning them off and relying on ambient light. Although the microscope's packaging promised magnification up to 60×, in practice it was impossible to obtain good focus beyond medium power (~20×). The best results were produced with a combination of the phone's digital zoom, careful adjustment of the autofocus, and a steady hand.

Although this device clearly will not replace a standard gemological microscope or even a loupe, it appears to provide a useful field tool in the gemologist's arsenal.

Figure 38. This inexpensive microscope accessory clips over a smartphone camera lens. Illumination is provided by LEDs. Photo by Robert Weldon.

Thomas W. Overton (toverton@gia.edu)
GIA, Carlsbad

SYNTHETICS AND SIMULANTS

Filled copal imitation of amber. Amber is one of the most popular gem materials for traditional Islamic prayer beads (*Mesbah* in Arabic). Specimens with inclusions of plants, insects, or even animals are often used. However, we have also seen amber imitations fashioned for this purpose.

We recently received a strand resembling amber that consisted of 33 yellow round beads (~12 mm in diameter) with two oval-shaped separators and a fancy-shaped link (figure 40). The round beads contained dark brown plant debris and a variety of insects: ants, mosquitoes, ladybugs, and flies, all in good condition. They were inert to short-wave UV radiation, but their reaction to long-wave UV was striking. They displayed a moderate chalky greenish yellow fluorescence, which appeared to be confined to the surface, together with distinctive chalky blue circular areas (figure 41)—most located near drill holes—that strongly suggested assemblages.

We obtained spot RI readings of 1.52 on the circular zones and 1.54 elsewhere. Observation between crossed polarizers revealed strong anomalous double refraction with

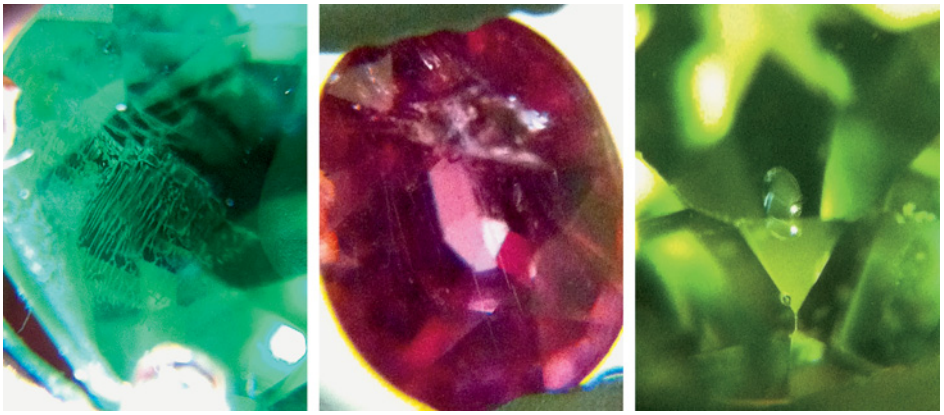

Figure 39. Taken with an Apple iPhone and the clip-on microscope in figure 38, these images show flux inclusions in synthetic emerald (left), needle-like inclusions in corundum, and a "lilypad" inclusion in peridot. Photomicrographs by T. W. Overton; fields of view ~4.0 mm.

strain colors. With the client's permission, we conducted hot-point and acetone tests on very small, inconspicuous areas. The main portion of the beads had a resinous odor, while the circular zones had an acrid odor. During acetone tests, the main areas revealed slightly softened and etched surfaces, while the circular portions showed even stronger surface etching. The characteristics of the bulk of the beads were consistent with copal, while those of the circular portions were consistent with plastic. This was the case for all 33 round beads, while the separators and link of the strand only showed characteristics consistent with copal, with no circular portions or insects.

Microscopic observation clearly revealed a separation plane between the main part of the beads and the circular blue-fluorescing areas, denoted by curved polish marks beneath the surface (figure 42, left). Examination with immersion (in water) indicated that all the round beads were cored and filled with a colorless to light yellow plastic, along with insects (figure 42, right). Gas bubbles were seen adjacent to insects within the plastic. In addition, a separation plane was visible between the beads' plastic core (containing the insects) and a plastic outer layer that formed the circular-fluorescing zones (which contained plant debris). The plant debris resembled that which was present in the copal, and apparently was added to the plastic to make it less noticeable.

On the basis of the evidence, we concluded that the beads consisted of copal filled with plastic to imitate insect-bearing amber. It appears that each round copal bead was subjected to the following process: (1) drilling

Figure 40. The beads in this rosary (~12 mm in diameter) proved to be copal filled and assembled with plastic to imitate amber. Photo by S. Singbamroong, © Dubai Central Laboratory.

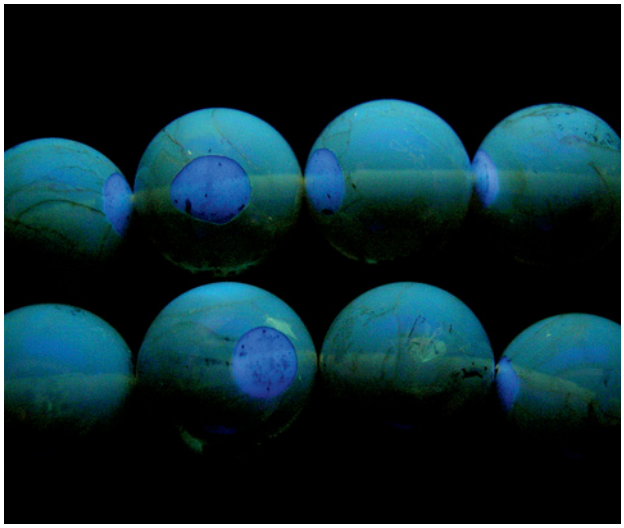

Figure 41. When exposed to long-wave UV radiation, the beads display a moderate chalky greenish yellow fluorescence, as well as chalky blue circular patterns. Photo by S. Singbamroong, © Dubai Central Laboratory.

and hollowing out the interior, (2) filling with plastic that contained insects, and (3) masking the hole with plastic containing plant debris. The inner filling material containing the insects was exposed on a small portion of the surface of a few beads, and acetone and hot-point testing of those areas gave results consistent with plastic.

Sutas Singbamroong (sssutas@dm.gov.ae) and Moza Rashed Al Falasi
Gemstone Unit, Dubai Central Laboratory
Dubai, United Arab Emirates

Glass with crystalline aggregates. Glass is the most common gem simulant and can show a wide variety of colors, transparencies, and optical effects. Most examples display similar features—namely gas bubbles, swirl marks, and devitrification effects—but in the last few years this contributor has encountered some interesting and unusual glass specimens (see, e.g., Summer 2007 GNI, pp. 174–175; Summer 2010 GNI, pp. 155–156).

Recently, the Gem Testing Laboratory of Jaipur, India, received a green 25.04 ct step cut measuring 20.04 × 14.86 × 6.36 mm (figure 43). It had the translucency of chalcedony and the color of emerald. None of emerald's distinct inclusions were observed microscopically, however, and the heft was sufficiently high to rule out emerald or chalcedony. Microscopic examination with fiber-optic light revealed aggregates of colorless crystalline features throughout the sample (figure 44). The crystals were easily resolved at higher magnification and were much larger than those found in cryptocrystalline materials such as chalcedony. The presence of these crystals initially suggested a natural origin.

Standard gemological testing, however, revealed the

Figure 42. Microscopic observation clearly reveals a separation plane between the main part of the beads and the blue-fluorescing round areas, denoted by circular polish marks beneath the surface (left). Immersion in water revealed they were copal beads that had been cored and filled with a colorless to light yellow material containing insects (right). Also visible are small bubbles next to the insect (white arrows) and a separation plane between the insect-bearing plastic in the core and an outer plastic layer containing plant debris (red arrows). Photomicrographs by S. Singbamroong, © Dubai Central Laboratory; magnified 10×.

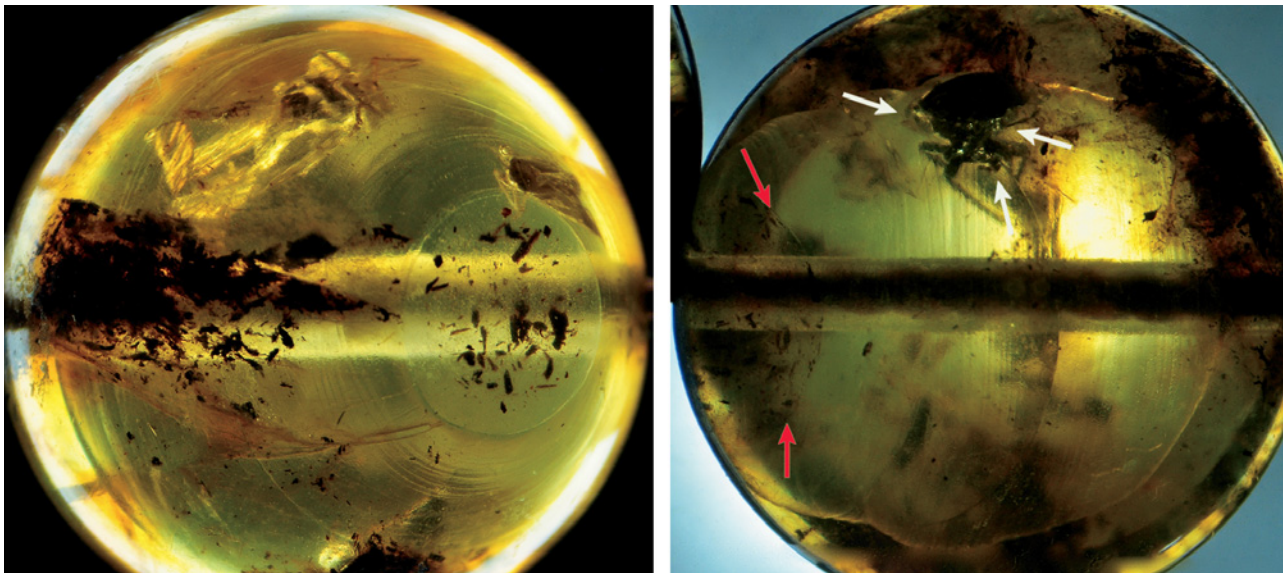

Figure 43. This 25.04 ct translucent green specimen, which proved to be glass, is unusual for its crystalline features. Photo by G. Choudhary.

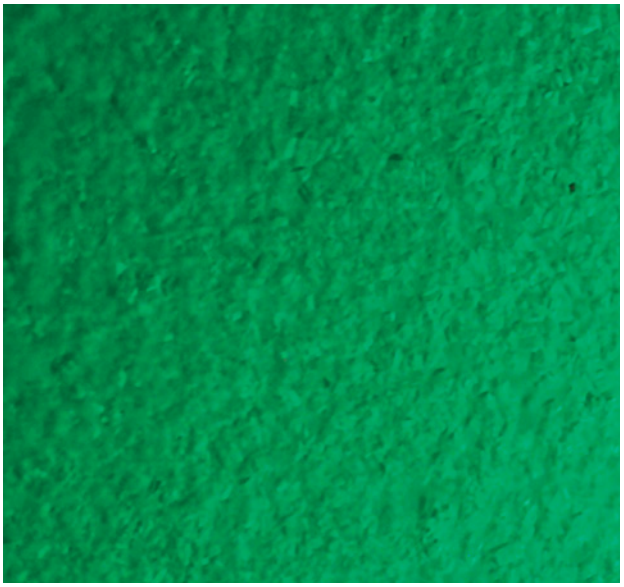

Figure 44. The glass specimen in figure 43 displays homogeneous colorless crystals throughout, giving it an aggregate structure. Photomicrograph by G. Choudhary; magnified 60×.

following properties: RI—1.745; hydrostatic SG—4.33; aggregate reaction in the polariscope; UV fluorescence—chalky blue to short-wave, and inert to long-wave UV. These properties indicated a glass, which was confirmed by FTIR and EDXRF analysis. The IR spectrum displayed twin humps between 3600 and 2600 cm^{-1} and complete absorption up to 2500 cm^{-1}, while qualitative EDXRF revealed the presence of Si, Ca, and Pb, the last being responsible for the high RI and SG values. During a subsequent microscopic examination of the sample, one gas bubble was finally resolved.

Crystalline features have been reported previously as inclusions in glass (see, e.g., H. A. Hänni et al., "A glass imitation of blue chalcedony," *Journal of Gemmology*, Vol. 27, No. 5, 2001, pp. 275–285; Lab Notes: Spring 2008, pp. 70–71; Summer 2010, pp. 144); these are attributed to partial devitrification. Hänni et al. (2001) identified the transparent and colorless crystalline inclusions as wollastonite, but those in our sample could not be identified with the techniques available.

Such specimens make very convincing gem simulants. In the absence of proper gemological testing and FTIR/EDXRF analysis, there is a strong possibility of misidentification.

Gagan Choudhary

Synthetic ruby specimen sold as natural. *G&G* has reported on a number of synthetic rubies sold as natural crystals (see Fall 1993 Lab Notes, p. 204; Fall 2001 GNI, pp. 243–245). A recent case underscores the importance of taking precautions against such frauds.

Dubai is a relatively new market for rough and polished colored stones, and an intersection between African sources and the Asian trade. It has also seen a variety of imitations of natural gem crystals. In fact, within the past two years, these contributors have reported on imitations of diamond and emerald crystals (Fall 2009 GNI, pp. 230–231; Winter 2009 GNI, pp. 305–306).

Recently, the Dubai Central Laboratory received a rough specimen for identification. The red "crystal" (figure 45) had a distorted hexagonal shape and was attached to some matrix material. It was identified as ruby by its absorption spectrum with a handheld spectroscope, a finding confirmed by UV-Vis-NIR spectroscopy. Using a microscope, we observed curved striae and filled cavities; gas bubbles were visible in the filling material. We therefore identified this sample as synthetic ruby with filled fractures. Raman spectroscopy identified the matrix as quartz, which had been joined to the synthetic ruby by some type of glue. Since quartz is geologically incompatible with corundum, the matrix provided another clue that this specimen was a fake.

This case again illustrates the importance of gem laboratory reports and the necessity of thoroughly examining a piece before purchase.

Nazar Ahmed (nanezar@dm.gov.ae)
and Hassan Al Marzooqi
Gemstone Unit, Dubai Central Laboratory
Dubai, United Arab Emirates

MISCELLANEOUS

Louis XV's Golden Fleece—recreated. In 1743, King Louis XV of France became a knight of the Order of the Golden

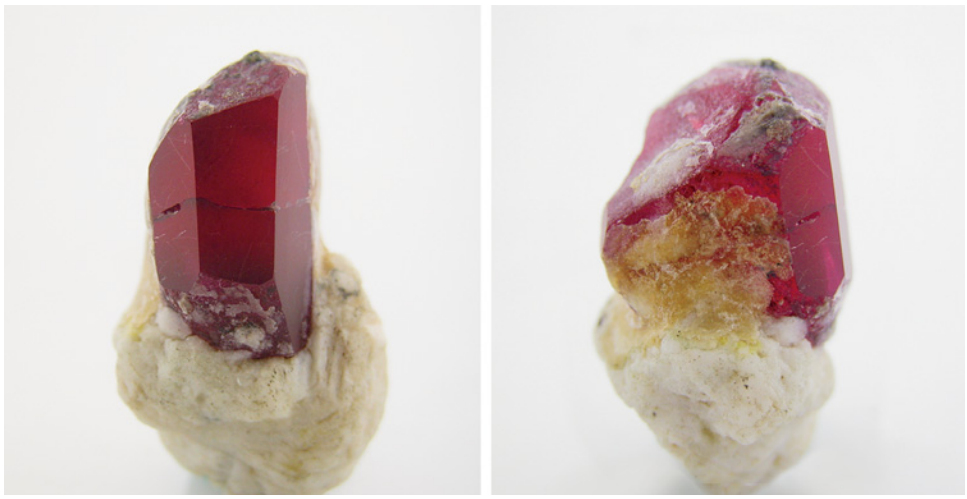

Figure 45. This synthetic ruby "crystal" (2.7 cm tall) was fashioned to imitate natural ruby in matrix. Photos by N. Ahmed, © Dubai Gemstone Laboratory.

Fleece, the first French ruler to receive this distinction since its founding in Burgundy three centuries earlier. In 1749, the king's jeweler, Jacqumin, created an emblem of this order for the king. It was composed of three exceptional gems: the 69 ct French Blue diamond; a 32.62 ct light blue diamond later named the Bazu; and the 107 ct Côte de Bretagne, a spinel carved as a dragon. This masterpiece of French rococo jewelry was stolen and disassembled in 1792 during the revolution; only the spinel carving remained intact, and it now resides in the Louvre. Many historians have since tried to reconstruct this emblem on paper (e.g., B. Morel, *The French Crown Jewels*, Fonds Mercator, Antwerp, 1988; H. Tillander, *Diamond Cuts in Historic Jewelry: 1381–1910*, Art Books Intl. Ltd., London, 1995).

Recently, these contributors recreated the Golden Fleece as accurately as possible, based on a 2008 painting (see figure 15 in Farges et al., "The French Blue and the Hope: New data from the discovery of a historical lead cast," Spring 2009 *G&G*, pp. 2–17) as well as a drawing of the original piece that was discovered in the 1980s in Switzerland. We tried to incorporate Jacqumin's techniques and *savoir faire* by using 3D rendering for the design and analyzing historical elements (such as diamond setting) that were not available to, or not considered by, previous investigators.

Replicas of the two blue diamonds were created from cubic zirconia. The Côte de Bretagne dragon was carved from lead glass using a wax replica based on 3D-scaled pictures of the original. Gold and manganese pigments in the glass were used to simulate the color of the spinel. The emblem's 500+ remaining "diamonds" were fashioned from cubic zirconia using a baroque cushion cut. The red and yellow stones, which adorned the dragon's flames and the golden fleece, were made from colorless CZ and then painted on their backs, following Jacqumin's original method.

Since the emblem was most likely made of silver-plated gold, as was the custom for French royal jewelry at the time (the setting of diamonds in gold was considered tasteless by royal French jewelers), we decided to create a setting constructed primarily of sterling silver. The metal was carved to recreate the delicate distribution of the dragon's wings and tail, as well as the palms over which the dragon is suspended. Some parts of the silver setting were gilded to recreate the elegant combination of gold and silver that likely prevailed in the original, and all the stones were set using 18th century techniques.

After three years of work, the recreated Golden Fleece (figure 46) was unveiled on June 30, 2010, at the site where the original jewel was stolen in 1792: the former royal storehouse, now the Hôtel de la Marine on Place de la Concorde in Paris. The event was filmed for a documentary on the French Blue, and an English-language version titled "Secrets of the Hope Diamond" will be broadcast in the U.S. in 2011 on the National Geographic channel.

Herbert Horovitz
Geneva, Switzerland

François Farges (farges@mnhn.fr)
Muséum National d'Histoire Naturelle
Paris, France

CONFERENCE REPORTS

20th Annual Goldschmidt Conference. The geochemistry-focused Goldschmidt Conference was held June 13–18, 2010, in Knoxville, Tennessee. The meeting featured a session titled "Geochemistry and Trace Elements in Gem Materials," chaired by **Drs. Emmanuel Fritsch** and **Benjamin Rondeau** (both from the University of Nantes, France), who opened with a brief discussion on the increasing importance of trace-element chemistry for investigating gemological problems. Their remarks were followed by several interesting talks. Abstracts can be viewed at www.goldschmidt2010.org/abstracts/view.

This contributor demonstrated the use of LA-ICP-MS analysis in separating amethyst, citrine, and malachite from their laboratory-grown equivalents. **Dr. Adolf Peretti** (GRS Gemresearch Swisslab, Lucerne) presented data showing small-scale chemical variations within single

Figure 46. This photo of the reconstructed Golden Fleece (~16 × 5 cm) shows a CZ replica of the 69 ct French Blue that is set above the fleece composed of about one hundred yellow paint–backed cubic zirconias, and set below a glass replica of the 107 ct Côte de Bretagne spinel. Photo by F. Farges.

crystals of Paraíba-type tourmaline, and cautioned against using color-specific geochemical criteria to identify geographic origin. **Dr. Laurence Galoisy** (University of Paris) discussed the role of chromium and other transition elements in the color of garnets from Thailand and East Africa. **Kaifan Hu** (Pennsylvania State University, University Park) showed how gem pietersite from Namibia can be separated from similar Chinese material on the basis of microstructures.

Both session leaders examined the chemical composition of opal. **Dr. Fritsch** described how differences in uranium content affect the occurrence of green and blue UV

luminescence. **Dr. Rondeau** presented geochemical data for opals from Wollo, Ethiopia (see Summer 2010 *G&G*, pp. 90–105). Of particular note were elevated barium concentrations, which are atypical of opal from volcanic environments.

Two talks dealt with trace elements in diamond. **Yakov Weiss** (Hebrew University of Jerusalem) categorized the trace-element composition of fluids trapped in fibrous diamonds into three groups that might prove useful in determining geographic origin. **Dr. Eloïse Gaillou** (Smithsonian Institution, Washington, DC) set forth a method for calculating total boron concentration in type IIb blue diamonds and compared that with existing methods using FTIR analysis.

Three posters also were displayed as part of the gem session. **W. Bieri** (GRS Gemresearch Swisslab) showed how the chemical composition of apatite inclusions in corundum and spinel can help specify the geographic origin of the host gem. **Dr. Andy H. Shen** (GIA Laboratory, Carlsbad) presented detailed data showing the possibility of using LA-ICP-MS analysis to measure trace concentrations of silicon in sapphire; this element may have an important effect on color centers in corundum. Finally, **Kristen Yetter** (New Mexico State University, Las Cruces) showed how LIBS analysis can provide a preliminary indication of geographic origin in some rubies and sapphires.

Christopher M. Breeding (mbreedin@gia.edu)
GIA Laboratory, Carlsbad

20th General Meeting of the International Mineralogical Association (IMA). This meeting was held August 21–27 at Eötvös Lorand University in Budapest. Some 1,700 participants from 74 countries attended, making it the largest IMA event to date. The conference featured several presentations of gemological interest, some of which are summarized here. Abstracts of all oral and poster presentations can be found at www.ima2010.hu/img/doc/ima2010_abstracts.pdf.

In an invited presentation, **Thomas Hainschwang** (Gemlab Laboratory, Balzers, Liechtenstein) reviewed the challenges of separating natural- and treated-color diamonds using visible, infrared, and photoluminescence spectroscopy. These techniques allow researchers to characterize optical defects in diamonds, some of which can be created, modified, or destroyed by laboratory treatment processes. The behavior of optical defects during treatment is a key to colored diamond identification. **Dr. Thomas Stachel** (University of Alberta, Edmonton, Canada) showed that most gem diamonds originate from several source rocks in portions of the lithospheric mantle beneath cratons. **Dr. Richard Taylor** (University of Saint Andrews, Scotland) discussed the chemical analysis of trace elements in gem feldspars using two analytical techniques: X-ray absorption fine structure (XAFS) and X-ray excited optical luminescence (XEOL). **Dr. Alessandra Costanzo** (National University of Ireland, Galway) described the results of a study of fluid inclusions in emeralds from the Piteiras mine in Minas Gerais, Brazil. **Dr. Bertrand Devouard** (Blaise Pascal University, Clermont-Ferrand, France) presented detailed chemical composition data on pezzottaite samples from Madagascar, Afghanistan, and Myanmar. Some specimens from Myanmar displayed hourglass-shaped color zoning, with significantly greater cesium content in the more strongly colored sectors.

One of these contributors (SK) compared microradiography with X-ray computed microtomography for imaging the internal structure of pearls. Despite a data-collection time lasting several hours, computed microtomography offered improved resolution over conventional imaging techniques. A study of the internal features and chemical composition of 170 alexandrite samples from various sources was presented by **Anna-Kathrin Malsy** (Gübelin Gem Lab, Lucerne, Switzerland). On the basis of LA-ICP-MS analyses, most sources could be differentiated on a triangular plot of boron, tin, and magnesium contents. The chemical composition data proved far more valuable than microscopic examination, since there were no diagnostic inclusions.

Dr. Pornsawat Wathanakul (Kasetsart University, Bangkok) compared the properties of blue-green-yellow sapphires from the Nam Khun–Nam Yuen region of Thailand and Garba Tula in Kenya. Both groups of sapphires come from basaltic host rocks, but slight differences in their visible absorption spectra appear to distinguish them. **Somruedee Satitkune**, also of Kasetsart University, examined mineral inclusions in diamonds from the Koffiefontein and Finsch mines in South Africa. She showed that inclusions with cubic symmetry (such as pyrope and chromite) exhibit nearly the same angular orientation to the {111} crystal face of diamond, whereas inclusions of minerals with lower symmetry (diopside and olivine) display more variable angular orientations.

Dr. Gaston Giuliani (Institute of Research for Development, and Center for Petrographic and Geochemical Research, Nancy, France) described how metamorphism of evaporates associated with sedimentary carbonate rocks provided the fluids partly responsible for the formation of some important colored stone deposits. **Dr. Dorrit Jacob** (Johannes Gutenberg University, Mainz, Germany) detailed the use of chemical composition data obtained by LA-ICP-MS analysis to differentiate freshwater cultured pearls from various geographic sources using the ratio of Ba/Sr versus B concentrations. **Tashia Dzikowski** (University of British Columbia, Vancouver, Canada) reported on the discovery of a ruby and sapphire deposit hosted in marbles near Revelstoke, British Columbia. She also provided details on the geologic conditions of corundum formation. **Dr. Tobias Häger** (Johannes Gutenberg University) described an interesting occurrence of ruby and sapphire, rimmed by spinel, from

the Luc Yen–Yen Bai mining area in Vietnam. Microscopic evidence suggests the spinel formed by an alteration reaction between corundum and dolomite.

During the conference, a meeting of the IMA Commission on Gem Materials (CGM) was held under the direction of the chair of the commission, **Dr. Lee Groat** (University of British Columbia, Vancouver). Among the items discussed was the creation of a CGM website, which may include an online atlas of gem deposits and also links to gem museums throughout the world.

James E. Shigley (jshigley@gia.edu)
GIA Research, Carlsbad
Stefanos Karampelas

Carpathian and Balkan Geological Association (CBGA) meeting. The 19th meeting of the CBGA took place in Thessaloniki, Greece, August 23–26, 2010. About 700 participants from 15 countries attended the event, which for the first time featured a session on gemology, with a particular focus on archeogemology as well as gems from the Carpathian and Balkan regions.

In the keynote lecture, **Dr. Emmanuel Fritsch** (University of Nantes, France) gave an update on the origin of color in minerals and gems. **This contributor** presented a nondestructive study of four late-16th and early-17th century religious artifacts from the Benedictine Abbey of Einsiedeln, Switzerland. The results of this analysis were compared with observations recorded at the end of the 17th century (for more details, see the article on pp. 292–296 of this issue).

Elisabeth Strack (Gemmological Institute of Hamburg, Germany) used "classical gemology" to investigate three jewelry pieces uncovered from the ruins at Veliki Preslav, Bulgaria, that date from the 9th century. These items contained a garnet, purple sapphires, emeralds with indications of Egyptian origin, and saltwater pearls. **Dr. Corina Ionescu** (Babes-Bolyai University, Cluj-Napoca, Romania) examined some unusual 5th century garnet-set jewelry (see the GNI entry on pp. 316–318 of this issue). A report on Bulgarian gem carvings from the Neolithic and Chalcolithic periods and their impact on the history of gemology was presented by **Dr. Ruslan I. Kostov** (St. Ivan Rilski University of Mining and Geology, Sofia). He indicated that these carvings represent the earliest record of fashioned nephrite from Bulgaria (figure 47) and the earliest known turquoise from the eastern Rhodope Mountains.

In the poster session, **Zoran Miladinović** (University of Belgrade, Serbia) discussed some deposits of gem-quality silica minerals (e.g., amethyst) found in a volcanic complex extending from southern Serbia to northern Greece (the Lece-Chalkidiki metallogenic zone). **Dr. Ludmila Illašová** (Constantine the Philosopher University, Nitra, Slovakia) reviewed opals and other gem-quality silica minerals from various locations in Slovakia. **Dr. Magdalena Dumańska-Słowik** (University of Krakow, Poland) offered preliminary results from a fluid inclusion study of topaz crystals from Volodarsk-Volynski, Ukraine, that apparently formed at about 360–385°C. Preliminary results from an FTIR and powder X-ray diffraction study of heated and unheated freshwater cultured pearls were presented by **Eleni Theodosoglou** (Aristotle University of Thessaloniki, Greece). Color differences were observed after heating at 250°C for one hour in air (5°C/min heating rate). The samples' XRD patterns did not change after heating, but some infrared bands showed slight differences related to organic matter and water.

Figure 47. This zoomorphic nephrite amulet from Bulgaria measures 4.2 × 3.7 cm and is from the early Neolithic period (i.e., end of the 7th millennium BC). Courtesy of the Regional Historical Museum, Kurdjali, Bulgaria (collection no. 4532); photo by Vladimir Alexeev.

The 20th CBGA meeting will take place in Albania in 2014.

Stefanos Karampelas

European Diamond Conference. More than 300 delegates attended the 21st European Conference on Diamond, Diamond-Like Materials, Carbon Nanotubes, and Nitrides, held September 5–9, 2010, in Budapest. Highlights of gemological interest from the ~330 oral and poster presentations are summarized here.

Several researchers, including **Dr. Mikhail Lukin** (Harvard University) and **Dr. Mark Newton** (University of Warwick, England) presented new research on nitrogen vacancy (NV) centers that occur—or have been created

after growth—in synthetic diamond. NV centers are common in natural diamonds as well, and have proven important for the detection of HPHT treatment since the late 1990s.

Dr. Bert Willems (HRD, Antwerp) presented a study of six CVD synthetic diamond samples grown at LIMHP-CNRS (Villetaneuse, France). These high-quality plates contained varying nitrogen contents (up to 200 ppm) and were characterized by a 525 nm band in the UV-Vis absorption spectra, along with strong NV centers and a silicon peak at 737 nm.

Dr. Riadh Issaoui (LIMHP-CNRS) provided the latest results of growing free-standing type IIb CVD synthetic diamond plates. Good-quality plates (measuring 5 × 5 mm and 200 µm thick) were grown at an intermediate microwave power density of 80 W/cm^3, a substrate surface temperature of 800–1000°C, a total feed-gas rate of 200 standard cubic centimeters per minute, a boron-to-carbon ratio of 3000 ppm, and a 5% methane concentration.

Dr. Andrey Bolshakov (Russian Academy of Sciences, Moscow) grew thin films of CVD synthetic diamond that mimicked the structure of opal, resulting in novel three-dimensional photonic crystals. Using porous synthetic opal as a template, he and his colleagues grew CVD synthetic diamond either in the voids between the silica spheres or in place of the etched silica. With the recent interest in diamond-like coatings applied to gemstones, the implications of this work may someday be seen in the jewelry industry.

This contributor compared the phosphorescence spectra results of 357 natural type IIb diamonds with those of HPHT-treated and HPHT-grown synthetic diamonds. The only phosphorescence bands observed in the natural diamonds were centered at 500 and 660 nm. None of the treated or synthetic diamonds showed the 660 nm band, but all did display the 500 nm band, usually at higher intensity than in the comparable natural diamonds.

Sally Eaton-Magaña (smagana@gia.edu)
GIA Laboratory, Carlsbad

5th International Workshop on Provenance and Properties of Gems and Geo-materials. Since 1997, these workshops have been held approximately every two years in Hanoi. The most recent session took place October 18–24, 2010, at the Vietnamese Academy of Science and Technology, with more than 60 participants from 13 countries in attendance. The workshop started with a one-day field trip to an akoya pearl farm at Ha Long Bay (figure 48). Over the next three days, about 40 talks and posters were presented.

Dr. Christoph Hauzenberger (University of Graz, Austria) discussed the petrology and geochemical characteristics of spinel rims surrounding some ruby and sapphire samples from Truc Lau in northern Vietnam. **Dr. Chakkapan Sutthirat** (Gem and Jewelry Institute of Thailand and Chulalongkorn University, Bangkok) compared the spectroscopic, chemical, and microscopic characteristics of Vietnamese rubies from two different regions, Luc Yen and Quy Chau. **Dr. Visut Pisutha-Arnond**, representing the same institutions as Dr. Sutthirat, gave an update on the spectroscopic, chemical, and microscopic characteristics of gem-quality purplish red almandine from Houaphan Province in northeastern Laos. **Dr. Pornsawat Wathanakul** (Gem and Jewelry Institute of Thailand and Kasetsart University, Bangkok) offered preliminary means of identifying the origin of some alexandrites. **Walter Balmer** (Chulalongkorn University) delivered a portion of his Ph.D. research on the possible genetic link between the marble-hosted ruby deposits in Luc Yen and those near Yuan Jiang in the Ailao Shan Mountains of China.

Dr. Boontawee Sriprasert (Department of Mineral Resources, Bangkok) summarized heating experiments on the coloration of tourmaline. **Dr. Bhuwadol Wanthanachaisaeng** (Burapha University, Chanthaburi, Thailand) outlined the identification of heat-treated zircons by their FTIR spectra. **Dr. Kanphot Thongcham** (Ramkhamhaeng University, Bangkok) examined the effects of annealing on the color of zircon. **Dr. Vu Phi Tuyen** (Vietnamese Academy of Science and Technology, Hanoi) presented the results of photoluminescence and thermoluminescence studies of zircon during annealing.

Dr. Tobias Häger (Johannes Gutenberg University, Mainz, Germany) described gemological applications of Cr^{3+} luminescence. In some spinels, Dr. Häger reported, the FWHM (full width at half maximum) of chromium bands at ~700 nm increases after heat treatment. **Dr. Lutz Nasdala** (University of Vienna, Austria) described defect luminescence of ion-irradiated gem materials, focusing on diamond and zircon.

One of these contributors (SK) described the structures and pigments observed in natural pearls, focusing on non-nacreous types such as melo, scallop, and quahog. **Dr. Jayshree Panjikar** (Institute of Gem & Jewellery, Pune, India) reviewed the microscopic and crystallographic features of gem-quality beryl from India.

The last day of the presentations took place at the headquarters of Doji Gold & Gems Group, where participants were briefed on the company's gem mining activities and their cutting factory. In addition, **Dr. Dietmar Schwarz** (Gübelin Gem Laboratory, Lucerne, Switzerland) reviewed ruby, sapphire, and emerald mining and marketing. The conference closed with a three-day field trip, led by Doji vice chairman **Duong Anh Tuan**, to a primary marble-hosted spinel mine and a secondary ruby and spinel mine in the Yen Bai region.

Stefanos Karampelas
Le Thi-Thu Huong
Faculty of Geology, Vietnam National University
Hanoi

Figure 48. This akoya cultured pearl farm is located at Ha Long Bay in northeastern Vietnam. Photo by Christoph Hauzenberger.

ERRATA

1. The Summer 2008 GNI section (pp. 184–185) erroneously reported the yellow vanadinite locality as the Democratic Republic of the Congo. Dr. Lavinsky's supplier has now admitted that the material was actually found in Otjitheka, Kaokoland, northwest Namibia.
2. The business retrospective article by R. Shor and R. Weldon in the Fall 2010 issue (pp. 166–187) incorrectly stated that the American Gem Society Laboratory was the first grading lab to issue a cut grade on diamond grading reports. A number of smaller labs were in fact issuing cut grades prior to AGS. We thank David Atlas for bringing this to our attention.
3. There were two errors in table 1 of the gem localities retrospective article by J. E. Shigley et al. in the Fall 2010 issue (pp. 188–216). On page 203, the Hiddenite emerald locality is located in Alexander County, not Mitchell County. On page 214, Malawi should not have been listed as a tourmaline locality; the Canary deposit is actually located in Lundazi, Zambia.
4. The C. M. Breeding et al. technology retrospective article in the Fall 2010 issue (pp. 241–257) incorrectly referred to the Holloway Cut Adviser as Holloway Cut Analysis. In addition, The Lexus M-Box software referred to in the article was developed by OctoNus (Lexus is the distributor) and the image in figure 10 shows the Oxygen software user interface. The rough diamond planning system also makes use of DiamCalc, which OctoNus developed in the late 1990s and today is used widely to assist in the evaluation of diamond cutting. Our thanks to Sergey Sivovolenko for providing this additional information.

EDITORS
Susan B. Johnson
Jana E. Miyahira-Smith
Thomas W. Overton

Blood on the Stone: Greed, Corruption, and War in the Global Diamond Trade

By Ian Smillie, 252 pp., publ. by Anthem Press [www.anthempress.com], London, 2010. US$29.95

Ian Smillie starts his new book by saying that it will address how diamonds fueled some of the most brutal wars in Africa. *Blood on the Stone* achieves this goal comprehensively and compellingly. More importantly, it also explores the larger issue behind this story—that of the extraction of mineral resources from developing countries and the struggle to force corporate accountability for the abuses and imbalances that have resulted.

The prologue relates the history of Smillie's own involvement in the conflict diamond issue, beginning with a meeting in the Ottawa offices of the nongovernmental organization Partnership Africa Canada, where he worked in 1997, and leading into his travels as a UN-appointed expert, which took him from war-torn regions of Africa to the White House.

Over a period of 10 years, Smillie became renowned for his knowledge of the conflict diamond issue and as an advocate for change. He takes pains to stress that diamonds did not *cause* the rebel wars in Sierra Leone, Angola, and the Democratic Republic of Congo. But they did prolong these conflicts by providing huge amounts of money to finance them. There has been much debate as to whether greed or grievance was the cause—the answer, according to Smillie, was both.

During the 1990s, perhaps 25% of the world's trade in rough diamonds was infected by some sort of illicit activity. The context for how this activity came to be so commonplace lies in the nature of the product and the trade: the portability and accessibility of diamonds, the industry's inherent secrecy and preference to avoid paperwork, the lack of government controls, and the difficulty of obtaining accurate data to track the flow of goods. Diamonds have long been linked to tax evasion and money laundering. In the 1990s, though, they were used to bankroll wars that claimed millions of lives and caused untold suffering.

Students of gemology will appreciate Smillie's review of the history of diamonds, with its concise and precise descriptions of their geology and timelines of important discoveries. Unlike many popular accounts of the diamond trade, this section is both scientifically accurate and well researched. Background on De Beers and its control of much of the rough diamond trade sets the scene for how combatants were able to use diamonds to fund conflict.

But it is in the surprisingly even-handed historical accounts of the diamond trade and politics in Angola, Liberia, Sierra Leone, and the DRC that Smillie's measured analysis and historical knowledge comes into its own. In these chapters, the reader is taken deep into the sordid tales of African history since independence. From the De Beers–funded International Diamond Security Organisation in West Africa during the 1950s to the shadowy 1980s terrorist training camps in Libya, the training grounds for the perpetrators of the madness that gripped Sierra Leone and Liberia in the 1990s, Smillie paints a grim picture of the damage wreaked by the sale of diamonds.

Any consumer who has recently purchased a diamond will learn that there is a 60% chance it came from Africa, and a 90% chance it traveled to the cutting centers of both Antwerp and India. They will also learn that before the 2003 implementation of the Kimberley Process Certification Scheme (KPCS), one out of four diamonds were at some point likely stolen, illegally mined, or used to launder money or evade taxes.

The book ends with a discussion of how the NGOs forced the diamond industry to accept responsibility for the problems occurring in Africa and their search for a solution. The drawn-out negotiations and politicking between governments, industry representatives, and NGOs to establish the KPCS makes for compelling reading. It took a dozen meetings between May 2000 and November 2002 to set up an international certification system for rough diamonds, which was launched in January 2003.

Yet Smillie is critical of the current state of the KPCS and argues that it will fail unless it can deal decisively and effectively with new problems as they arise. What the author does not discuss is the fact that he himself resigned from involvement in the scheme in May 2009. He is now active with the Diamond Development Initiative, which seeks to redress some of the imbalances caused by the global trade in diamonds.

Smillie's skill is the ability to write a scholarly record of the circumstances that created conflict diamonds

while also providing an entertaining, fast-paced read full of intrigue. It is unfortunate, then, that the book lacked the attention of an experienced editor. Each of the 13 chapters feels self-contained, and consequently there is considerable overlap between them, at times almost verbatim.

Blood on the Stone will be welcomed by anyone interested in Africa, corporate social responsibility, and geopolitics. Though a troubling book for many in the jewelry trade, it provides an important lesson for those keen to learn more about the topical issue of accountability and traceability of the product they sell. As the author points out, the diamond trade is disjointed. It portrays the romance and beauty of diamonds from gleaming showcases in major cities. Yet the product often starts its journey in an alluvial river bend in West Africa, where ownership is often fleeting and dangerous, and never *forever*.

EDWARD JOHNSON
GIA London

Jewellery in the Age of Queen Victoria: A Mirror to the World

By Charlotte Gere and Judy Rudoe, 552 pp., illus., publ. by The British Museum Press [www.britishmuseumshoponline.org], London, 2010. £50.00

This book is a welcome addition to the literature on 19th century jewelry. The authors have done a remarkable job of interpreting how jewelry was designed and worn during this prosperous age. Rather than presenting the subject in a strictly chronological manner or by describing the work of individual jewelers, their approach is to identify the cultural and emotional significance of jewelry in Victorian society.

I must warn you that nothing about this work is lightweight. It is a heavy book, literally and figuratively. There is no cozy reading in bed with this tome—it requires a library table to support its weight! Gere and Rudoe have done exhaustive research on every cultural aspect that might have had any bearing on Victorian jewelry, as is evident in the six-page bibliography and 33 pages of footnotes. Keep a bookmark placed in the footnotes as you read each chapter, as they contain many tidbits of additional information you won't want to miss.

The book is also heavily illustrated with images of jewelry, portraits (both rendered and photographic), as well as newspaper articles and jewelry advertisements. Be sure to read all the captions, as they provide valuable information to support the text. Happily, the authors have a light touch, making the book enjoyable and absorbing.

Ten chapters focus on the various cultural influences of the era. The first chapter, by far the longest, is an overview of Queen Victoria's life (1819–1901). It shows how jewelry fashion and styles were influenced by her coronation, her marriage to Prince Albert, the birth of her children, the tragedy of her husband's early death, her 40-year widowhood, and her management of a burgeoning empire.

The next four chapters address social factors of jewelry design. Gere and Rudoe explore the role jewelry played in public and private life as dictated by etiquette (jewelry appropriate for wear during the stages of mourning, for example), and how jewelry interacted with the prevailing clothing fashions. The authors decipher the hidden messages jewelry carried during this sentimental age, as well as the fascination with novelty that pervaded the 19th century and how this was manifested in jewelry.

Chapter 6, "Britain and the World," underscores the enormous impact of the International Exhibitions. From the first Great International Exhibition in London in 1853 to the Paris Exposition of 1900, these extraordinary events introduced art and artifacts from India, the Islamic world, China, and Japan to Europe and the West. This cultural integration had a profound effect on jewelry design and manufacture.

The wide range of historical and archeological revival styles are covered next. The authors do a great service by neatly categorizing the different influences, as they are often intermingled in a single piece of jewelry. Gothic and Renaissance revival styles are deciphered in chapter 7, followed by the different motifs that emerged from archeological discoveries in Egypt, Italy, Greece, Ireland, and Scandinavia.

Cameos—arguably the quintessential jewel of the Victorian era—are examined in chapter 9. We learn why these mini-sculptures in hardstone and shell were so highly prized. The final chapter is devoted to the various types of souvenir jewelry brought back from travels abroad. These include painted enamels from Switzerland; Italian *pietra dura*, micromosaics, and carved coral; and delicate ivory carvings from Germany.

It is important to understand that *Jewellery in the Age of Queen Victoria* deals with the jewelry worn by royalty and the very wealthy. Jewelry of the Arts & Crafts movement and Art Nouveau style were not favored by the Victorian elite, so readers should not be surprised that these are not mentioned. Gere and Rudoe have masterfully interwoven the cultural influences of the age into a marvelous and colorful tapestry, providing a clearer understanding of why fine jewelry took the forms that it did during Queen Victoria's reign.

ELISE B. MISIOROWSKI
Exhibit Curator
"All That Glitters: The Splendor and Science of Gems and Minerals"
San Diego Natural History Museum

Amethyst Uruguay

By Reinhard Balzer, 304 pp., illus., publ. by Christian Weise Verlag [www.lapis.de], Munich, 2009. US$65

This is a well-written historical account of how the gem cutting industry in Idar–Oberstein, Germany, fueled the mining and trading of agates in South America during the early 19th century. The promise of land and new resources was the driving force that led German families in the gem cutting business to settle in

South America.

The author supports the historical information by reproducing original letters between German miners in South America and their families in Idar-Oberstein, which offers a very real connection with these early miners. Overall, the book is thorough in both the information presented and the period photography. The text reads well, though the dual-language German-English format makes the book rather bulky. The highlight for this reviewer lies in the photos of the modern mining areas, as well as the amethyst specimens, which are nothing short of spectacular. The quality of the photography reveals tremendous detail. The final chapter showcasing these specimens leaves little room for the imagination, painting a vivid picture of the treasures these early miners would likely have discovered.

While the history and lore of a mining area contributes to the value of many gems, amethyst is not typically considered one of them. Nevertheless, this book makes a noteworthy attempt to give the reader a deeper understanding and appreciation for this material and its rich history in Uruguay.

Overall, this book is recommended for anyone interested in gems and their history, and it is an essential read for those with particular interest in amethyst.

NATHAN RENFRO
GIA Laboratory
Carlsbad, California

The Fancy Color Diamond Book: Facts & Secrets of Trading in Rarities

By Eden Rachminov, 231 pp., illus., publ. by Diamond Odyssey [www.diamondodyssey.org], Tel Aviv, 2009. US$215.00

This attractive book by third-generation gem dealer Eden Rachminov was created for fancy-color diamond enthusiasts and trade professionals. Filled with photos of rough and faceted colored diamonds, it offers a wealth of information. Nine chapters cover diamond colors, cuts, and shapes; how to read a diamond grading report; diamond trade nicknames (e.g., traditional terms such as *cape*, *canary*, etc.); treated diamonds; and diamond formation. The book's structure closely follows the GIA diamond grading course and applies it to colored diamonds.

One of the book's merits is that it impresses on the reader the rarity of fancy-color diamonds. It also reinforces the basic principles that govern diamond cut, shape, and grading. The inclusion photomicrographs deserve special mention for their quality. The book clearly compares the color grading process for near-colorless diamonds to that for fancy-color diamonds (with the latter far more complex), and presents color reference charts for yellows, pinks, and blues. Through simple scientific explanations, it also presents a brief overview of color origin in diamonds.

Unfortunately, because the colors in the charts are represented in the purest hues, the reader cannot appreciate the subtle nuances that give colored diamonds their distinctiveness and are critical to appreciating their rarity and value. For instance, a very pale colored diamond might be much more valuable than one of greater intensity if its hue is more desirable. Colored diamond hues, saturations, and tone are very specific. Rachminov does a superb job, however, of covering the vast palette, including the rarely featured chameleon, gray, brown, and black varieties. While the book includes an overview of treated diamonds, the lack of scientific explanation or photos in this section makes it difficult to grasp the complexities of diamond enhancements.

One of the book's greatest strengths is that it addresses (from a dealer's perspective) one of the most frequently asked questions: Which colors are the rarest and most expensive? Another is the value scale comparison for each of the different colors of colored diamonds, though it is disappointing that the prices are quoted in broad generalities, despite publicly available auction results. Additionally, the book gives an interesting answer to the important question of which color intensity is most valuable: deep, intense, or dark? The author emphasizes very clearly the importance of cut and openly explains the fact—well known in the trade—that fancy shapes help lengthen the light rays within the stones and make colors look more intense. Therefore, traditional shapes are rarer and more valuable for colored diamonds. The author further explains that blue fluorescence has far less impact on a colored diamond than on a colorless one. The reader will learn how to read a diamond report, which information is the most important, and which is a potential deal-breaker.

Fancy-color diamonds are not for everyone, but for those who do their homework and choose selectively, they are prized possessions. With its lavish illustrations on a variety of subjects, the book delivers a complete overview of colored diamonds, one that will stimulate further interest in this fascinating topic.

DELPHINE A. LEBLANC
Hoboken, New Jersey

OTHER BOOKS RECEIVED

Agates and Jaspers. *By Ron Gibbs, 239 pp., illus., publ. by theimage.com [www.theimagebooks.com], Wedington, NC, 2009, US$40.00.* This comprehensive, meticulously photographed work sets out to be a complete guide to agates and succeeds admirably. Agate formation, properties, structure, and identification are reviewed in detail, with more than 1,000 photos and diagrams describing the structural features of agates and jaspers. TWO

Minerals & Precious Stones of Brazil. *By Carlos Cornejo and Andrea Bartorelli, 704 pp., illus., publ. by Solaris [www.solariseditora.com.br], São Paulo, Brazil, 2010, R$148.00.* This massive volume presents a comprehensive historical and iconographic review of Brazil's minerals and precious stones. In addition to a detailed history of Brazilian gems, it provides a photographic record of the most important specimens of beryl, tourmaline, garnet, topaz, amethyst, and diamond, among others. TWO

2010 GEMOLOGICAL ABSTRACTS

COLORED STONES AND ORGANIC MATERIALS

Appearance of new bead material in cultured pearls. H. A. Hänni [info@gemexpert.ch], M. S. Krzemnicki, and L. Cartier, *Journal of Gemmology*, Vol. 32, No. 1–4, 2010, pp. 31–37.

Following a brief description of conventional shell beads and unusual materials recently used for culturing pearls, the authors describe the feasibility, characterization, and detection of Chinese freshwater cultured pearls (CFCPs) used to nucleate pearls in oysters. Some other unusual bead materials include bironite and pressed barium sulfate. One new technique utilizes irregularly shaped shell beads to produce baroque South Sea cultured pearls. Radiographs of the latter reveal the nature of the shell core, making them easily identifiable.

As traditional bead materials become less viable due to cost and scarcity, the abundance of nearly round CFCPs offers a possible alternative for pearl culturing. To study the method's effectiveness and the identifying characteristics of the resulting cultured pearls, the authors nucleated 200 *Pinctada maxima* and 200 *Pinctada margaritifera* oysters with 6.5 mm CFCPs. They found that the rejection rate was slightly lower than for shell beads, and that CFCPs larger than 9 mm could be used in a second nucleation. The cultured pearls were harvested after 13 months and compared with conventionally produced samples by slicing to reveal cross sections and also using microtomography and conventional radiography. Features typical of CFCPs—such as a complex central cavity, undulating hairlines, and fine fissures between layers—can be used to readily identify these cultured pearls. The advantages of CFCPs over

shell beads include abundance and ease of drilling, but the comparative costs will determine whether they become the preferred bead material.

Much more difficult to identify are samples produced using low-quality natural pearls as beads.

EAS

Boron and lithium isotopic compositions as provenance indicators of Cu-bearing tourmalines. B. M. Shabaga, M. Fayek [fayek@cc.umanitoba.ca], and F. C. Hawthorne, *Mineralogical Magazine*, Vol. 74, No. 2, 2010, pp. 241–245.

Eight samples of Cu-bearing tourmaline were analyzed for this study: four from Paraíba State, Brazil; two from Nigeria; and two from Mozambique. Electron microprobe analysis revealed that the samples had similar chemical compositions and were classified as fluor-elbaite. Secondary-ion mass spectrometry (SIMS) was used to measure the stable isotopes of B and Li to develop criteria to distinguish their origin and identify the source of fluids that precipitated these tourmalines.

The $\delta^{11}B$ values of the tourmaline from Paraíba ranged from –42.4 to –32.9‰, while the values of the samples from Nigeria and Mozambique ranged from –30.5 to –22.7‰ and –20.8 to –19.1‰, respectively. The $\delta^{11}B$ values were relatively homogeneous and displayed no overlap. There was some overlap in the $\delta^{7}Li$ values in samples from the three localities. Nevertheless, Cu-bearing tourmalines from each locality could be fingerprinted by their combination of $\delta^{11}B$ and $\delta^{7}Li$ values.

The very low $\delta^{11}B$ values are among the lowest reported for magmatic systems, expanding the global range of B isotopic composition for tourmaline by 12‰. The corresponding $\delta^{7}Li$ values +24.5–+46.8‰ are among the highest reported, though they are less diagnostic of the Li source. The combination of high $\delta^{7}Li$ values and low $\delta^{11}B$ values suggests a nonmarine evaporite or brine as the source for Li and B, either as constituents of the magma source region or through assimilation during magma ascent. The wide range in $\delta^{11}B$ and $\delta^{7}Li$ values suggests that B and Li isotope fractionation occurred during magmatic degassing and late-stage magmatic-hydrothermal evolution of the granitic pegmatite systems that produced these tourmalines.

GL

The formation of agate structures: Models for silica transport, agate layer accretion, and for flow patterns and flow regimes in infiltration channels. E. Walger, G. Mattheb, V. V. Seckendorff [volker.von_seckendorff@uni-wuerzburg.de], and F. Liebau, *Neues Jahrbuch für Mineralogie, Abhandlungen*, Vol. 186, No. 2, 2009, pp. 113–152.

An agate may contain one or more of three different structures: common agate banding, horizontal layering, and/or infiltration channel banding. Common agate banding is a three-dimensional layered structure, with each layer measuring a few microns thick. This structure can be formed by either an externally controlled accumulation process or an internally controlled differentiation process. Horizontal layering features parallel layers that can be quite extensive. Infiltration channel banding develops in a cavity that has been lined by layers of common agate banding. An infiltration channel is formed by fluid (silica) jets, which enter through one or more capillary fissures that penetrate the first layer of silica gel lining the inner surface of the cavity. Occasionally, the capillary fissure may be filled with non-silica minerals such as barite and calcite.

The authors propose a new model for agate formation that explains these three structures through water molecule cluster size, Brownian motion and limiting velocity, the penetration depth of the silica jet, and the duration of the cavity-filling process. Syneresis or aging (i.e., spontaneous dehydration, crystallization, and shrinking) occurs immediately after the formation of the first layer of silica gel (composed of disorderly packed spheres) in the cavity. This is followed by the supply of silica from the host rock. A relaxation mechanism is essential to achieving the typical agate texture of multiple silica (chalcedony) layers. This mechanism also controls the thickness of each layer. The agate structure can be formed either with an infiltration channel (by injection) or without one (by a direct process).

The rate of silica transport can be measured by the ratio of total surface area of the innermost active silica layer and the cross-sectional area of the capillary fissure. This ratio increases as the cavity becomes larger. Thus, the time needed for silica gel to fill a large cavity or a small one may be about the same. Silica gel starts to precipitate when it reaches the minimum level of supersaturation. Non-silica minerals as precursors of agate formation or as part of the agate structure suggest that the silica supply also contains other mobile chemical species from the host rock. Thin sections show that silica fibers in the agate layers always form perpendicular to the growth surface, though they appear to be deformed. The calculated duration of agate formation ranged from a few hundred to more than 10,000 years. *KSM*

"Real" hiddenite and real names. R. C. Tacker [christopher.tacker@ncdenr.gov], *Rocks & Minerals*, Vol. 85, No. 3, 2010, pp. 264–268.

Named in honor of William Earl Hidden, who documented specimens in North Carolina during the late 1800s, the Cr-bearing green spodumene known as hiddenite is also found in the Tuva Republic of Siberia; Kabbur, India; and Minas Gerais, Brazil. Some controversy surrounds the varietal name, since J. A. D. Stephenson described green spodumene from North Carolina prior to Hidden. While the International Mineralogical Association does not differentiate the variety names *hiddenite* and *kunzite* from spodumene, CIBJO recognizes hiddenite as green spodumene that owes its color to chromium. *EAS*

Spessartin: Von Sammlerstein zum Topseller [Spessartine garnet: From collector stone to top seller]. C. C. Milisenda [info@gemcertificate.com], T. Lind, and U. Henn, *Gemmologie: Zeitschrift der Deutschen Gemmologische Gesellschaft*, Vol. 59, No. 1–2, 2010, pp. 3–18 [in German].

Named after the Spessart Mountains of northwestern Bavaria, spessartine ($Mn_3Al_2SiO_4$) is an orange garnet that is sometimes known as "Mandarin garnet" in the trade. Production has always been erratic, and there are only a handful of traditional sources: Amelia, Virginia; Ramona, California; Minas Gerais, Brazil; Sri Lanka; and various locations in Africa. Because of their scarcity, these garnets were traditionally collectors' stones.

In 1992, a new occurrence was discovered in Namibia, followed a year later by a discovery in the Neelum Valley of Azad Kashmir. Spessartines emerged from Nigeria in 1998 and from Tanzania in 2007. The stones from Namibia and Tanzania are predominantly spessartine-pyrope garnets, with Tanzanian stones having a higher pyrope content. Samples from Azad Kashmir and Ramona are spessartine-almandine. Nigerian samples commonly have a high spessartine content, up to 95 mol.%, and varying traces of pyrope and almandine. The supply has dwindled in recent years, a trend that could return the gem to collector status.

GL

DIAMONDS

Diamond formation in the deep mantle: The record of mineral inclusions and their distribution in relation to mantle dehydration zones. B. Harte [ben.harte@ed.ac.uk], *Mineralogical Magazine*, Vol. 74, No. 2, 2010, pp. 189–215.

As natural diamonds are believed to crystallize in fluids/melts, the author proposes that diamonds and inclusions of particular compositions are restricted to two depth intervals (the lower asthenosphere and upper transition zone, and the upper/lower mantle) because they are controlled by locations of fluid/melt occurrence. Explanations for the depth restrictions and compositional restrictions of diamond inclusions are explored. The author gives a lengthy overview of past research related to diamonds, their inclusions, and mantle xenoliths formed in the diamond stability field in the earth's mantle lithosphere. A comparison of the inclusions and associations found in diamonds with experimentally determined silicate assemblages to depths of ~800 km shows a close correspondence between the data. The formation of mafic and ultramafic deep-mantle rocks and their diamonds is associated with subduction zones, where dehydration reactions occurred in subducted material or at the subduction interface.

EAS

Diamonds through time. J. J. Gurney [john.gurney@minserv.co.za], H. H. Helmstaedt, S. H. Richardson, and S. B. Shirey, *Economic Geology*, Vol. 105, No. 3, 2010, pp. 689–712.

The vast majority of gem diamonds formed during episodic events in the lithospheric mantle beneath continental cratons and were transported to the surface during a span from at least the Archean to the Phanerozoic. Harzburgite and eclogite are important diamond source rocks in the mantle. Most diamonds formed 1–3 billion years ago, and geologic evidence suggests that they spent long periods in the mantle before being transported to the earth's surface. There is also evidence that during these periods, the crystals underwent partial resorption and recrystallization. With improved methods of isotope analysis, diamond formation ages can now be correlated with processes in the upper mantle such as craton accretion and craton edge subduction.

JES

Lithoprobe's impact on the Canadian diamond-exploration industry. D. B. Snyder [dsnyder@nrcan.gc.ca] and H. S. Grütter, *Canadian Journal of Earth Sciences*, Vol. 47, No. 5, 2010, pp. 783–800.

Lithoprobe is a Canadian national research project established in 1984 to better understand the evolution of the northern part of North America. Using geologic and geophysical methods, Lithoprobe has demonstrated the very different geologic settings for the parageneses of peridotitic and eclogitic diamonds found across Canada. On a regional scale, seismic methods have delineated many of the oldest cratonic mantle blocks, as well as associated Archean and Proterozoic suture zones, where larger percentages of diamondiferous eclogites may occur. On a local scale, geophysical surveys have resulted in high-resolution (meter-scale) mapping of diamond-bearing kimberlite pipes and shallow-dipping dikes, allowing more precise volume estimation and more efficient mining.

JES

GEM LOCALITIES

The alluvial sapphire profiles of Mayo Kewol placer in the Adamawa region (North-Cameroon): Granulometric and mineralogical features. M. L. Boaka à Koul [boakami@yahoo.fr], R. Yongue-Fouateu, and P.-D. Ndjigui, *Journal of African Earth Sciences*, Vol. 56, No. 2/3, 2010, pp. 121–126.

Blue sapphires, along with other gems and heavy minerals, have been found in alluvial placers in several areas of Cameroon. The Mayo Kewol (Kewol River) placer covers an ~170 km^2 area in the western portion of Adamawa Province. Based on sediment samples and profiles, the gem minerals were found to occur along several horizons within the alluvial sequence. The authors were able to recognize several populations of sapphires based on their crystal

shape and degree of abrasion (indicated by roundness). Sapphires could not be found in any rocks exposed in the study area, so their primary source is unknown.

JES

Andradite from Antetezambato, north Madagascar. F. Pezzotta [fpezzotta@yahoo.com], *Mineralogical Record*, Vol. 41, May–June 2010, pp. 209–229.

In 2006, spectacular demantoid and topazolite (andradite) crystals on matrix were found in northern Madagascar. The location of the andradite occurrence—in a mangrove swamp subject to tidal surges—makes it difficult to extract the gem material, but the quality is very high. Initially identified as tourmaline, zircon, or sapphire, the green crystals were properly identified by the University of Nantes as demantoid.

JEC

Demantoid und Topazolith aus Antetezambato, Nordmadagaskar [Demantoid and topazolite from Antetezambato, northern Madagascar]. F. Pezzotta [fpezzotta@yahoo.com], *Lapis*, Vol. 35, No. 10, 2010, pp. 31–39, 90 [in German]; **Eine Reise zu den Demantoiden von Antetezambato [A travel to the demantoids of Antetezambato].** J. Hintze [jentschmineral@aol.com], *Lapis*, Vol. 35, No. 10, 2010, pp. 40–43 [in German].

These two articles provide an update on the demantoid deposit at Antetezambato. The mining rush of 2009 is clearly over, and almost all the diggers have moved to a new gold deposit. Consequently, the production and quality of the demantoid have dropped, while prices have increased. Many specimens offered for sale are manufactured fakes.

RT

Conditions for Early Cretaceous emerald formation at Dyakou, China: Fluid inclusion, Ar-Ar, and stable isotope studies. G. Xue, D. Marshall [marshall@sfu.ca], S. Zhang, T. D. Ullrich, T. Bishop, L. A. Groat, D. J. Thorkelson, G. Giuliani, and A. E. Fallick, *Economic Geology*, Vol. 105, No. 2, 2010, pp. 339–349.

In 1992, prospectors accidentally discovered emeralds near the Chinese village of Dyakou, in southeastern Yunnan Province near the border with Vietnam. The emeralds occur in quartz and quartz-pegmatite veins that intrude deformed metamorphic rocks (granofels and schists) of Proterozoic age. Ar-Ar dating of micas in the veins indicates they are of Cretaceous age (124 ± 1 million years). Oxygen isotope data suggest that vein formation occurred at temperatures of 365–420°C and pressures of 1.5–3.3 kbar. The Be- and Cr-rich fluids that produced the emeralds resulted from the intrusion of evolved granitic magmas into the metamorphic rocks.

JES

Le district minier à "tsavorite" de Lemshuku, Tanzanie [The tsavorite mining district of Lemshuku, Tanzania]. J. Feneyrol, G. Giuliani, D. Ohnenstetter, M. Saul, E. Saul, and J. M. Saul, *Revue de Gemmologie*, No. 172, 2010, pp. 11–22 [in French].

Tsavorite [$Ca_2Al_3(SiO_4)$] is a vanadium-bearing green grossular garnet discovered in the late 1960s by Campbell Bridges near Komolo in northeastern Tanzania. It has since been found elsewhere in Tanzania and in Kenya, Madagascar, Pakistan, and Antarctica. The three Tanzanian deposits lie in the Lelatema Fold Belt at Merelani, Namalulu, and Lemshuku.

At Lemshuku, two types of mineralization have been recognized: (1) primary deposits in graphitic gneiss, where tsavorite occurs in quartz-bearing veins associated with graphite and pyrite; and (2) a secondary deposit in an alluvial basin. Mechanized mining of the Lemshuku placer produces 12 g per day, with stones ranging from 0.5 to 3 cm. The hues vary from yellow-green to dark green; the intensity of the color corresponds to the vanadium and chromium content. No treatment is needed to enhance color or clarity.

GL

Estrazione di granato grossularia (var. essonite) a Kamburupitiya, Sri-Lanka [Mining of grossularite garnet (variety hessonite) at Kamburupitiya, Sri Lanka]. F. Troilo and E. Costa, *Rivista Gemmologica Italiana*, Vol. 4, No. 3, 2009, pp. 165–174 [in Italian].

Sri Lanka is a leading producer of hessonite, almost all of it coming from a mine at Kamburupitiya about 60 km north of Matara. The authors visited a typical small-scale mine in that area with a shaft extending 25 m down to the gem-bearing gravels. Because the deposit is eluvial, the hessonites occur mainly as fragments. Cuttable pieces generally weigh 2–5 g, but 50 g stones also have been recovered. The material goes directly to the cutter, and very few rough stones are available. The hessonites from Kamburupitiya are relatively pure grossular, with an andradite component of ~10%. Typical inclusions are apatite and possibly calcite.

RT

Gem-quality transparent diaspore (Zultanite) in bauxite deposits of the İlbir Mountains, Menderes Massif, SW Turkey. M. Hatipoğlu [murat.hatipoglu@deu.edu.tr], N. Türk, S. C. Chamberlain, and A. M. Akgün, *Mineralium Deposita*, Vol. 45, No. 2, 2010, pp. 201–205.

Yellowish green transparent diaspore crystals occur within two metamorphosed bauxite horizons in bedded marbles of the İlbir Mountains in southwest Turkey. The horizons are several meters thick. The diaspore crystals typically display a tabular habit and "dovetail" contact twinning, and some show color-change behavior under different

lighting. Their average length is 5 cm, but crystals up to 35 cm have been found. They occur (along with muscovite, hematite, ilmenite, chloritoid, and calcite) in small open spaces within fracture zones that crosscut the bauxite horizons. Diaspore and the associated minerals formed by hydrothermal remobilization of chemical components from the bauxite horizons. The diaspore from this locality is marketed as Zultanite. *JES*

Petrography and chemistry of SiO_2 filling phases in the amethyst geodes from the Serra Geral Formation deposit, Rio Grande do Sul, Brazil. A. Commin-Fischer, G. Berger [berger@lmtg.obs-mip.fr], M. Polvé, M. Dubois, P. Sardini, D. Beaufort, and M. Formoso, *Journal of South American Earth Sciences*, Vol. 29, No. 3, 2010, pp. 751–760.

Important sources of amethyst in the form of crystal-filled geodes and crystal-lined fractures are found in basalts of Rio Grande do Sul State in Brazil and in areas of neighboring Uruguay. The amethyst typically occurs with chalcedony and colorless quartz. Textural relationships and trace-element data suggest that these three phases formed in a single growth event at temperatures below 100°C. The host basalt or an underlying sandstone formation are considered possible sources of silica that was mobilized into a mineralizing fluid by a regional hydrothermal event. Silica precipitation occurred in open spaces in the basalt upon cooling and oxidation of this percolating fluid, first as chalcedony and then as colorless quartz. Over time, the fluid's silica content decreased, with amethyst forming during the final oxidizing stage of geode mineralization.

JES

Spinels from Ywathit deposit, Kayah State, Myanmar. U T. Hlaing, [p.tinhlaing@gmail.com], W. Atichat, and C. Sutthirat, *Australian Gemmologist*, Vol. 24, No. 3, 2010, pp. 61–63.

Pink, red, and orange spinel occurs in alluvial deposits near Ywathit in eastern Myanmar. Most of the pieces range from 1.0 to 2.5 cm; the larger stones (up to 6 g) are waterworn and have pitted and etched faces. Eight electron microprobe analyses demonstrated that they are almost pure spinel, with only minor amounts of Fe and Zn. Their inclusions consist of partially healed fractures, dark clouds, and some crystallites.

RAH

INSTRUMENTS AND TECHNIQUES

EDXRF quantitative analysis of chromophore chemical elements in corundum samples. L. Bonizzoni, A. Galli [anna.galli@mater.unimib.it], G. Spinolo, and V. Palanza, *Analytical and Bioanalytical Chemistry*, Vol. 395, 2009, pp. 2021–2027.

In recent decades, a considerable amount of research has dealt with the physicochemical causes of different colors of corundum. Much of it focused on optical absorption studies of corundum from various geographic origins, natural and synthetic, treated and untreated. The attribution of some of the absorption bands is still a matter of debate. This study examines the absorption bands in the NIR and visible ranges that do not involve intervalence-charge-transfer transitions ($Fe^{2+} \rightarrow Fe^{3+}$ and $Fe^{2+} \rightarrow Ti^{4+}$), commonly thought to be responsible for blue color in sapphire.

EDXRF analysis revealed the presence of Cr, Ti, Fe, V, and Ga in the corundum samples, in percentages that depend on the samples' characteristics (color, provenance, and origin). The data were compared to the results obtained by techniques such as optical absorption photoluminescence, not only for the correct attribution of some absorption bands, but also to match the luminescence and absorption spectra and their relative intensities in a semi-quantitative manner. This matched interpretation may be performed by taking into account the ion concentrations in the corundum structure, the spectral location and the probability of the induced absorption, and spontaneous emission processes in the samples.

ERB

Towards the differentiation of non-treated and treated corundum minerals by ion-beam-induced luminescence and other complementary techniques. H. Calvo del Castillo [hcalvo@ulg.ac.be], N. Deprez, T. Dupuis, F. Mathis, A. Deneckere, P. Vandenabeele, T. Calderón, and D. Strivay, *Analytical and Bioanalytical Chemistry*, Vol. 394, 2009, pp. 1043–1058.

A set of 78 red, pink, and yellow rough and faceted corundums of known origin, both treated and untreated, were examined by ion-beam-induced luminescence (IBIL, or ionoluminescence), micro-Raman spectroscopy, proton-induced X-ray emission (PIXE), and proton-induced gamma-ray emission (PIGE) to explore new methods for separating treated and untreated corundum. PIXE elemental concentrations showed enriched calcium and lead, which in some cases could be linked to treatment with fluxes or lead oxide. This technique was useful in detecting lead glass–filling treatment. Based on the concentrations of chromium and iron, it was possible to distinguish various origins for the different groups of samples. Raman spectroscopy corroborated PIXE analysis in detecting lead oxides.

IBIL could differentiate treated and untreated samples of the same type by their luminescence features. Micro-Raman and PIXE were complementary techniques that worked well for the samples containing lead glass, though neither conventional heating nor beryllium treatment could be identified without IBIL. PIGE could not detect beryllium due to the low cross section of the nuclear reaction chosen for Be identification.

ERB

X-ray fluorescence analyzers: Science fiction comes to life in this handheld device. S. Voynick, *Rock & Gem*, Vol. 40, No. 9, 2010, pp. 20–28.

When X-rays bombard atoms, certain electrons become energized; when the atoms return to their normal state, these electrons release their excess energy as secondary or fluorescent X-rays. Handheld X-ray fluorescence (XRF) analyzers began appearing in the mid-1990s, and continued refinement has produced the remarkable instruments in use today. Lightweight handheld models such as the Thermo Scientific Niton XL3t analyzer have recently become available. The nondestructive analysis requires only a few seconds and provides both laboratory-grade accuracy and a permanent data record. The instrument is configured specifically for geochemical analysis and can identify 29 elements selected for their importance in general mining and mineral exploration. It can analyze minerals, ores, and drill-hole samples; monitor ore grades in working mines; and measure the elemental compositions of mill tailings, mill concentrates, and smelter products. One drawback is the cost: Because of the research and development expenses and the low volume of instruments produced, the Niton XL3t analyzer sells for $42,000.

GL

JEWELRY RETAILING

Female empowerment gathers pace as self-purchases continue to rise. *New York Diamonds*, Vol. 118, May 2010, pp. 22–26.

As women command higher salaries and seek jewelry that reflects their lifestyle and personality, female self-purchasing has become a trend. Analysts believe the trend started last decade with the De Beers ad campaign for the right-hand ring. Powerful female politicians and entertainers have also influenced the self-purchase market. Because women self-purchase for many reasons and through many venues, it is difficult to assess the value of this market. But given its annual growth of around 20%, the jewelry industry should develop more marketing programs aimed at women.

MK

SYNTHETICS AND SIMULANTS

A different kind of composite. G. Choudhary [gtl@gjepindia.com], *Gems & Jewellery*, Vol. 19, No. 1, 2010, pp. 10–12.

Two unusual composite gems were submitted to the Gem Testing Laboratory of India. Presumably fashioned to simulate emerald, the specimens had a moderate to highly saturated green color. Microscopic examination revealed inclusions found in natural emeralds, as well as flattened gas bubbles visible near the pavilion. Diffused light and immersion in bromoform showed areas of varying saturation on the pavilion facets that followed the profile of the stone, along with pale yellow junctions and a nearly colorless central region. A chalky blue UV fluorescence reaction along the yellow junctions appeared to indicate glue. Gemological properties confirmed beryl at the center (table), surrounded by pieces of glass attached to the pavilion. While careful observation revealed the nature of these composites, they could be difficult to detect in a mixed parcel.

EAS

New data for distinguishing between hydrothermal synthetic, flux synthetic and natural corundum. A. S. Bidny [alexei.bidny@gmail.com], O. S. Dolgova, I. A. Baksheev, and I. A. Ekimenkova, *Journal of Gemmology*, Vol. 32, No. 1–4, 2010, pp. 7–13.

To provide more-reliable criteria for distinguishing natural and synthetic (flux and hydrothermally grown) corundum, excitation spectroscopy and oxygen-isotope analysis were used to study 35 samples. The natural corundum was from Russia, Madagascar, Tanzania, and Vietnam, and the synthetic samples were from various laboratories. Photoluminescence (PL) spectroscopy revealed a 290 nm excitation band in synthetic rubies, but not in natural samples. UV-Vis absorption spectroscopy showed a narrow band at 342 nm in flux-grown corundum but not in natural or hydrothermally grown samples. FTIR spectra showing so-called water bands related to OH complexes were distinctly different in natural and hydrothermal samples and altogether absent from flux-grown material. EDXRF data showed varying proportions of chromium, iron, and gallium impurities in samples from different laboratories and geographic localities. Although isotopic analysis is destructive, this technique could identify synthetic corundum and also help determine the type of deposit from which natural material was obtained. The technique even showed potential for determining geographic origin of samples from various Russian localities representing igneous, skarn, hydrothermal, and metamorphic deposits. The oxygen-isotope values reflected the source compositions of the water involved in their crystallization; anomalous results for samples from Khitostrovskoye were believed to be the result of contamination by meteoric water, which was negligible in samples from the other localities.

EAS

Recent advances in high-growth rate single-crystal CVD diamond. Q. Liang [qliang@ciw.edu], C. Yan, Y. Meng, J. Lai, S. Krasnicki, H. Mao, and R. J. Hemley, *Diamond and Related Materials*, Vol. 18, 2009, pp. 698–703.

The authors employed microwave plasma chemical vapor deposition (MPCVD) with varying atmospheres to grow thick films of high-quality synthetic diamond at elevated rates of 40–100 μm/hr. Post-growth treatments enhanced the crystals' mechanical, optical, and electrical

properties. The synthetic diamonds were characterized using an array of techniques, including electron paramagnetic resonance (EPR), photoluminescence, and ultraviolet, visible, infrared, and Raman spectroscopy. The authors also used Vickers indentation to test the mechanical properties and SIMS analysis to measure nitrogen impurity contents.

Near-colorless and flawless single-crystal CVD synthetic diamonds up to 2 ct were grown; these were difficult to distinguish from natural type IIa diamond. To enhance their mechanical properties, samples with higher nitrogen content were grown and subsequently treated by high-pressure, high-temperature annealing at 2000°C and 57 GPa pressure for 10 minutes. These treated synthetics were found to be harder and tougher than natural diamonds. Finally, low-pressure, high-temperature (LPHT) treatments were performed to produce more transparent and colorless crystals. Significantly, the samples that were free of visible inclusions had a lower tendency to form graphite under LPHT conditions than natural diamond. Their defect structures with respect to incorporated nitrogen, incorporated hydrogen, and vacancy clusters differed significantly from those found in natural diamonds. These differences led to special properties in both the as-grown and treated synthetic diamonds.

JS-S

TREATMENTS

APHT treatment of brown type Ia natural diamonds: Dislocation movement or vacancy cluster destruction? V. G. Vins [vgvins@gmail.com], A. P. Yelisseyev, S. S. Lobanov, D. V. Afonin, A. Yu. Maksimov, and A. Ye. Blinkov, *Diamond and Related Materials*, Vol. 19, No. 7/9, 2010, pp. 829–832.

Using a specially designed apparatus, type Ia brown diamonds were subjected to high-temperature heating (up to 2100°C) in an inert gas at atmospheric pressure (APHT). The heating was performed in five or six successive thermal shocks, each lasting about two seconds. The total exposure time was kept very brief to minimize graphitization of the diamond. Prior to heating, the diamonds were dark brown and exhibited evidence of strong plastic deformation (e.g., uneven color distribution in the form of parallel bands of brown color). After treatment, they were light brown or yellowish brown due to the destruction of lattice defects responsible for the dark brown color. Details of the changes in lattice defects were revealed by infrared and photoluminescence spectroscopy.

The article also describes the results of preliminary experiments on APHT color treatment of yellow, red, and purple-red synthetic diamonds. Many of these color and lattice-defect changes have been observed as a result of traditional HPHT diamond treatment.

JES

Detection of beryllium treatment of natural sapphires by NRA. P. C. Gutiérrez [carolina.gutierrez@uam.es], M.-D. Ynsa, A. Climent-Font, and T. Calligaro, *Nuclear Instruments and Methods in Physics Research B*, Vol. 268, 2010, pp. 2038–2041.

The possibility of using a nondestructive nuclear reaction analysis (NRA) technique for detecting Be diffusion in corundum was investigated. Be diffusion is usually detected with techniques such as laser ablation–inductively coupled plasma–mass spectrometry (LA-ICP-MS) or laser-induced breakdown spectrometry (LIBS), which are microdestructive (leaving 50–100 μm diameter craters on the gems). NRA involves examining nuclear reaction products such as protons, alpha particles, and gamma rays generated by a helium ion beam. The radiation fingerprint identifies individual light isotopes and quantifies them with ppm sensitivity. Tests were conducted to optimize beam energy and dose to obtain the appropriate peak-to-background ratio for detecting Be. With a 2.8 MeV external He beam and a beam dose of 200 μC, beryllium concentrations of 5–16 ppm were measured in the samples, with a detection limit of 1 ppm.

GL

Determination of the potential for extrinsic color development in natural colorless quartz. E. H. Nunes, V. Melo, F. Lameiras [fernando.lameiras@pq.cnpq.br], O. Liz, A. Pinheiro, G. Machado, and W. Vasconcelos, *American Mineralogist*, Vol. 94, 2009, pp. 935–941.

Colorless quartz can become colorized after exposure to ionizing radiation (e.g., gamma rays, X-rays, and high-energy electron beams) and heat, due to trace elements such as aluminum, iron, hydrogen, lithium, and sodium. Infrared spectroscopy was used to identify the color potential of several thousand samples from Brazil, Uruguay, Bolivia, and Colombia. At room temperature, all the colorless samples showed bands at 3063, 2935, 2771, 2677, 2600, and 2499 cm^{-1}. The samples that remained colorless after irradiation also displayed bands at 3304 and 3202 cm^{-1}. The samples that became grayish to black after irradiation contained additional bands at 3483, 3433, and 3381 cm^{-1}; the 3483 cm^{-1} band is related to greenish yellow, yellow (citrine), or brown colors after irradiation and heating. The samples that became grayish "olive" green after irradiation and "olive" green after further heating showed an additional pair of bands at 3510 and 3304 cm^{-1}. The samples that became violet (amethyst) or green (prasiolite) after irradiation, or "sky" blue after irradiation plus heating, displayed a broad band at ~3341 cm^{-1} and a band at 3585 cm^{-1}.

ERB

Identificazione di acquamarine trattate termicamente [Identification of heat-treated aquamarines]. I. Cascione, F. Caucia, I. Adamo, and V. Bordoni, *Rivista Gemmologica Italiana*, Vol. 5, No. 1, 2010, pp. 23–31 [in Italian].

Ten aquamarine samples from Nigeria and Minas Gerais, Brazil, were heated and their property changes documented. The stones were heated in four stages from approximately 300 to 480°C, which in each case led to distinct color changes from green to blue. Weight, density, and refractive index before and after heating were compared. Based on qualitative and quantitative electron microprobe analyses as well as UV-Vis-NIR and mid-infrared spectroscopy, the color changes could generally be linked to an Fe^{3+}-Fe^{2+} intervalence charge transfer. Aside from color, the most significant change was a higher RI. Despite the small sample size tested, the increased refractive index might offer a clue in identifying heat treatment. [*Abstractor's note*: There appears to be too much overlap in RI to reliably distinguish between heated and unheated stones.]

RT

MISCELLANEOUS

Dangerous dust. D. Hamilton, *Rock & Gem*, Vol. 40, No. 8, 2010, pp. 26–29.

Dust is the lapidary's forgotten hazard. Whether it is inhaled or ingested or comes in contact with exposed skin, lapidary dust can cause serious health problems. Some dust is poisonous, and the worst contains copper oxide, which can damage the endocrine and central nervous systems. Gems that pose this hazard include turquoise, chrysocolla, malachite, and azurite. Silicates such as quartz can cause silicosis, a respiratory disease. Asbestos can be found in tiger's-eye and soapstone. Some fossils are radioactive, and care should be taken when collecting and polishing them. A few simple precautions can minimize the dangers and keep a workshop safe.

MK

Los minerales de colección como recurso económico en países en vías de desarrollo [Minerals for collectors as a source of income in developing countries]. J. C. Melgarejo [joan.carlos.melgarejo.draper@ub.edu], M. Campeny, J. Sanz, C. Curto, and J. Viñals, *Bolétin de la Sociedad Geológica Mexicana*, Vol. 62, No. 1, 2010, pp. 55–100 [in Spanish].

The production of minerals for collectors offers a good opportunity to create additional income in rural areas of developing countries. Unfortunately, rural populations usually have little knowledge about the mining and marketing of mineral specimens. This article provides the basic knowledge and deals systematically with a wide range of questions, such as: What types of collections are there? What are the usual sizes of mineral specimens? What do they look like? Which criteria determine the value of a specimen? How are the specimens prepared for sale and transport? Which marketing channels are there for minerals? Each subject is illustrated by color photographs. Lists of mineralogical laboratories and useful websites are provided.

RT

Volume 46 Index 2010

Numbers 1–4

SUBJECT INDEX

This index gives the first author (in parentheses), issue, and inclusive pages of the article in which the subject occurs for all feature articles, Notes & New Techniques, and Rapid Communications that appeared in Volume 46 of *Gems & Gemology*. For the Gem News International (GNI) and Lab Notes (LN) sections, inclusive pages are given for the item. The Book Reviews section is available only as an online supplement, beginning with page S1. The Author Index (p. S18) provides the full title and coauthors (if any) of the articles cited.

C

D

E

F

G

H

I

J

K

L

AUTHOR INDEX

This index lists, in alphabetical order, the authors of all feature articles, Notes & New Techniques, and Rapid Communications that appeared in the four issues of Volume 46 of *Gems & Gemology*, together with the full title and inclusive page numbers of each article and the issue (in parentheses). Full citation is given under the first author only, with reference made from coauthors.

Because Public Education Happens At The Counter.

GIA's Retailer Support Kit and website

A $97.00 value, shipping and handling extra.

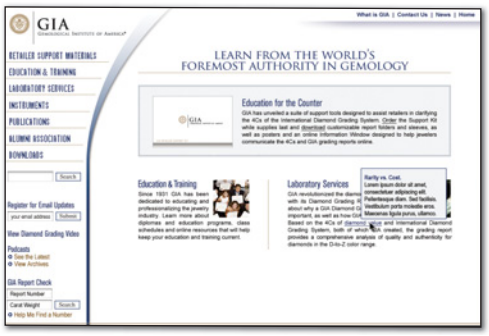

GIA's Retailer Support Kit has been developed to help sales associates educate the public about diamonds, the 4Cs, and thoroughly explain a GIA grading report. Take full advantage of all that GIA has to offer by visiting www.retailer.gia.edu

To order your FREE kit, log on to www.retailer.gia.edu

GIA®

GGW110

GIA®

80th ANNIVERSARY
SINCE 1931